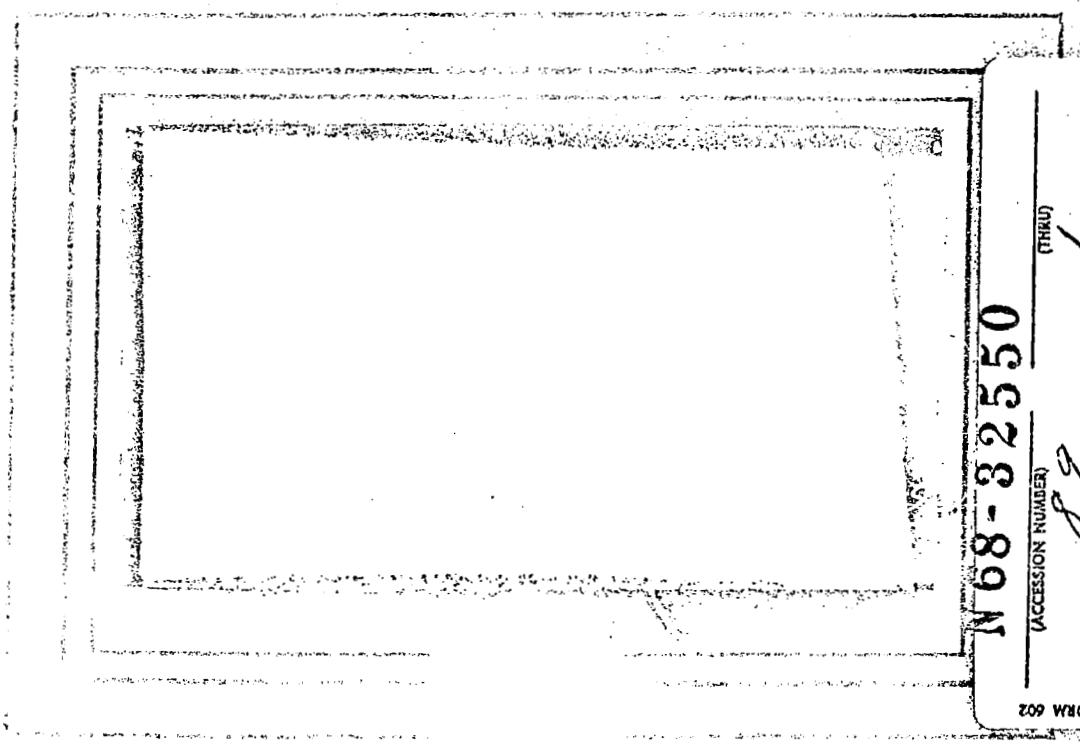

NGL-31-001-005
(NsG-306/31-001-005)
(NASA Grant NsG-306-63)
Supplement No. 5

National Aeronautics
and Space Administration

PULSED ELECTROMAGNETIC GAS ACCELERATION

12th Semi-annual Progress Report
1 January 1968 to 30 June 1968

Report 634k

Prepared by: Robert G. Jahn
Robert G. Jahn
Professor
and Research Leader

and: Woldemar v Jaskowsky
Woldemar F. von Jaskowsky
Senior Research Engineer
and Lecturer

July 1, 1968

School of Engineering and Applied Science
Department of Aerospace and Mechanical Sciences
Guggenheim Aerospace Propulsion Laboratories
PRINCETON UNIVERSITY
Princeton, New Jersey

Abstract

Studies of the spontaneous transition of a parallel-plate accelerator from a transient "sweeping" mode to a quasi-steady "blowing" mode have been extended to sufficiently long pulse times that the influence of externally injected mass flow can be clearly discerned. By Kerr-cell photography of the downstream flow over a wedge, and by terminal voltage signatures, it is possible to distinguish situations of adequate mass flow injection, of mass-"starvation," and of mass overload of a given quasi-steady discharge configuration. A shock tube gas injection system for a high-power magneto-plasmadynamic arc simulator has been devised which can provide mass flows up to 50 gm/sec of argon for three milliseconds, with a rise time of one millisecond. Optimization of the efficiency of energy transfer from a capacitor line to a gas-sweeping current sheet has been achieved in terms of the ratio of the line impedance to the dynamical impedance of the propagating discharge, and in terms of the ratio of driving pulse length to a characteristic time of the gas-sweeping process. Correlation has been found between the resistive voltage drop across a propagating sheet discharge and the size of the anode surface available for attachment of that sheet, an effect which appears related to the development of a diffuse "anode foot" at the anode terminus of the current sheet. The influence of gasdynamic interferences on high-speed pressure transducers and on electric probes has been found significant enough to distort the interpretation of current sheet structure made with such devices unless special precautions are taken. The feasibility of gas laser interferometric determination of electron density profiles through propagating current sheets has been established in a calibration experiment, encouraging application of this technique to the parallel-plate and quasi-steady MPD accelerators.

CONTENTS

LIST OF ILLUSTRATIONS

LIST OF ILLUSTRATIONS-contd

CURRENT STUDENT PARTICIPATION

Student	Period	Degree	Thesis Topic
BOYLE, Michael J.	1968-	B.S.E. Cand.	Plasma Velocity Measurements
BRUCKNER, Adam P.	1966-	Ph.D. Cand.	Gas Laser Interferometry of Closed Chamber Discharges
CLARK, Kenn E.	1965-	Ph.D. Cand.	Magnetoplasmadynamic Arc Simulation
DI CAPUA, Marco S.	1966-	Ph.D. Cand.	Current-voltage Characteristics of High-current Discharges
ECKBRETH, Alan C.	1964-	Ph.D. Cand.	Stabilization of a Current Sheet for Quasi-steady Plasma Acceleration
OBERTH, Ronald C.	1966-	Ph.D. Cand.	Current Sheet Anode Foot Phenomena
TURCHI, Peter J.	1963-	Ph.D. Cand.	Unsteady Plasma Diagnostics
VAN WOERKOM, Paul	1968-	Visiting Scholar	Static Breakdown Characteristics of Various Electrode Configurations
WILBUR, Paul J.	1966-	Ph.D. Cand.	Optimization of Energy Transfer to Accelerating Plasmas
YORK, Thomas M.	1965-	Ph.D. Cand.	Gas Pressure Distributions in Accelerating Plasmas

I. INTRODUCTION

The flavor of this semi-annual report differs somewhat from its typical predecessors, for two reasons. First, the educational aspects of the program are in an unusual phase where no less than four of our eight graduate students are just completing their Ph.D. theses. Impressive as this constellation may be from an academic standpoint, it raises problems of reporting significant elements of their work here, without preempting their thesis publications, all of which will be issued within the next reporting period. For this reason, the studies involved are presented rather concisely, with an eye to the more detailed accounts to follow.

Second, several of the laboratory efforts, for different reasons, have recently taken on a strong gasdynamic flavor, and this report reflects more pure gasdynamic research than one might normally expect from a basically plasmadynamic and electrodynamic program. Gasdynamic questions of proper mass flow supply have arisen in both the parallel-plate accelerator work (Sec. II), and in the MPD simulator (Sec. III); questions of gasdynamic interference and boundary layer effects have been resolved in connection with the transient pressure measurements in closed chamber discharges (Sec. VI); and the influence of stagnation point gasdynamics on electric probe response has been clearly demonstrated (Sec. IX). In a sense, these simultaneous excursions into several gasdynamic studies may have a salutory effect on the entire laboratory program, for in retrospect, gasdynamic aspects have received considerably less attention here, as in other laboratories, than the somewhat more dramatic plasmadynamic phenomena. Yet it is clear that an equivalent sophistication in handling gasdynamic processes must precede effective implementation of any plasma thruster concept, and the background and training of our particular group should be appropriate to this aspect of the task.

II. TRANSITION FROM UNSTEADY TO STEADY PLASMA ACCELERATION IN A PARALLEL-PLATE CHANNEL (Eckbreth)

The process of stabilization of a propagating current sheet into a quasi-steady, plasma-"blowing" configuration has been described in some detail in the past several reports [47,48,51]. The most recent of these discussed the necessity of extending the test time in this experiment into the 100 μsec range if the complete gas flow pattern through the accelerator was to achieve a reasonably quasi-steady situation. To provide the driving current pulses of this duration, new inductors have been fabricated for the capacitor line. These consist of 14 turns of #8 TW wire wound on 7" lengths of 4" dia. plastic sewer pipe. Bench tests indicate that these coils each have an inductance of 12.8 μ henries. From these inductors and the same capacitors used previously, a set of four LC ladders have been assembled, such that when connected in series a nominal 5,000 amp x 500 μsec pulse is provided. Parallel connection yields a 20,000 amp x 125 μsec nominal pulse, and series-parallel alignment provides a 10,000 amp x 250 μsec pulse. When actually driving the parallel-plate accelerator, these lines deliver current pulses approximately 20 percent lower in amplitude and 20 percent longer in duration than their nominal values, but we shall use the design values when referring to a particular pulse. Typical signatures of the 10,000 amp x 250 μsec current pulse (hereafter denoted 10/250, etc.), and its time derivative are shown in Fig. 1. The rise time on the current pulse is approximately 20 μsec which is less than 10 percent of the pulse duration. The other pulses, 20/125 and 5/500, are qualitatively similar to that shown.

Before performing any detailed interior diagnostics on the long current pulses, voltage measurements were taken to see if any difference could be found between cases where the chamber was prefilled to an ambient pressure of 100 μ

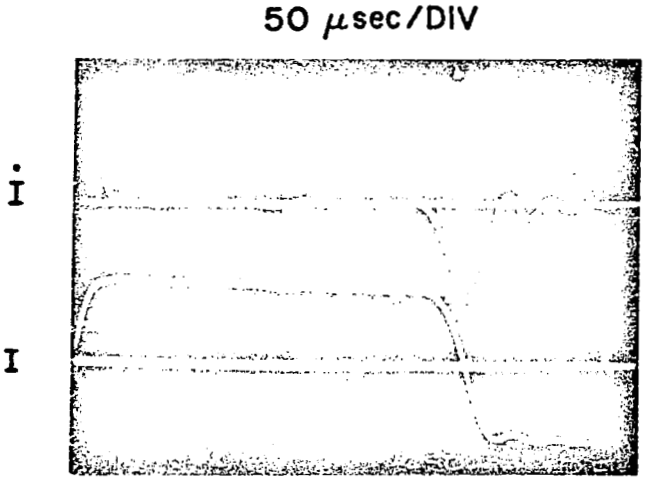

NOMINAL 10,000 amp × 250 μsec PULSE

AP 25 P-201 68

FIGURE 1

argon and those where the shock tube injection was used to bring the pressure in the breakdown gap abruptly to 100 μ from an initial hard vacuum. In order to enhance any possible mass starvation effects, some data were taken with the length of the metal electrode portion of the channel reduced to 2", in contrast to the normal 5-1/4" length. The voltage was monitored at the downstream end of the parallel-plate accelerator, where there are only two possible contributions to the total voltage, a resistive drop V_R representing the finite conductivity of the plasma, and a back emf component V_{uB} derived from plasma flow through the stabilized current distribution. Both of these components should respond in the same way to mass starvation of the discharge. In this pressure range the resistance of the discharge tends to decrease with increased gas pressure, and hence will increase if mass flow is depleted. The V_{uB} contribution should vary inversely with mass flow rate, since the fixed $\vec{j} \times \vec{B}$ body force is applied per unit volume. As longer and longer current pulses of correspondingly lower amplitudes are employed, V_{uB} tends to become small compared to V_R which typically is on the order of 50 to 100 volts for this range of operation. Figure 2 displays a plot of V_{uB} vs. current data for the case of 5-1/4" electrodes and 100 μ prefilling. Note that in the range of 1,000 to 10,000 amps the V_{uB} term can be expected to be less than 20 volts so that any differences in voltage signature between shock tube gas injection cases and ambient prefill cases will most likely be due to changes in V_R. This effect is shown in Fig. 3 where the total voltage, which is nearly equal to the resistive drop, is plotted against ambient prefill pressure.

In Fig. 4 voltage measurements are presented for the permanently insulated electrodes, 5-1/4" metal electrode portion, comparing 100 μ ambient prefill with shock tube injection which simulates 100 μ initially. These are presented for the 20/125 and 10/250 pulses. In Fig. 5 voltage measure-

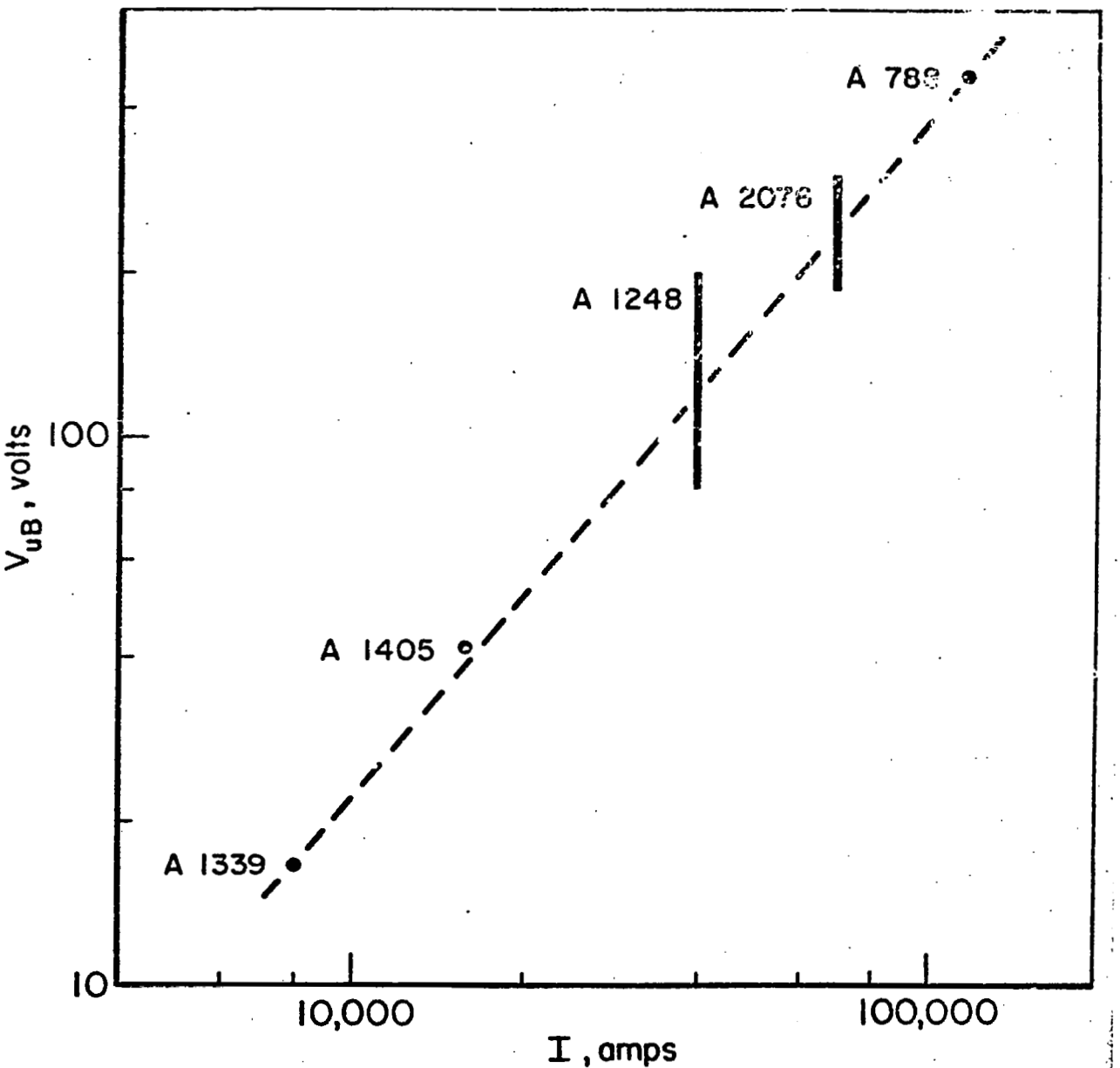

BACK EMF vs DISCHARGE CURRENT

FIGURE 2

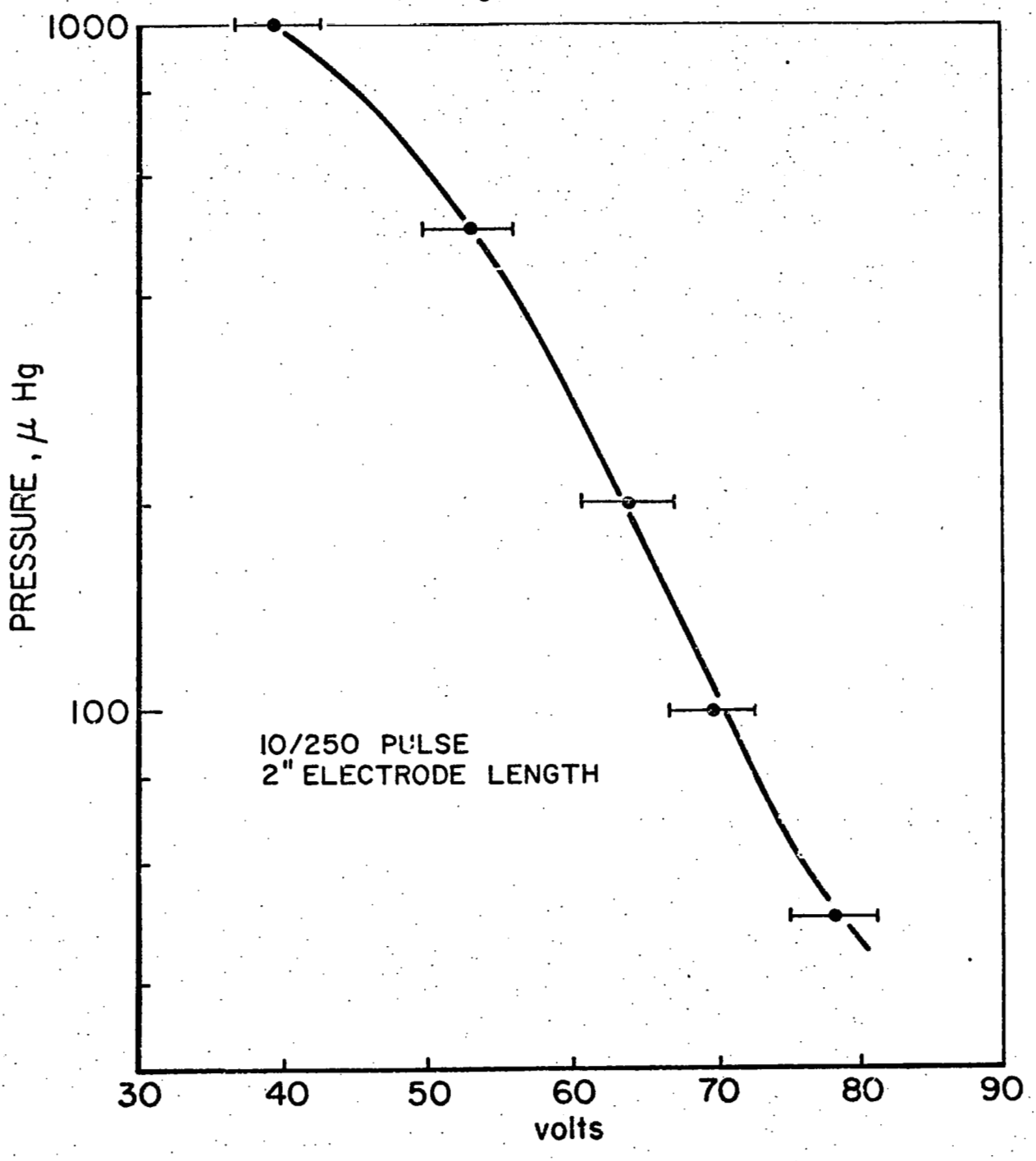

TOTAL ARC VOLTAGE vs AMBIENT PREFILL PRESSURE

FIGURE 2

AP 25 P-202. 68

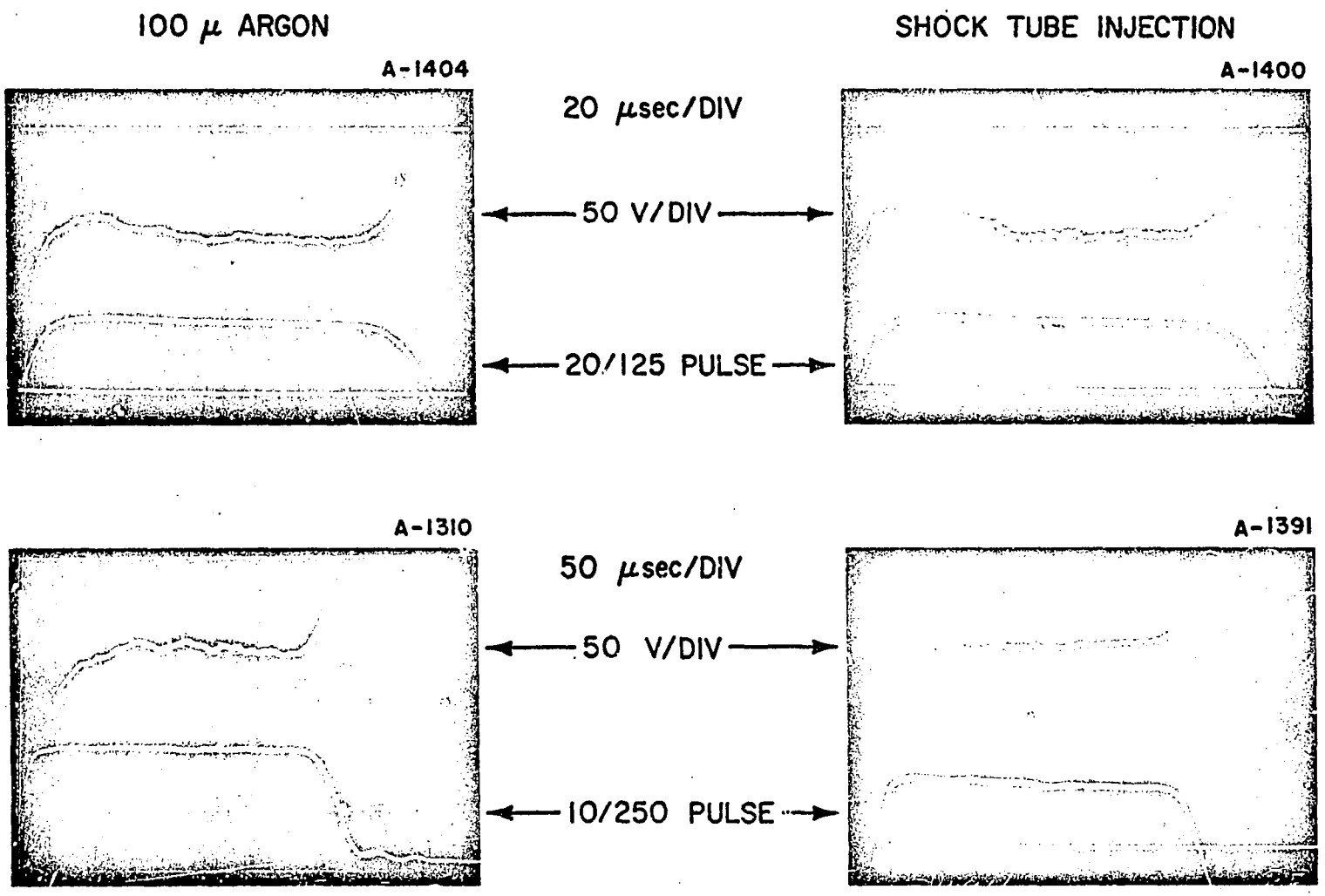

VOLTAGE SIGNATURES FOR 5 1/4" ELECTRODE LENGTH

FIGURE 4

ERRATA:
Replace Fig. 4, p. 7 of text with corrected figure.

AP 25 I-203 60

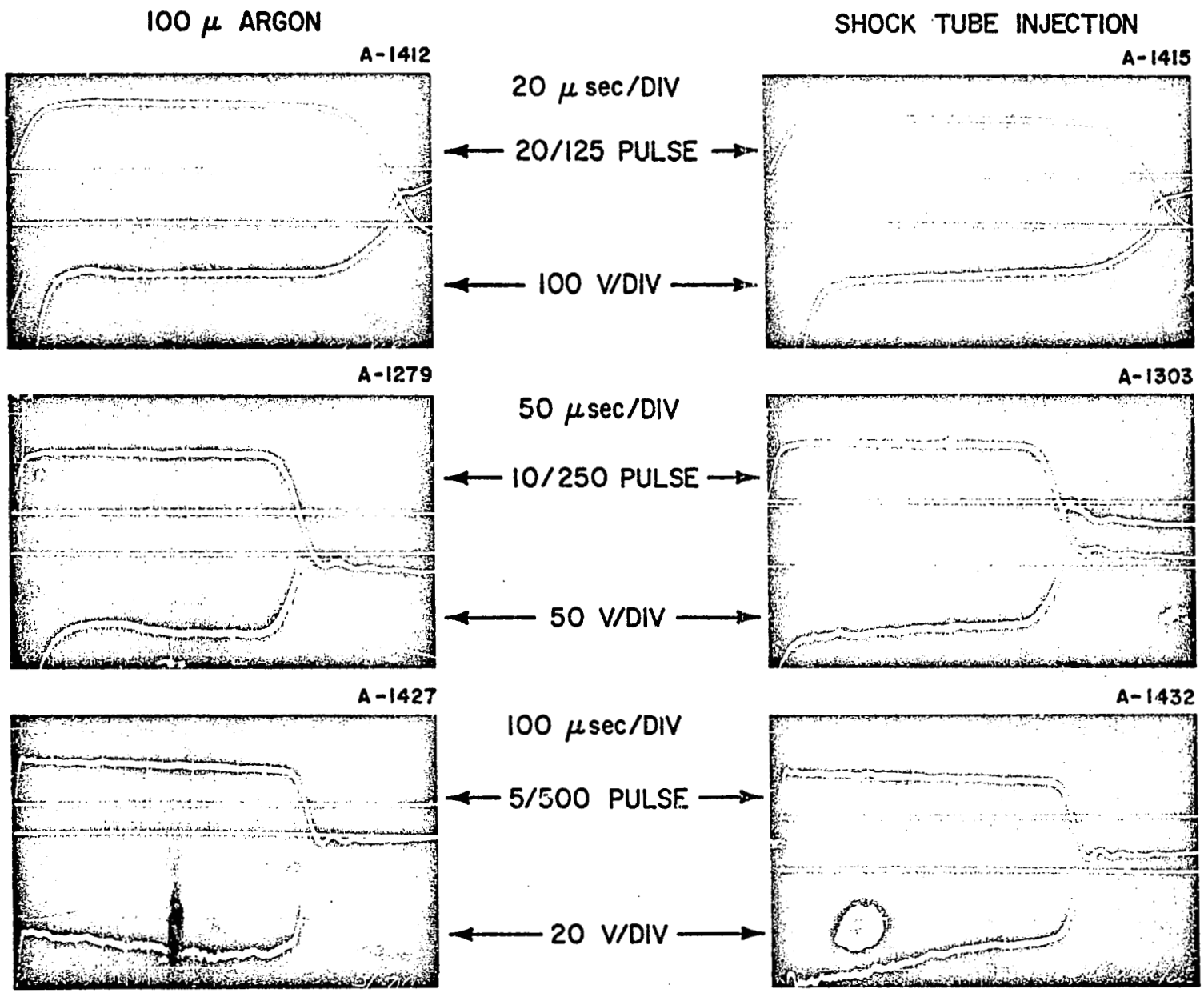

FIGURE 5

VOLTAGE SIGNATURES FOR 2" ELECTRODE LENGTH

ments are presented for a 2" metal electrode length comparing ambient and shock tube injection for the three pulses 20/125, 10/250, and 5/500. Note that for the 20/125 pulse, for both the 2" and 5-1/4" metal electrode length cases, voltage signatures for the shock tube and ambient cases are nearly identical. Presumably the shock tube is properly simulating 100 μ initially, but does not change the mass flow situation appreciably for the balance of the pulse length. However, for both electrode lengths in the 10/250 case, a difference arises between the shock tube and ambient cases in the voltage level toward the end of the pulse. The effect is most noticeable in the 2" electrode length case for the 5/500 pulse where, near the end of the pulse, the shock tube voltage is nearly 40 percent lower than the ambient value. In fact, the shape of the entire signature is markedly different for the long pulses. The shock tube signatures decrease with time, probably due to increased pressure in the arc region because of the mass flow supply, whereas the ambient signals increase with time, presumably due to a mass starvation of the arc. Thus, based on the voltage data, it appears that fresh gas can be supplied to the arc from the present shock tube injection system if the pulse length exceeds some 200 μsec.

One possible difficulty with the long pulses in the parallel-plate accelerator may be the lack of uniformity of the discharge. Fringing magnetic fields which exist because of the finite width of the accelerator may severely constrict the sheet discharge into an arc column when the current is maintained for very long periods of time. Such a constriction clearly would impair the operation of this device as an effective gas accelerator. To check on this possibility, the uniformity of the discharge has been studied in three ways: (a) Kerr-cell photography, (b) magnetic probing, and (c) observation of electrode pitting.

In order to perform Kerr-cell photography on the low

amplitude current pulses, it is necessary to replace the usual 50 nanosecond shutter with a new 5 μsec pulse-forming network to achieve sufficient film illumination. Figure 6 shows typical perspective photographs obtained with this shutter for the 10/250 discharge between 2" length electrodes with shock tube injection. Although some localization of discharge luminosity can be discerned, it appears that the entire electrode width contributes to the discharge pattern.

The discharge uniformity was also studied with magnetic probes. A simple probe carriage was constructed so that three magnetic probes could be positioned in the midplane of the discharge at different distances from the sidewalls. The magnetic field data were then reduced to contours of enclosed current in the horizontal midplane. In the particular survey to be displayed, all the data were taken on one side of the centerline of the device under a presumption of symmetry. The probes were all identical and equal calibrations were assumed for the probes. A rough calibration equating peak magnetic field with total discharge current was made, and a single integrator was used. Typical results are shown in Figs. 7a,b,c. From such data it is found that the discharge breaks down over the entire electrode surface and redistributes itself as a wave of current whose density is highest near the back insulator and along the midplane. The wave of current propagates downstream and also bows downstream slightly. The contours are smooth and indicate a distribution of current over the central region of the channel unlike a constricted arc column. Actually, the results are probably a bit pessimistic in their lack of one-dimensionality. The presence of three probes on one side of the channel clearly perturbs the current distribution as evidenced by electrode pitting and insulator deposition. Presumably the low current density at the insulator walls may be attributed to plasma cooling by the walls. The evidence of diffuse discharge initiation over the entire electrode surface is contrary to our experience with high current pulses

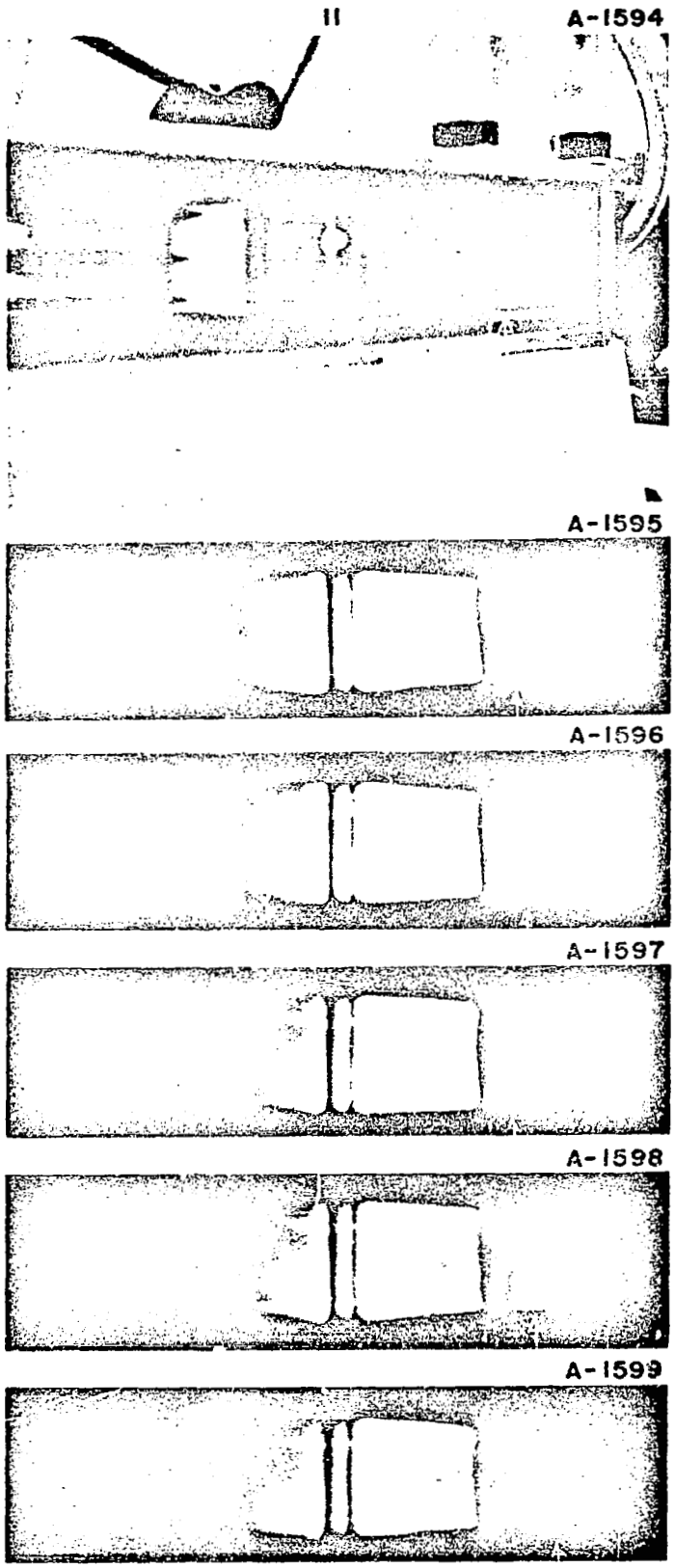

PERSPECTIVE PHOTOGRAPHS OF 10/250
DISCHARGE BETWEEN 2" ELECTRODES FIGURE 6

AP 25 P-204 68

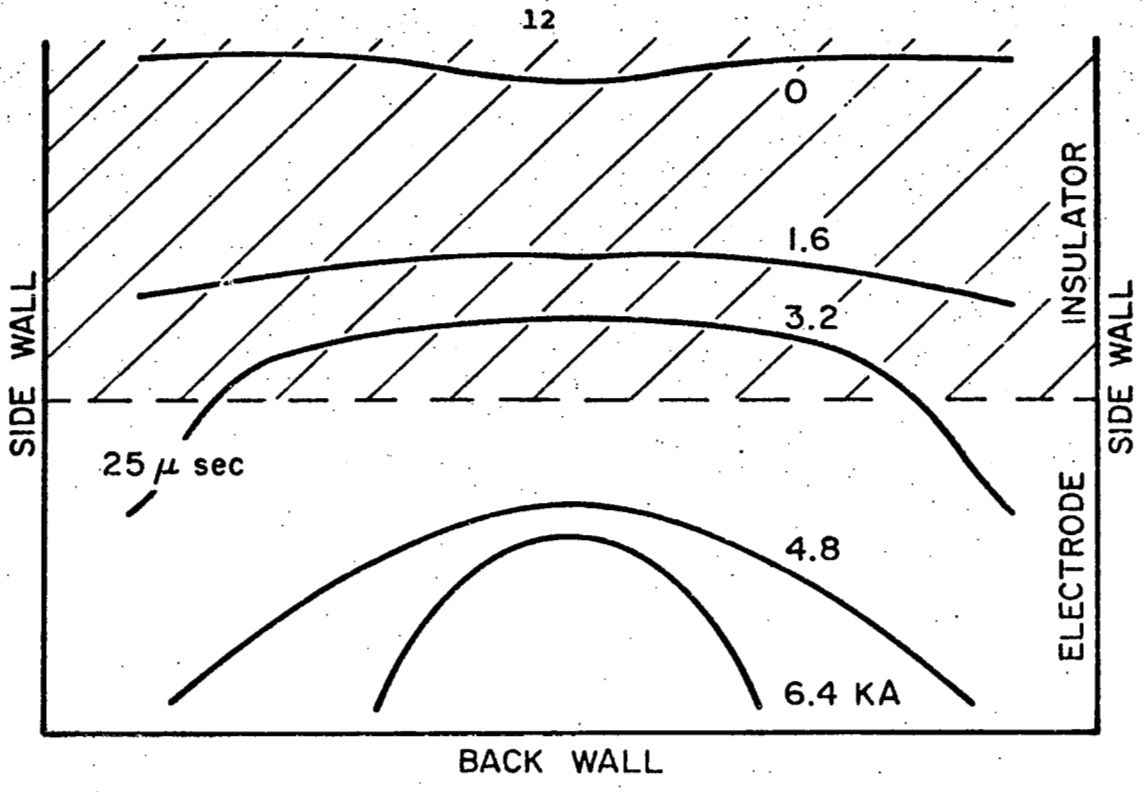

SHOCK TUBE INJECTION

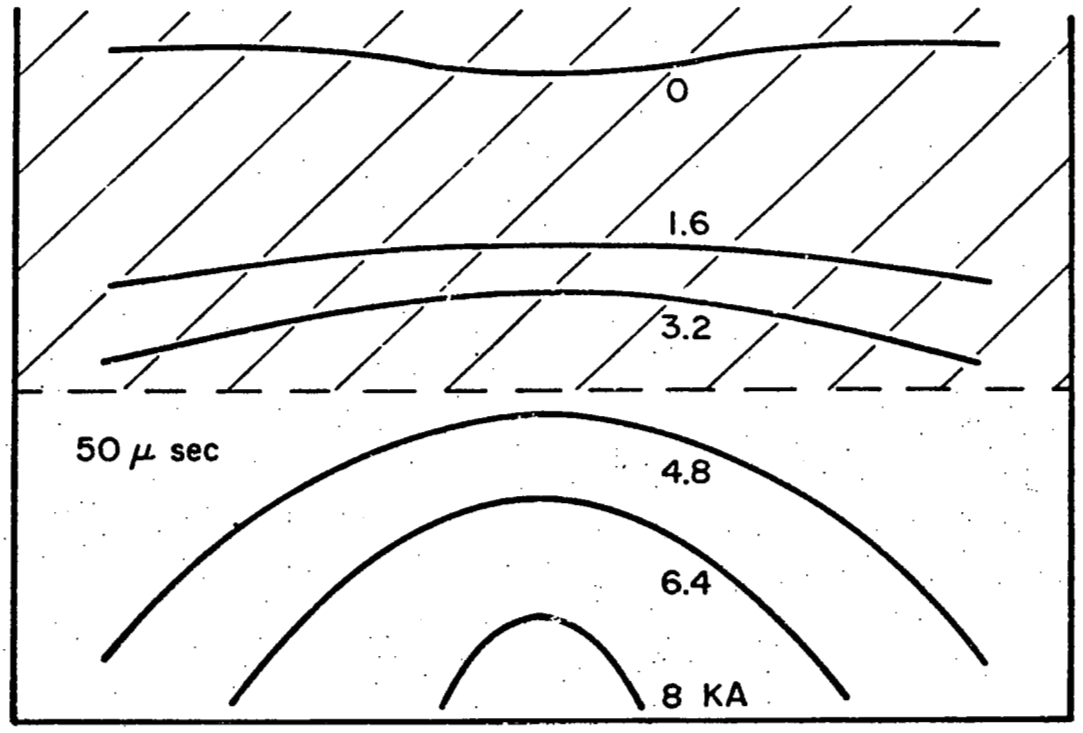

ENCLOSED CURRENT CONTOURS
FOR 10/250 DISCHARGE BETWEEN 2" ELECTRODES

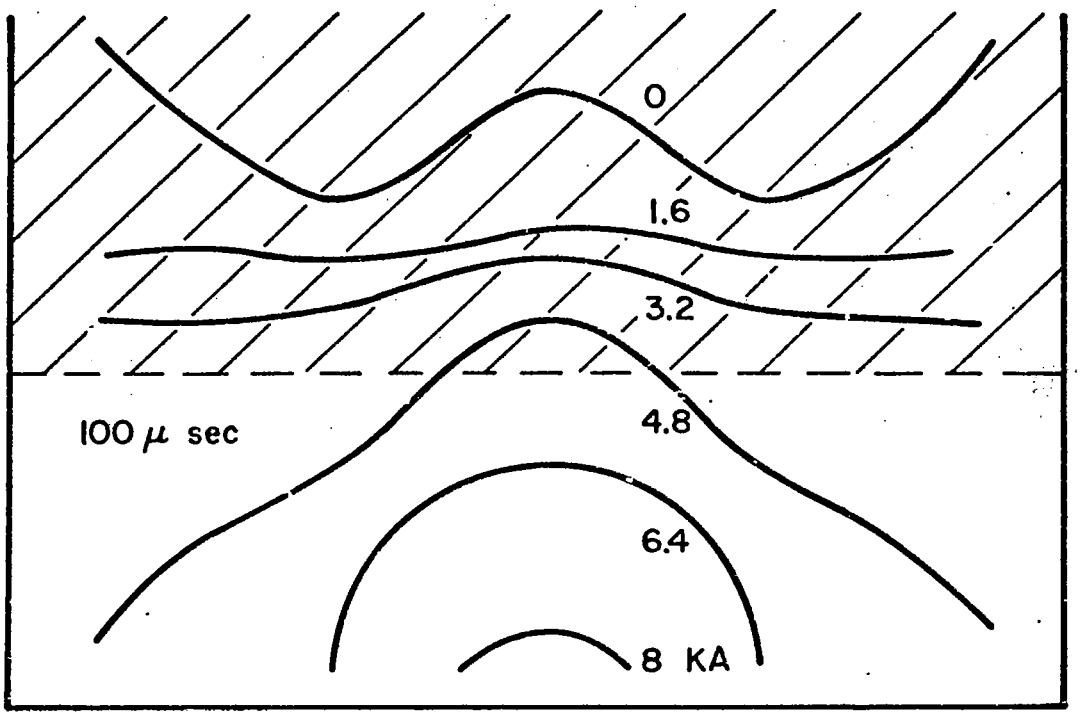

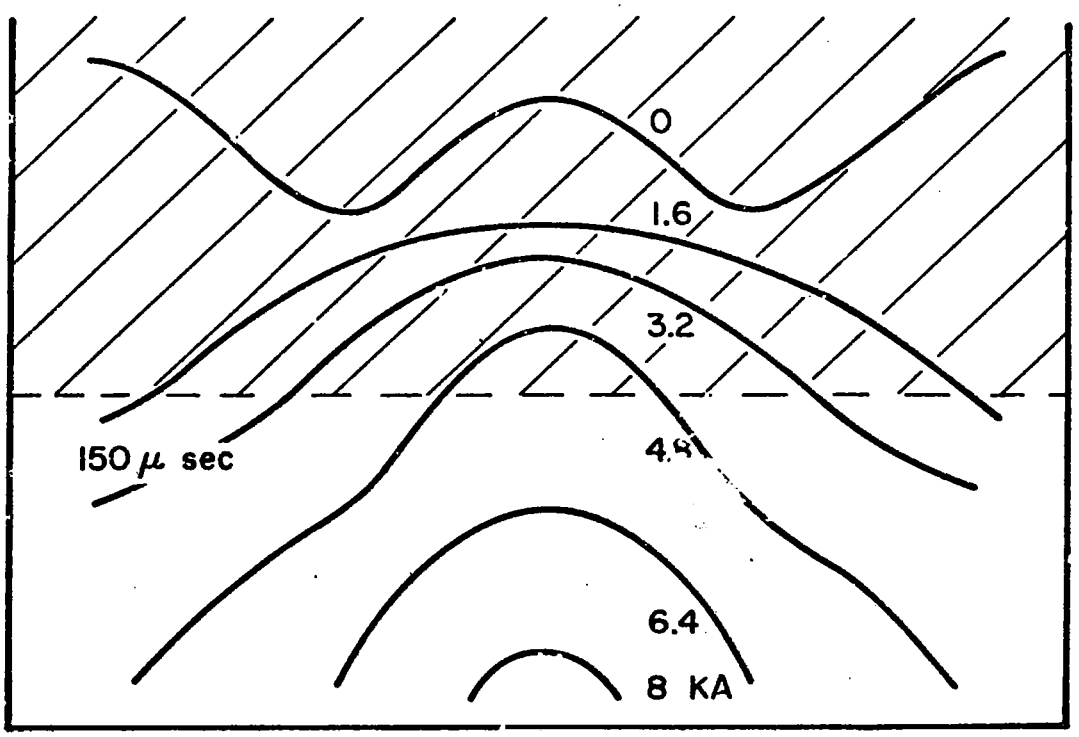

ENCLOSED CURRENT CONTOURS
FOR 10/250 DISCHARGE BETWEEN 2" ELECTRODES

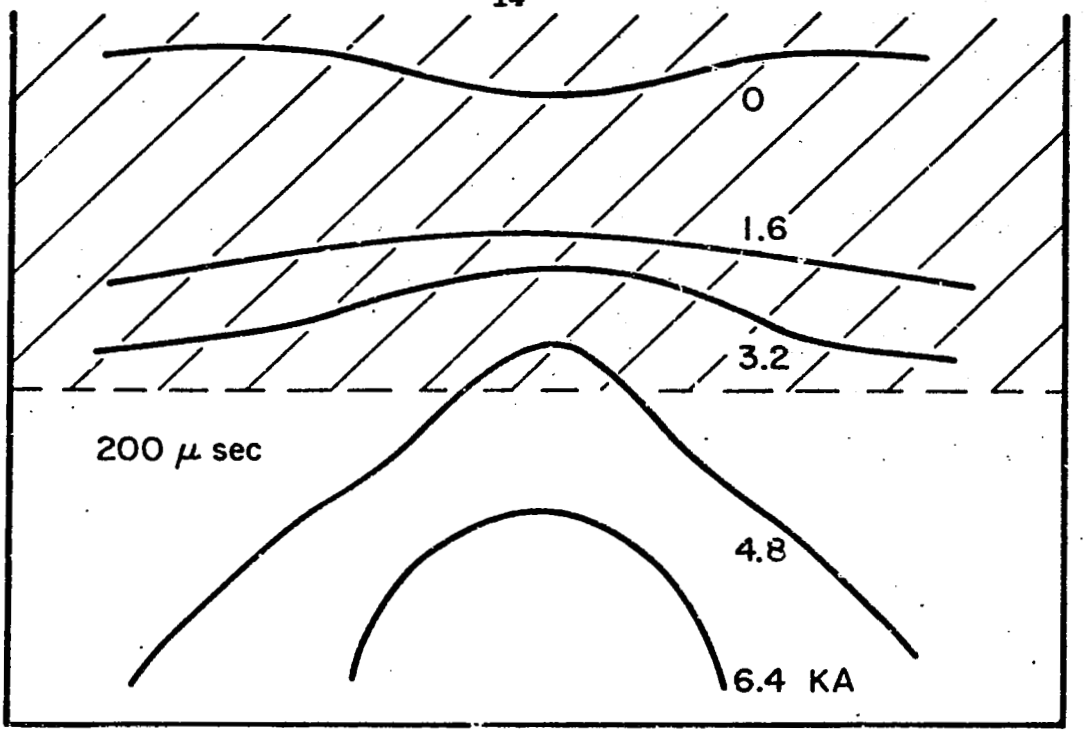

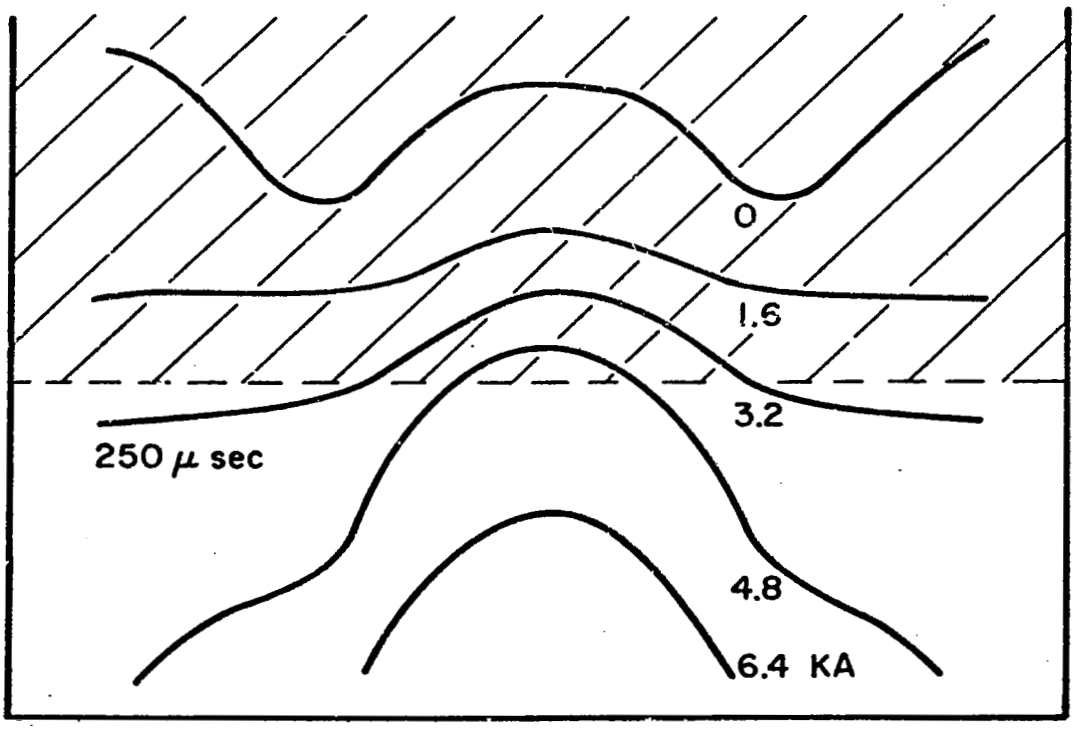

ENCLOSED CURRENT CONTOURS
FOR 10/250 DISCHARGE BETWEEN 2" ELECTRODES

where discrete current sheets arise near the minimum inductance configuration. The difference is probably attributable to the relatively long rise time of the long pulse, which predicates a skin effect comparable with the chamber dimensions.

Observations of electrode pitting and deposition on the insulation adjacent to the electrode also support the above picture. Electrode pitting is most severe in the central region of the channel and falls off nearer the walls as do burn marks on the insulation, but in no case is a discrete arc column or spoke indicated.

To ascertain whether the "fresh" gas which, based on the voltage measurements, appears to be feeding the discharge is accelerated by the current zone, a small 15° half-angle wedge was placed 2-1/4" downstream of the metal-to-insulation junction in the hope that luminous bow shocks could be observed. No results were obtained for the 5/500 pulse where the voltage decrements were the most striking, presumably because the luminosity is too weak to be photographed with our present equipment. For the 10/250 case some luminosity was observed in the flow field, but well-defined bow shocks were found at only one combination of orifice sizes to the switch and accelerator chamber, namely a 1/2":1/4" arrangement which provides the maximum mass flow possible with the existing equipment. With other orifice combinations, yielding less mass flow, no shocks were seen. Even in the one visible case, shown in Fig. 8a, the shocks are quite diffuse and suggest that the flow is rarefied. However, the shock angles are nearly those observed with the high current pulses, e.g., 120/20 or 60/40. The shocks can also be found in the flow further downstream (Fig. 8b), although a much faster lens, with less depth of field is needed for this purpose.

Although no shocks are visible for lower mass flow orifice combinations, an interesting new effect is seen in the form of an intensification of the luminous jets extending downstream of the electrode edges as the mass flow decreases.

10/250 PULSE, 2" ELECTRODE LENGTH
0.5" DIA. ORIFICE TO SWITCH
0.25" DIA. ORIFICE TO CHAMBER

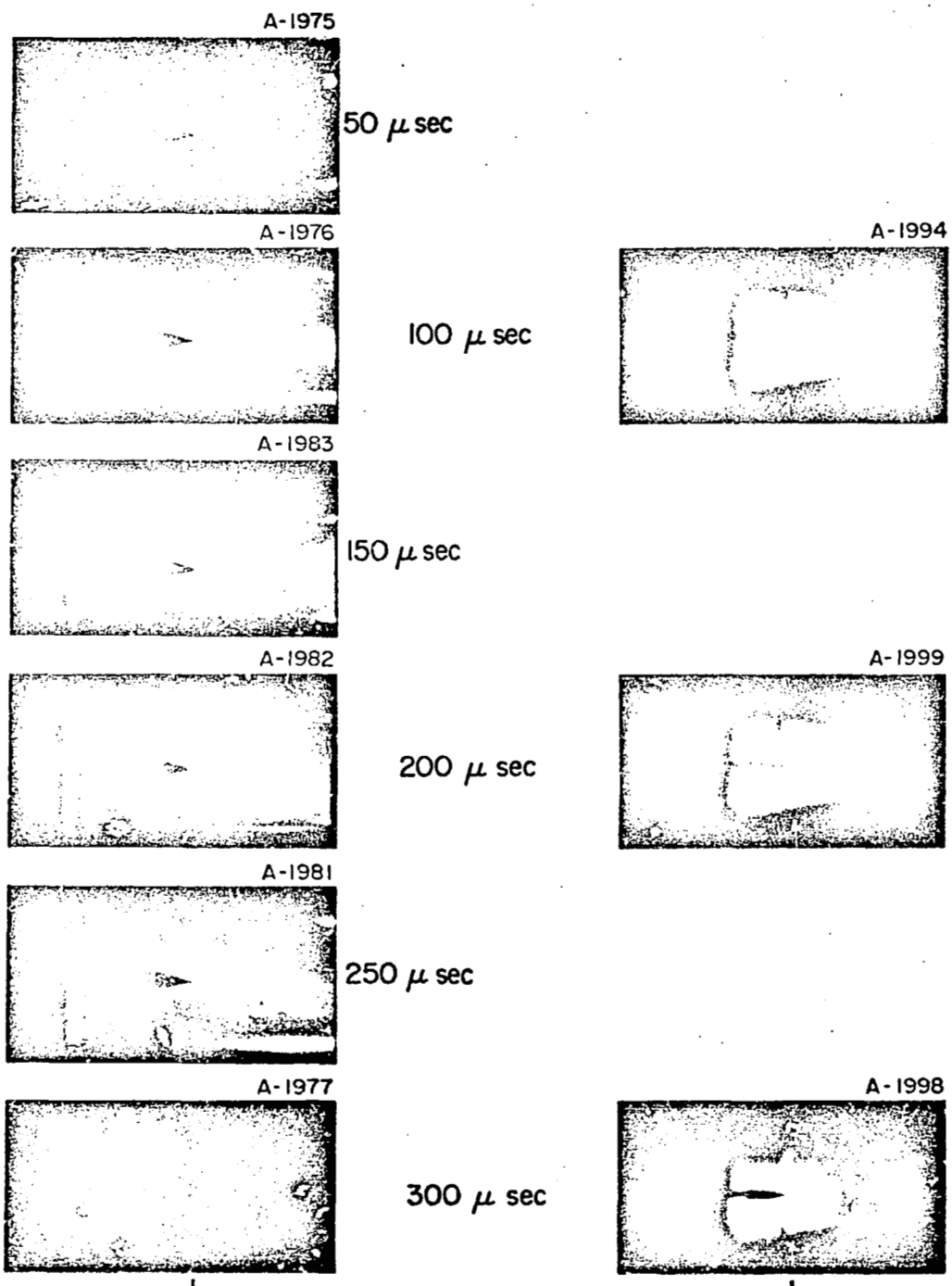

AP 25 P-205 68

FLOW OVER WEDGE DOWNSTREAM OF
ELECTRODE DISCONTINUITY

For example, Fig. 9 shows a sequence of photographs with a 1/2" switch orifice:1/8" chamber orifice; and also with a 1/2":1/16" combination, which when compared with each other, and with the 1/2":1/4" sequence of Fig. 8, illustrate this electrode jet effect clearly. One may speculate that these jets consist of electrode material vaporized by the arc in lieu of an adequate external mass supply. Spectroscopic studies are currently in progress to verify or deny this hypothesis.

Figure 10 shows a similar sequence of photographs taken with a higher current, shorter time driving pulse, 20/125, and the 1/2":1/8" orifice combination. Here one sees faint initiation shocks on the wedge at 40 and 60 μsec, but no shocks thereafter. Presumably the initiation burst is just dense enough for the faint wave structure to be visible, but the mass flow rate at later times is too low and rarefied for the shocks to be noticeable.

The shock tube system has just recently been modified in several ways to achieve much higher mass flows into the accelerator. On the basis of preliminary experiments with these systems, it appears possible to pass through a condition of adequate mass flow, to a condition of mass overload of the given discharge pattern. Specifically, as mass flow is increased, the bow shocks on the downstream airfoil are first observed to intensify in luminosity, and then to weaken and eventually to disappear entirely. By such studies, it is hoped that an optimum quasi-steady operating condition can be located, at which condition detailed interior diagnostics will be performed in an attempt to learn more about the acceleration processes in the discharge.

10/250 PULSE, 2" ELECTRODE LENGTH

0.5" DIA. ORIFICE TO SWITCH
0.125" DIA. ORIFICE TO CHAMBER

A-1968

50 μ sec

A-1970

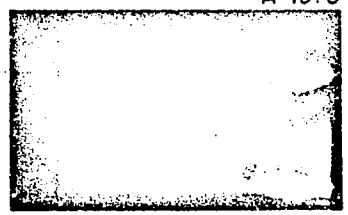

100 μ sec

A-1967

200 μ sec

A-1969

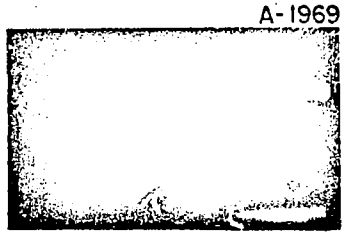

300 μ sec

2.3"

0.5" DIA. ORIFICE TO SWITCH
0.063" DIA. ORIFICE TO CHAMBER

A-1971

50 μ sec

A-1973

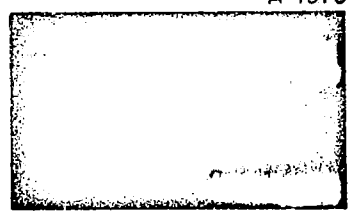

100 μ sec

A-1974

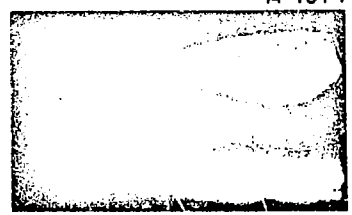

200 μ sec

2.3"

FIGURE 9

FLOW OVER WEDGE 2.3" DOWNSTREAM OF ELECTRODE DISCONTINUITY

20/125 PULSE, 2" ELECTRODE LENGTH
0.5" DIA. ORIFICE TO SWITCH.
0.125" DIA. ORIFICE TO CHAMBER

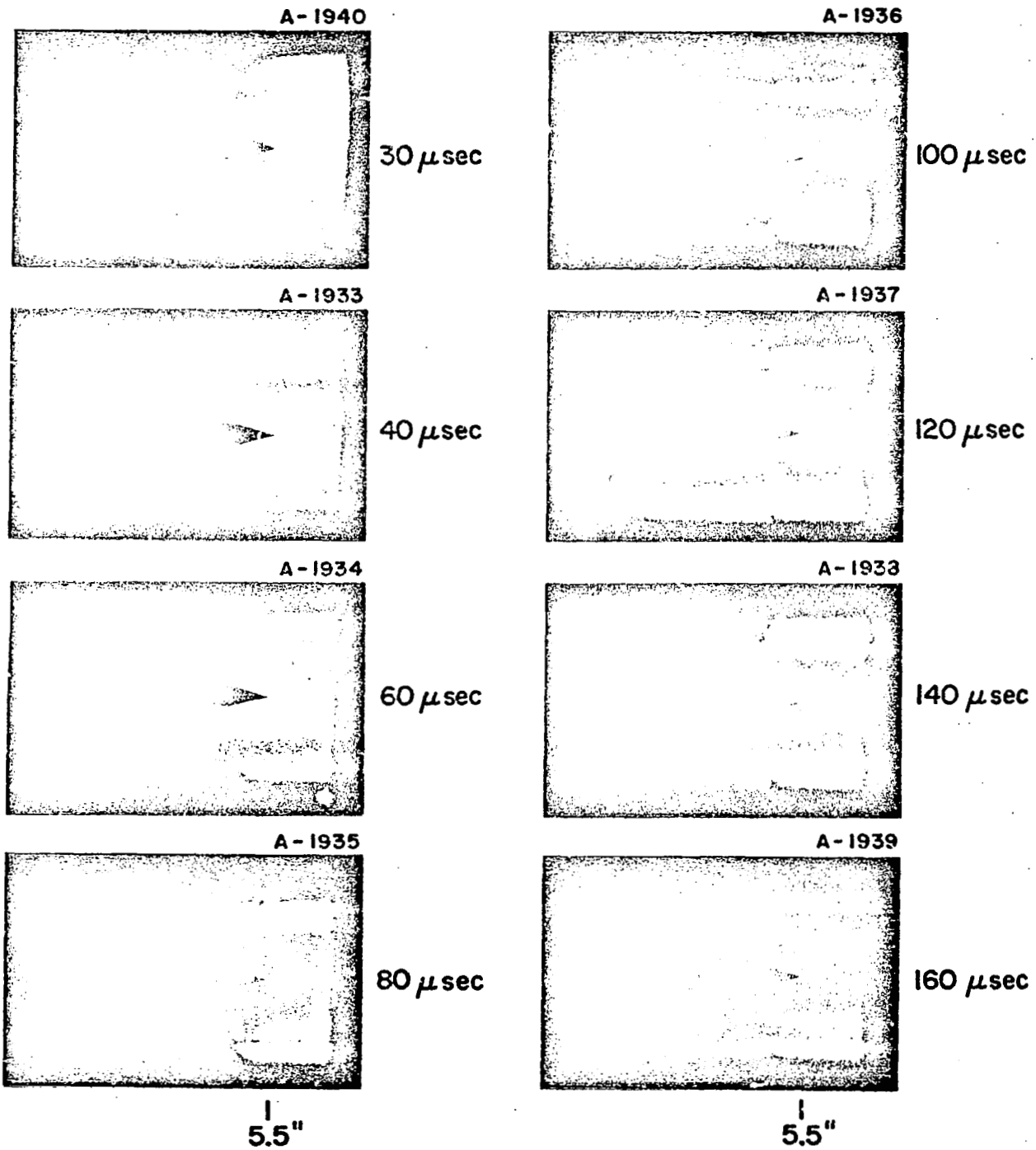

FLOW OVER WEDGE 5.5" DOWNSTREAM OF ELECTRODE DISCONTINUITY

FIGURE 10

III. MPD ARC SIMULATION (Clark)

The most recent reports [48,51] have discussed the modification of the electrode geometry and gas injection system of the previous pinch-orifice configuration in order to produce a plasma accelerator capable of simulating a steady-state magnetoplasmadynamic arcjet on a quasi-steady basis. The resulting ability to perform exhaust plume diagnostics at power levels inaccessible to steady-state experiments and at back pressures duplicating a space environment enables careful examination of the gas acceleration mechanisms, current conduction patterns, and electrode phenomena of high power density, self-field arcs. In addition, the ability to operate a pulsed plasma thruster in a stabilized mode for times considerably longer than the initial "snowplowing" phase bears on the problem of determining the optimum pulse length for combining the advantages of high power plasma acceleration with modest average power consumption.

As has been pointed out previously, proper quasi-steady operation must include stabilization of the mass flow pattern to a steady level in an operating range appropriate to the self-field thrust level, as well as stabilization of the current pattern and electrode processes to regular, effective situations. The latter were rather easily achieved; the gasdynamic stabilization has proven more difficult, and the preceding report dealt almost entirely with this aspect of the problem. In brief, a shock tube injection system was described in which a shock wave reflected off the end wall of the shock tube, generating a high pressure reservoir of gas which drove mass into the electrode region. This constant-pressure reservoir lasted for a time sufficiently long to enable a steady pressure distribution to be established in the electrode region and for the flattop current pulse to be completed. Argon was bled into the driven section of the

shock tube before diaphragm rupture at a sufficient rate to maintain that pressure in the continuum range ($\approx$ 1 mm Hg), while the leakage of the flow through the injection ports into the arc chamber was kept tolerable. The shock wave resulting from rupturing the diaphragm was thus well defined and acted like a valve with an opening time of less than 2 μsec. Details of the shock tube–arc chamber interface are repeated in Fig. 11. The injection ports and shock tube operating conditions were adjusted so that the capacitor bank self-triggered when the pressure in the electrode region reached its plateau value.

The calibration of such a mass injection system was performed within a framework of characteristic times which, since they will be referred to later, are again defined in Fig. 12. Note that one additional time, τ_D , the time from mass flow initiation until current initiation, has been included. The other characteristic times for the gasdynamic system as defined earlier are:

τ_R = the time required for the mass flow rate to reach its steady value

τ_M = the interval over which the mass flow rate is constant

τ_A = the time required for a steady pressure to be reached in the arc chamber after the mass flow rate has become constant

in terms of which the principle requirements of the gas injection system can be stated:

$\tau_R < \tau_M$ so that during τ_R the pressure distribution in the vacuum tank does not increase enough to compromise the space environment requirement

$(\tau_M - \tau_A) > \tau_I$ (where τ_I = the duration of the flattop current pulse), i.e., the current pulse should only occur after a steady arc chamber pressure has been reached and before the mass flow rate departs from its constant value.

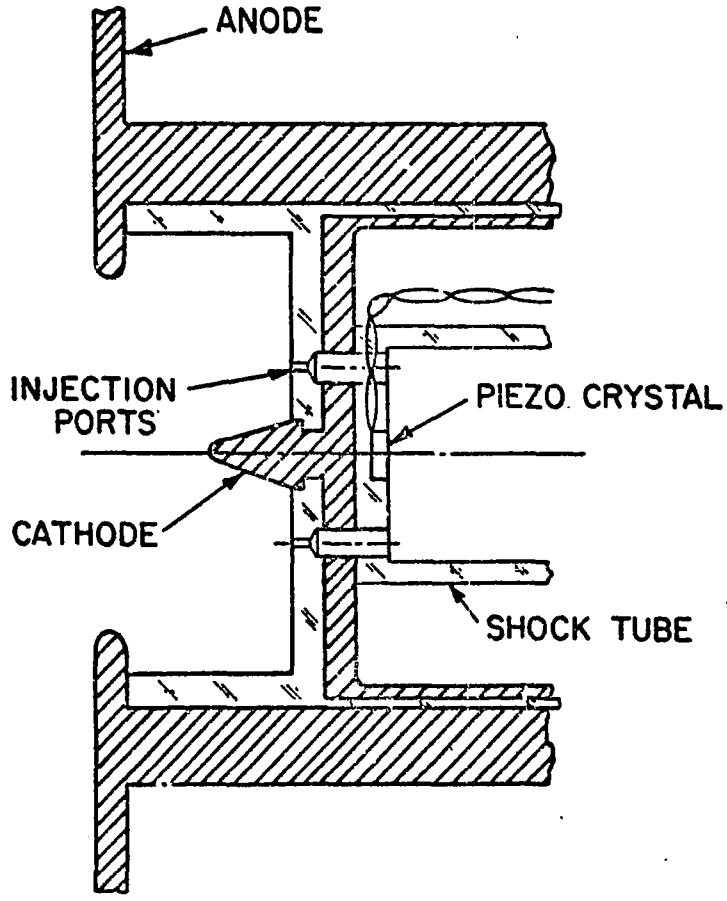

CROSS SECTION OF MPD ARC SIMULATOR

FIGURE 11

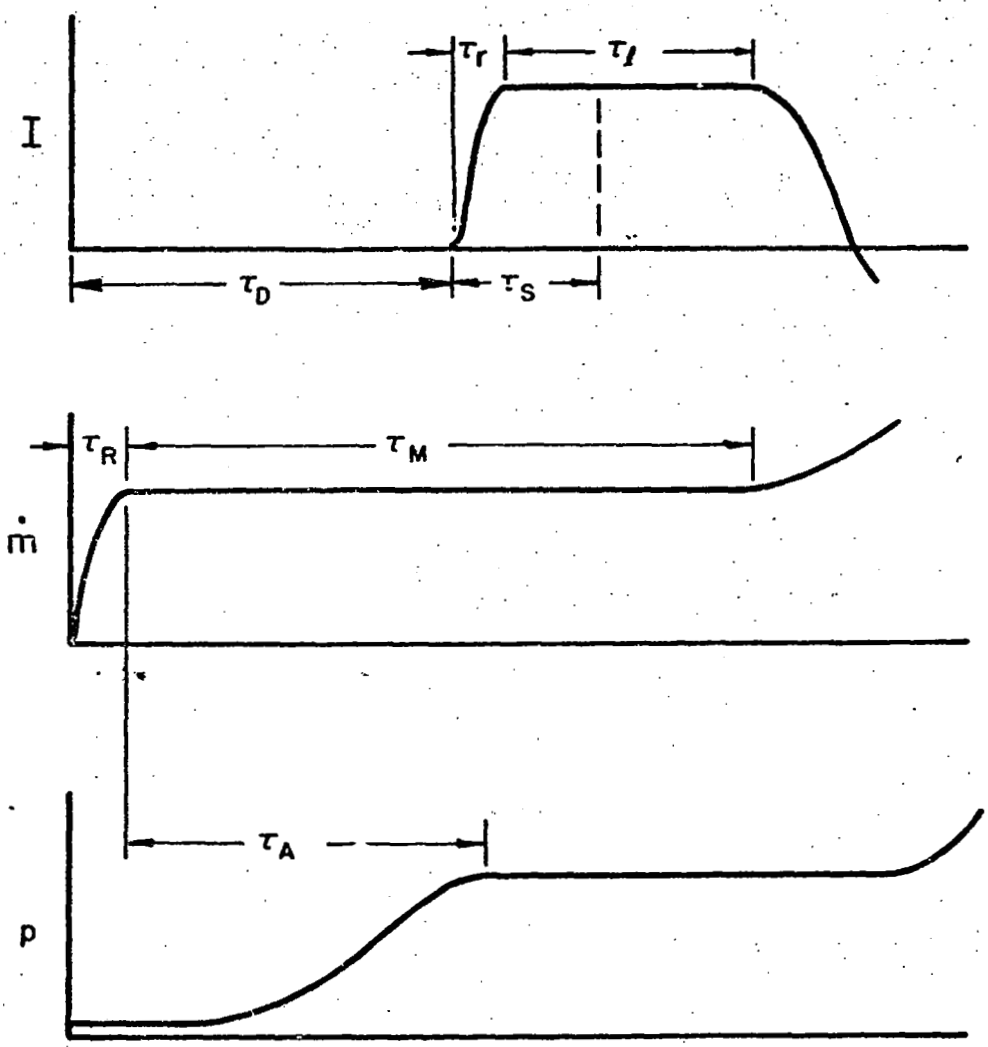

CHARACTERISTIC TIMES FOR CURRENT PULSE AND MASS FLOW

FIGURE 12

Using the experimental arrangement just described, magnetic field measurements and voltage signatures were recorded for currents covering the range from 4,000 to 120,000 amps using aluminum, molybdenum, and tungsten cathodes. In addition, Kerr-cell photographs were taken from a perspective angle for the 120,000 amp x 20 μsec amp pulse. These photographs, samples of which appear in Fig. 13, show rapid development of the exhaust plume into an azimuthally symmetric pattern distinctly confined near the cathode tip by the strong self-magnetic field. These data were acquired for a mass flow rate of about 0.05 gm/sec and a local pressure in the electrode chamber of about 25 μ at the time of breakdown.

However, the above data must be considered preliminary for the following two reasons. First, the delay time, τ_D, between the start of the shocked gas flow into the arc chamber and the onset of the self-triggered current pulse was irreproducible for all values of initial driven section pressure tried. This irreproducibility was of the order of $\pm$ 1 msec whereas the tolerable error dictated by the known values of τ_M, τ_A, and τ_f is $\pm$ 0.1 msec. Since the gas injection characteristics have been shown to be reproducible (as shown in Fig. 14 which is a triple overlay of the reservoir pressure time variation at the end of the shock tube), such a large variation of self-triggered breakdown time strongly suggests that the breakdown characteristic may be changing on a shot-to-shot basis. This may, in turn, be due to the intense heating and observed local melting of the cathode which causes small changes in surface texture and shape, thereby altering the breakdown pressure for the macroscopic electrode geometry. Evidence that the breakdown mechanism itself may vary from shot-to-shot is the observed tendency for the breakdown occasionally to begin with a glow discharge for a second or more before making the transition to a low-voltage, high-current sheet. This may also imply that the current initiation location, which magnetic probes have shown to be at the rear of the cathode cone for this configuration,

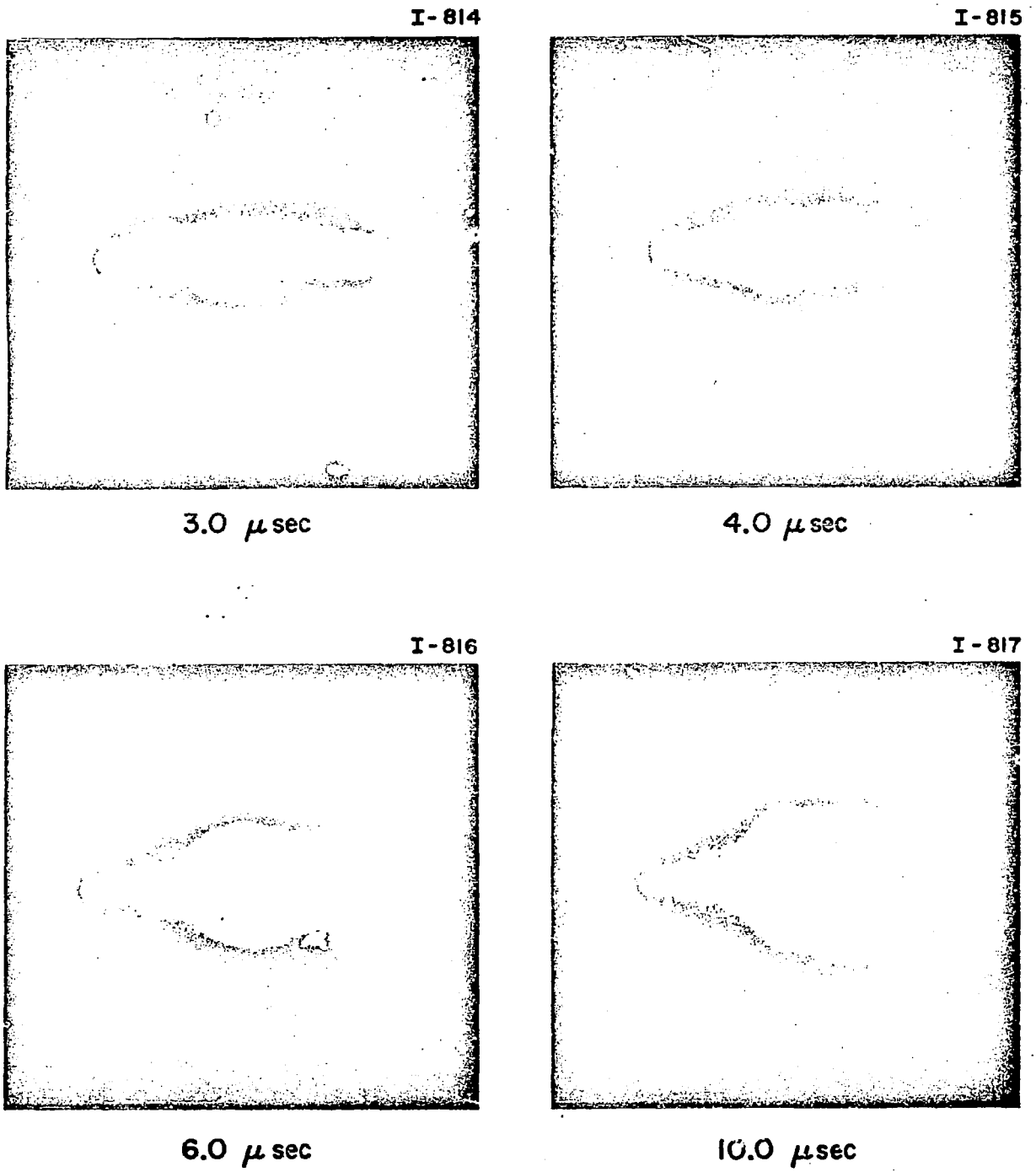

LUMINOUS PATTERNS OF MPD ARC SIMULATOR

FIGURE 13

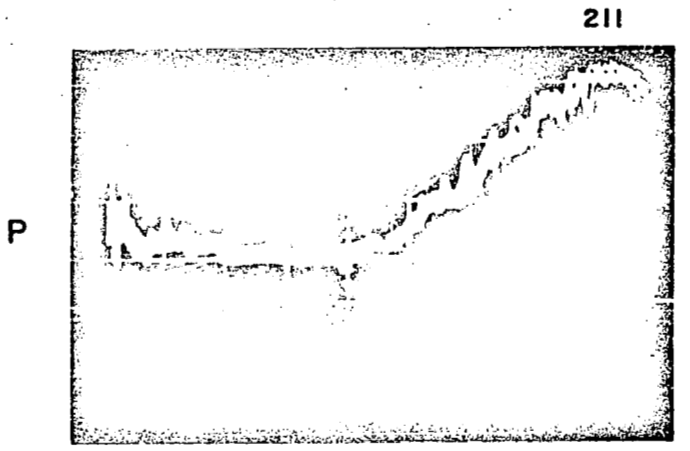

PIEZOELECTRIC PRESSURE RECORD
AT END OF SHOCK TUBE

FIGURE 14

is too close to the final current conduction region so that the severe arc heating may cause changes in the particular microstructural properties of the electrode surfaces which affect the breakdown process.

The second reason that the initial electrodynamic results must be considered preliminary is the inadequacy of the mass flow rate. The analysis in the previous report showed that mass flow rates from 0.002 to 0.040 gm/sec can be delivered to the arc chamber by the shock tube reservoir during its constant pressure phase behind the reflected shock. However, the required mass flow rate for propulsion purposes must conform to the thrusting capability of the self-field pattern for the desired specific impulse. For a purely self-magnetic thruster with a uniform cathode current distribution, the electromagnetic thrust generated has been shown to be [53]

$$F = \frac{\mu J^2}{4\pi}\left[\ell n\left(\frac{r_a}{r_c}\right) + \frac{3}{4}\right] \qquad (3\text{-}1)$$

where $\mu = 4\pi \times 10^{-7}$ (mks)
J = total current
r_a = effective anode radius of attachment
r_c = effective cathode radius of attachment

Since this thrust must be equal to the momentum increase of the working fluid, the appropriate mass flow rate can then be found for any specified exhaust velocity or specific impulse. Such a set of calculations is shown in Fig. 15 for the anode-to-cathode radius ratio of 30 indicated by our current density maps. It should be noted that for a current of 4,000 amps, the lowest value readily available from the capacitor bank at present, and for a specific impulse of 2,000 sec with argon, a mass flow rate of 0.35 gm/sec is dictated with higher currents requiring even higher values. Thus, for the 120,000 amp pulse used in the early experiments, the discharge was probably starved for mass which may have contributed to the electrode material erosion.

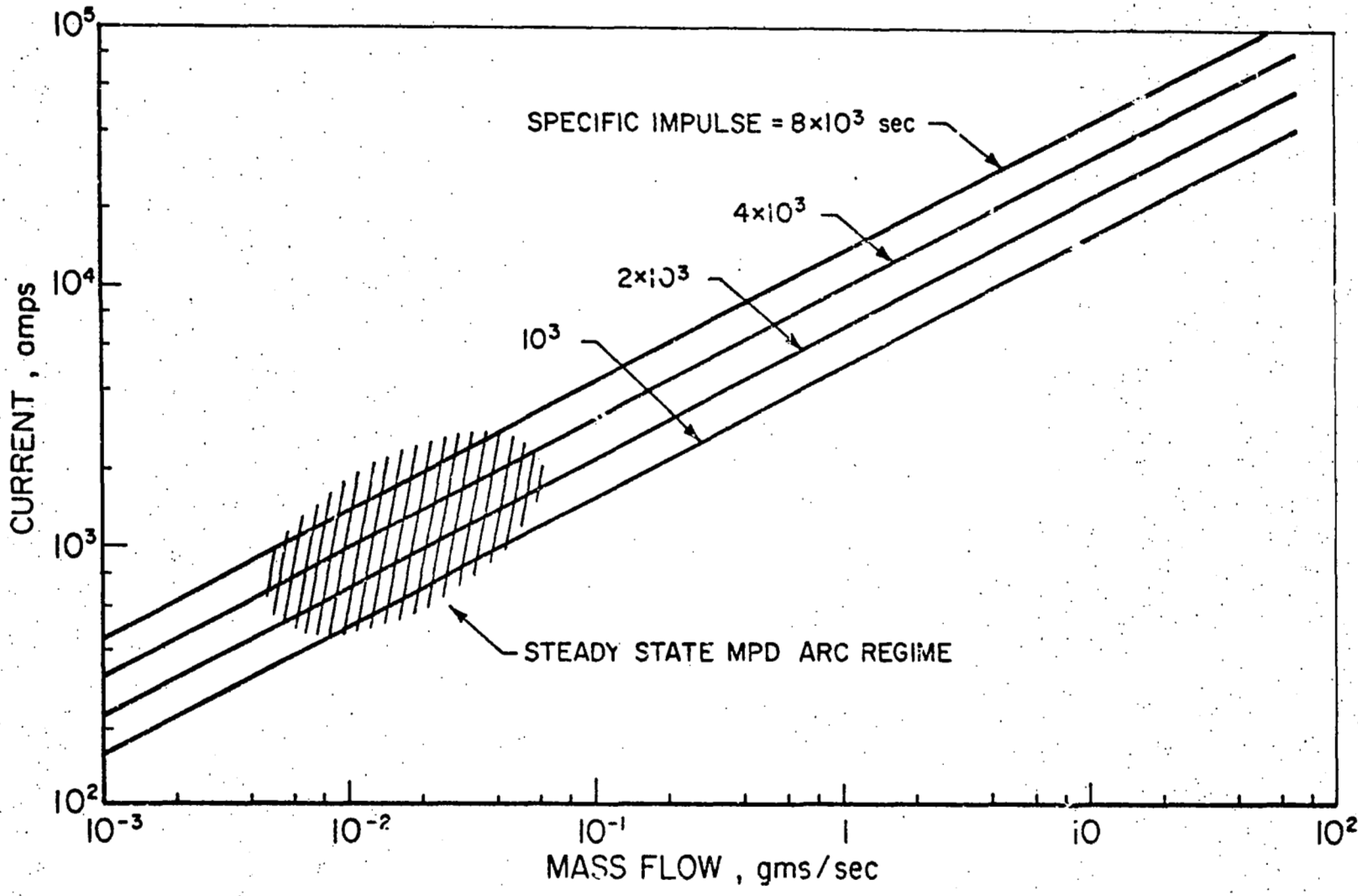

MASS FLOW FOR PURELY ELECTROMAGNETIC THRUST

In order for the appropriate mass flow rate to be delivered by the reservoir of gas behind the reflected shock, large initial pressures are required in the shock tube driven section, and the diameter of the injection holes must be substantially increased. However, attempted operation in this regime would result in a greatly increased leakage through the injection ports and corresponding increase in the back pressure in the exhaust tank to the point where any attempt to duplicate a space environment in the exhaust plume region would be negated.

This problem of insufficient mass flow rate has been resolved by operating the shock tube in an entirely different domain than described above. This new approach allows abrupt injection of large mass flow rates into the arc chamber, raising its pressure to a level where a separate gas-triggered switch is needed to delay the chamber breakdown time until a steady injection rate has been reached. Since the use of such a gas switch is a familiar and reproducible operation in the laboratory, the other problem of irreproducible delay time between gas injection and self-triggering of the capacitor bank is also resolved by the new configuration described below.

In Fig. 14, which shows the typical early time piezocrystal response at the end of the shock tube, the magnitude of the pressure plateau is 20 -- 40 mm Hg, depending on the initial pressure in the driven section. By putting a large resistor in series with the pressure sensing circuit, the effective time constant can be increased so that accurate pressure readings can be obtained for times of the order of tens of milliseconds. Figure 16a shows such a long time piezocrystal response for an initial pressure in the driven section of 1 mm Hg. Note that the total time depicted in Fig. 14 is now compressed to 2 mm (one small division) on this photograph and that the pressure level after 10 msec is nearly constant and at least an order of magnitude greater than the earlier plateau shown in Fig. 14. This trace is

5 m sec/DIV

325

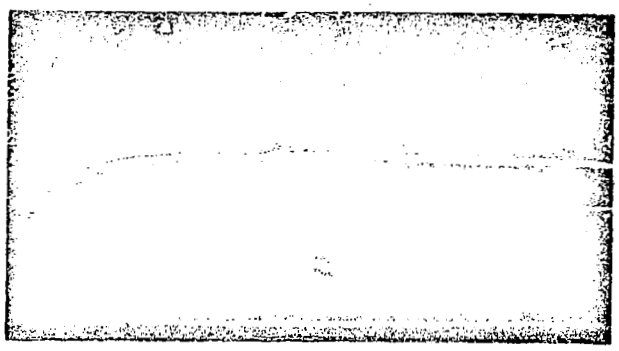

(a) P_i = 1 mm

324

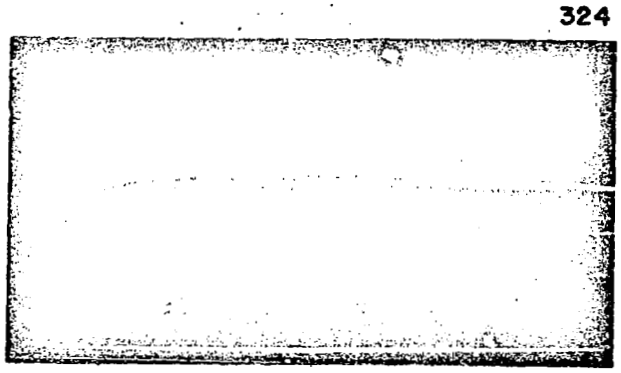

(b) $P_i < 10\,\mu$

AP 25 P-208 GD

LONG TIME PIEZO ELECTRIC PRESSURE RECORD AT END OF SHOCK TUBE

FIGURE 16

not unexpected since, for large pressure ratios across the diaphragm, the initial rarefaction (which propagates downstream as well as upstream) and the reflected rarefaction off the driver end wall dominate the pressure history until the reflected shock wave again returns to the driven section end wall. Thus it is reasonable to expect that even for very low pressures in the driven section (where the mean free path exceeds tube dimensions), the long time profile should appear the same. This is shown to be the case for $p_1 = 10\ \mu$ in Fig. 16b which in comparison with Fig. 16a is only slightly different for the first millisecond. Thus, by setting very low initial pressures in the driven section, the injection holes may be opened up, with negligible leakage flow to the chamber, but a much higher pressure reservoir of gas eventually obtains.

It should be noticed in Fig. 16 that the time required to effectively reach the new plateau is approximately 10 msec. Earlier neutral density measurements with a fast ionization gauge [48] have shown that a steep pressure profile of gas injected into the electrode region propagates outward into the large environmental tank at roughly 1 inch per 100 μsec. Hence, for the present exhaust vessel whose radius is 18", it is a requirement that the arc chamber pressure be stabilized and the current discharge initiated by about 2 msec in order that there be no communication between the discharge and the tank.

Since the onset of the pressure plateau is due to the reflected rarefaction arriving at the downstream end of the shock tube, shortening the driven and driver sections should reduce the time before the plateau is reached. Figure 17 shows the effects of such changes. In Fig. 17a, the piezocrystal response for the initial shock tube configuration is shown (driven section length $\equiv \ell = 7.5'$, driver section length $\equiv L = 2.0'$, and initial driven section pressure $\equiv P_1 < 10\ \mu$). Note that this is just Fig. 16b seen on

32

2 m sec/DIV

323

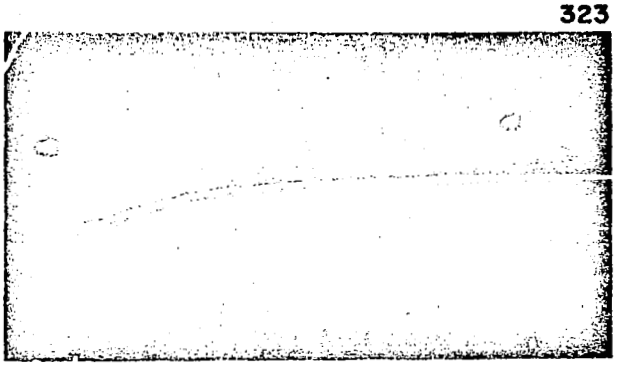

(a) $l = 7.5'$; $L = 2.0'$; $P_1 < 10\ \mu$

312

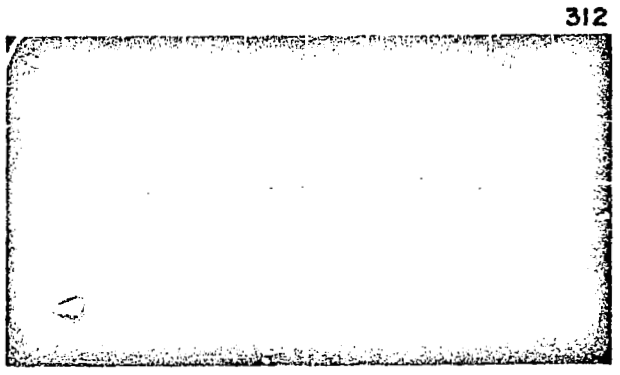

(b) $l = 2.5'$; $L = 2.0'$; $P_1 < 10\ \mu$

332

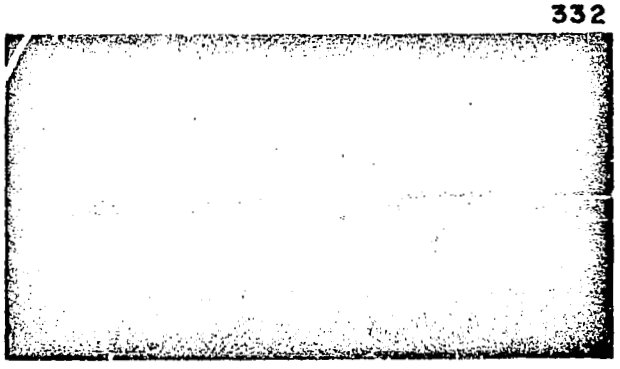

(c) $l = 2.5'$; $0.5'$; $P_1 < 10\ \mu$

AF 25 P-209 GB

EFFECTS OF DRIVEN AND DRIVER SECTION LENGTHS ON PRESSURE HISTORY AT END OF SHOCK TUBE

FIGURE 17

an expanded time scale. Figure 17b shows the effect of shortening the driven section from 7.5' to 2.5' while retaining the original driver section. The rise time to a pressure plateau has decreased from 10 msec down to 4 msec while decreasing the plateau level by approximately 50 percent. On the same time and voltage scales, Fig. 17c shows the effect of retaining the 2.5' shortened driven section while decreasing the driver section length from 2.5' to 0.5'. As expected, the rise time to a plateau has been further reduced accompanied by an additional plateau magnitude reduction. Figure 18 shows this last trace on amplified voltage and time scales and in a negative direction. It is apparent that the reflected rarefaction arrives after approximately 1 msec with the plateau then being constant to within 10 percent for at least an additional 3 msec. Since previous ionization gauge studies [51] have shown that the time constant for the arc chamber to reach a steady pressure for a nearly step input of mass flow rate is about 200 μsec, then the proper function of the gas-triggered discharge switch is to delay the discharge initiation until approximately 1.3 – 1.5 msec after the measurable pressure buildup begins at the end of the shock tube.

The calibrated piezocrystal yields the pressure level of the plateau which, when combined with the appropriate discharge coefficient and reservoir temperature, gives the mass flow rate into the arc chamber for a given injector hole size. For the reasons given above, 200 μsec after this plateau level has been reached, this calculated value will also be the mass flow rate out of the chamber into the environmental tank. Figure 19 shows the achievable mass flow rates for various injector sizes with pressure in the driver section as a parameter. Comparing this with Fig. 15, it is evident that from gasdynamic considerations, the present system is capable of MPD simulation for the current range from 60,000 amp down to less than 1,000 amp, i.e., the complete range down to the steady state MPD arc domain. At present, this mass injection

500 μ sec / DIV

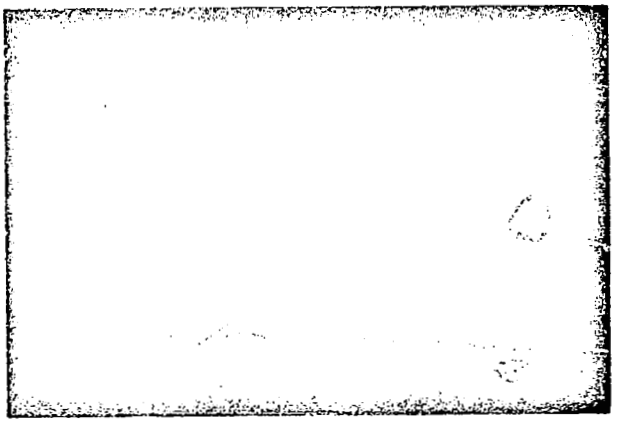

PIEZO ELECTRIC PRESSURE RECORD AT END OF SHOCK TUBE FOR l=2.5'; L= 0.5'; P_1<10 μ

FIGURE 18

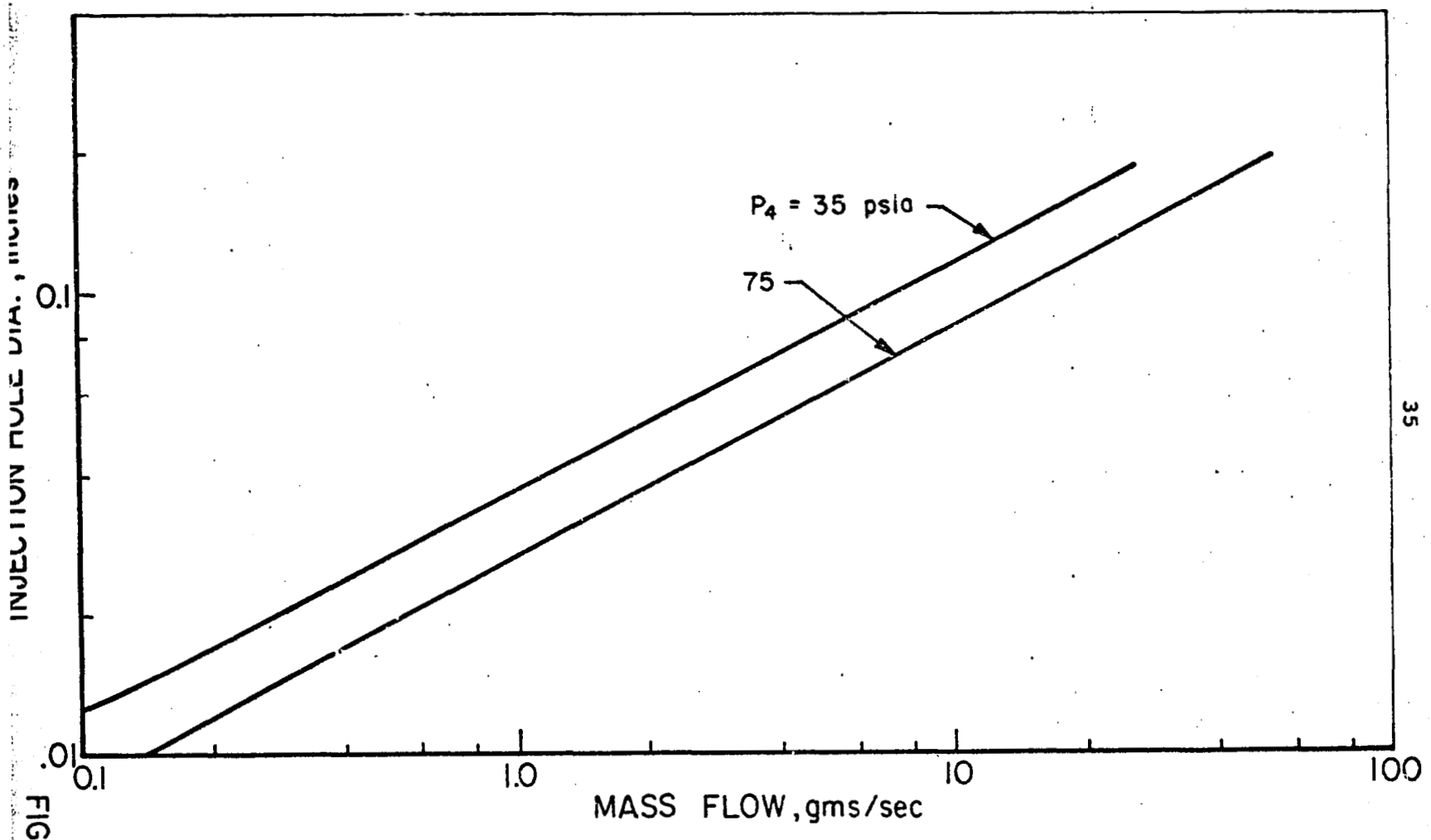

FIGURE 19

CALCULATED MASS FLOW FOR SHOCK TUBE INJECTION ; I = 2.5' ; L = 0.5'.

system provides steady flow rates for times considerably longer than the longest current pulse available with the capacitor bank and the present supply of inductors. As such, it will provide the basis for extension of the simulation program to longer pulses and for the investigation and evaluation of the long pulse mode of operation as an optimum pulsed plasma thruster technique.

The changes in the mass injection system can best be summarized in a table comparing the various characteristics of the old and new configurations:

	OLD	NEW
τ_R	2 μsec	1 msec
τ_M	0.3 – 1.0 msec	3 msec
τ_A	0.2 msec	0.2 msec
τ_D	irreproducible	controlled by switch
Back pressure	$1–5(10^{-3})$ mm Hg	10^{-5} mm Hg
$\dot{m}$	0.002 – 0.040 gm/sec	0.1 – 50 gm/sec

Thus, it appears that increased mass flow rate, longer constant pressure reservoir time, and decreased back pressure without reproducibility problems have been gained at the expense of a longer but tolerable mass flow rise time in going from the self-triggered mode to the externally triggered mode.

The gas-triggered discharge switch necessary to make the transition has been designed and constructed and is now being installed. Briefly, it is a 2" high by 5" diameter cylindrical pinch switch similar to that used in the previous pinch-orifice configuration. However, space limitations behind the arc chamber due to the necessity for the large shock

tube and small injector lengths have dictated that the switch not be coaxial to the discharge chamber but instead be mounted in series with the hot lead off the capacitor bank outside the environmental tank. This new switch and the modified gas injection system will first be tried with a familiar flat cathode configuration as in the pinch-orifice experiments. After proper operation and sequencing of the switch has been verified, the geometry will be altered to one with a shaped cathode for better simulation of the MPD arc.

IV. LONG-PULSE POWER SUPPLY ANALYSIS (Clark, Eckbreth, Wilbur)

In the past several months, experiments in both the parallel-plate geometry and in the quasi-steady coaxial exhaust configuration, for reasons discussed in Secs. II and III, have migrated toward longer pulse times and a consequent decrease in current amplitude. Figure 20, which shows the present capability of the capacitor line in terms of flattop current amplitude vs. half-cycle times, indicates that for pulses of adequate length to insure gasdynamic stabilization, say $>$ 250 μsec, currents are restricted to amplitudes below 10,000 amps. This limitation to lower currents may unnecessarily restrict or prejudice future experimental studies for the following reasons:

1. Since the electromagnetic force scales with the square of the current, low amplitude currents predicate weaker driving forces relative to pressure and viscous forces. Thus, current pulses long enough to allow observation of the complete transition process from a "snowplowing" mode to a "blowing" mode may not provide sufficient current amplitude to display sharply the fundamental features of the transition itself.

2. MPD simulation experiments should be able to investigate arc behavior, acceleration mechanisms, and thrust efficiency over an instantaneous power range from some 100 kw (current $\approx 10^3$ amps) up to about 100 mw (current $\approx 10^5$ amps), i.e., the range from present steady state self-field thrusters up to the optimum levels for primary manned-planetary propulsion.

3. Investigation of the quasi-steady pulse mode as an optimum thrust technique will require arbitrarily long pulses over a wide range of discharge currents.

Numerous schemes are available for providing these

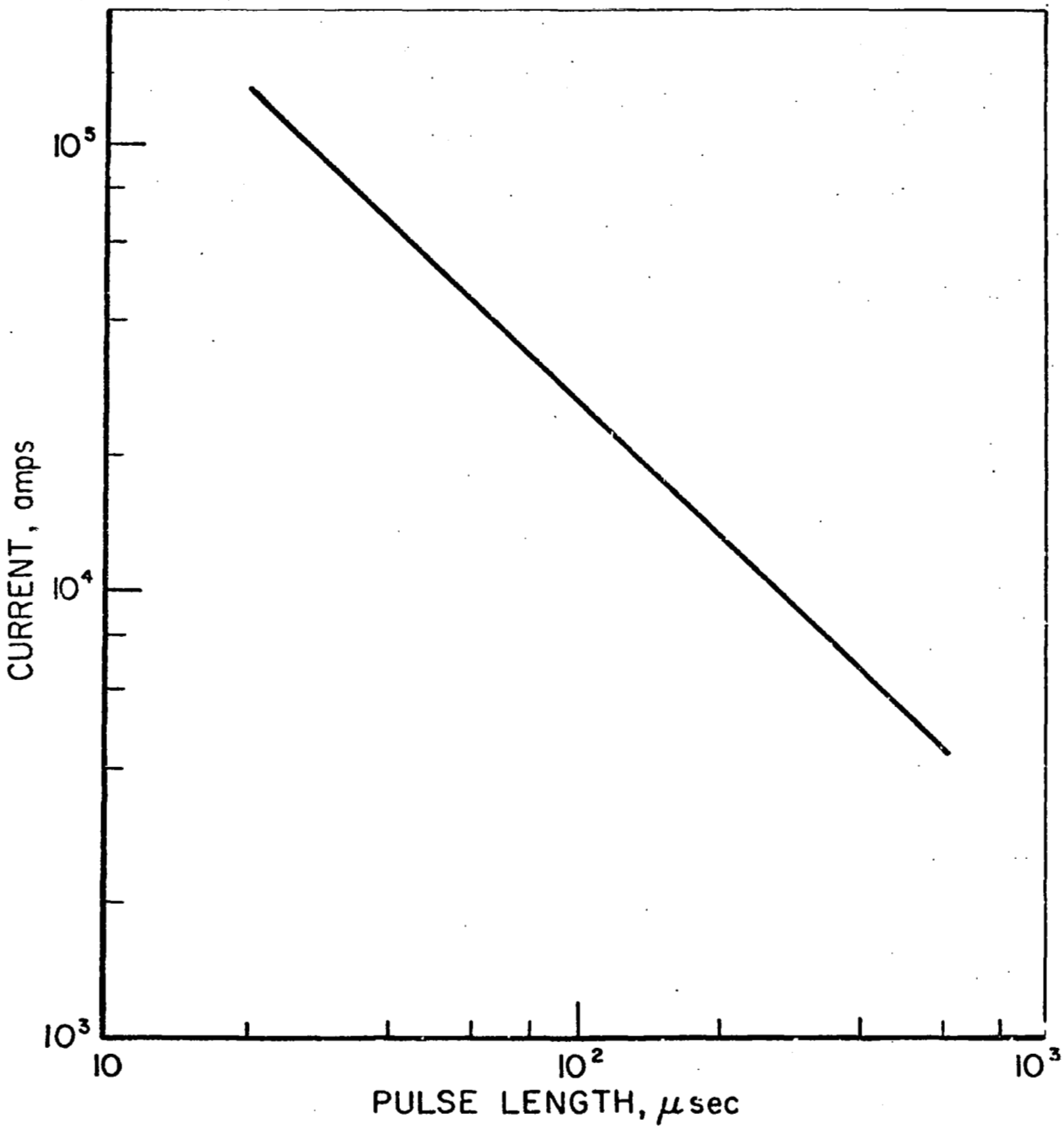

EXISTING CAPACITOR LINE CURRENT PULSE CAPABILITY

AP 25 E 4405 68

FIGURE 20

long duration, high-current pulses, each with its own advantages and disadvantages. For example, simply adding more capacitors is an obvious solution, but space, weight, cost and versatility must be considered carefully before such an approach is taken. Other possible solutions include: a pulse transformer between the capacitor bank and the plasma source which would increase the current for a given length pulse; a large collection of batteries which, by various series and parallel arrangements, would provide a wide spectrum of input power opportunities; an inductive storage facility; and the conversion of kinetic energy stored in rotating machinery into electrical energy by an appropriate generator.

As an initial step toward examining the feasibility of these different techniques and the eventual selection of one, analytical experience gained from related studies has been used to provide a preliminary look at the pulse transformer problem. The effect of a pulse transformer in a circuit consisting of a pulse-forming network and a load such as a stabilized current sheet in a high-current discharge apparatus can be investigated in terms of the following model:

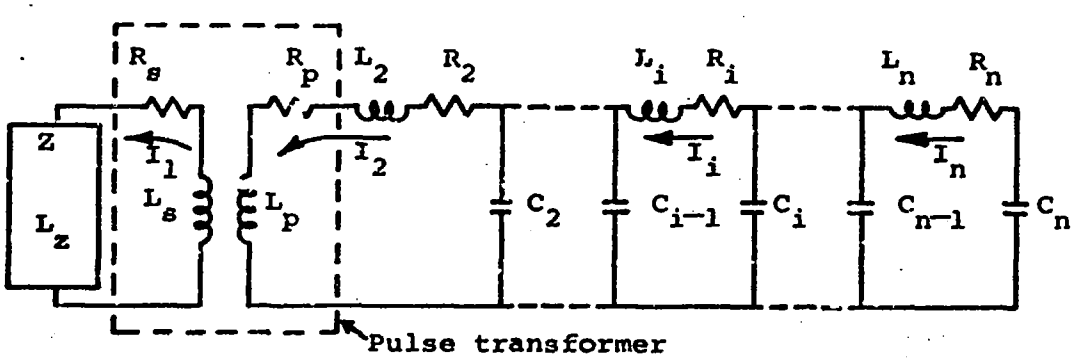

where Z = load impedance (real)

L_z = load inductance

R_s = resistance of the secondary side of the transformer

L_s = self inductance of the secondary side of the transformer

R_p = resistance of the primary side of the transformer

L_p = self inductance of the primary side of the transformer

R_2 = resistance of the first inductor in the pulse-forming network (includes switch resistance)

L_2 = inductance of the first inductor in the network (includes switch inductance)

C_2 = capacitance of the first capacitor in the network

R_i = resistance of the ith element of the network

L_i = inductance of the ith element of the network

C_i = capacitance of the ith element of the network

For illustration, this model is applied to the parallel-plate accelerator where the values of the load impedance and the load inductance are determined from the dynamics of the current sheet as expressed by the snowplow equation. After the current sheet reaches a prescribed stabilization position, experimentally observed impedances, Z, are specified as a function of the current flowing through the load.

The basic equations governing the above system are:

for the 1st loop

$$M \frac{dI_2}{dt} = (L_s + L_z) \frac{dI_1}{dt} + I_1(Z + R_s) \qquad (4\text{-}1)$$

for the 2nd loop

$$M \frac{dI_1}{dt} = -\frac{Q_2}{C_2} + I_2(R_2 + R_p) + (L_2 + L_p) \frac{dI_2}{dt} \qquad (4\text{-}2)$$

and

$$\frac{dQ_2}{dt} = -I_2 + I_3 \qquad (4\text{-}3)$$

for the ith loop

$$L_i \frac{dI_i}{dt} = \frac{Q_i}{C_i} - \frac{Q_{i-1}}{C_{i-1}} - R_i I_i \qquad (4\text{-}4)$$

and

$$\frac{dQ_i}{dt} = -I_i + I_{i+1} \qquad (4\text{-}5)$$

where Q_i = charge on capacitor C_i

M = mutual inductance of the transformer = $k\sqrt{L_s L_p}$

where k is the transformer coupling coefficient, and essentially expresses the degree to which magnetic flux generated by one coil of the transformer is linked to the other coil. k can be as high as 0.98 for an iron core transformer and will be somewhat lower for an air core unit.

This system of 2n-1 ordinary differential equations is combined and solved on the IBM 7094 computer using the Runge-Kutta technique. Several preliminary computer runs have been made using the existing pulse-forming network in a configuration which provides a pulse approximately 600 μsec long. The effect of the transformer coupling coefficient and secondary self inductance for a transformer turns ratio of 10 is illustrated in the current pulses shown in Fig. 21.

In comparing this figure with Fig. 20, it is seen that the computer solution predicts a discharge current about seven times greater than the amount experimentally supplied by the capacitor bank for the same length pulse, i.e., the current delivered to the primary of the 10/1 transformer is less than the value that would be delivered to the discharge if no transformer were in the circuit. This feature is due to the initial bank voltage being fixed and the total impedance in the primary circuit being greater with the transformer than without it. It is also obvious from the figure that k plays a very important role in determining the pulse

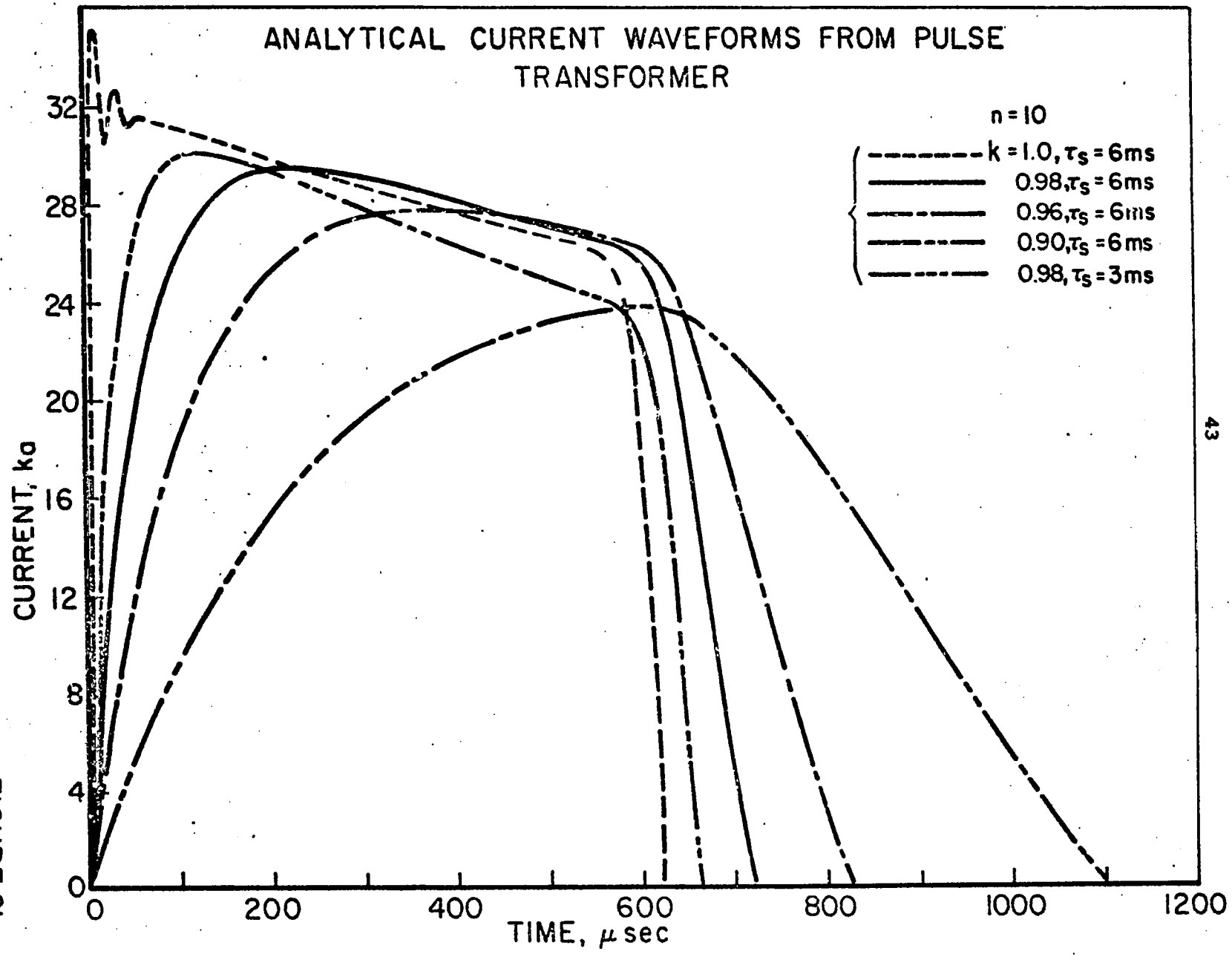
ANALYTICAL CURRENT WAVEFORMS FROM PULSE TRANSFORMER
n = 10
k = 1.0, τs = 6ms
0.98, τs = 6ms
0.96, τs = 6ms
0.90, τs = 6ms
0.98, τs = 3ms
CURRENT, ka
0
4
8
12
16
20
24
28
32
0
200
400
600
800
1000
1200
TIME, μ sec

FIGURE 21

rise time and protraction. Finally, it should be noted that there is a droop in the flattop portion of the current pulse, regardless of the value of k. This droop is caused by the decay time constant ($\tau_s \approx \frac{I_s}{Z}$) in the secondary circuit which is 6 msec for all cases studied except one where it is half that value.

A series of preliminary investigation like that above serves to provide insight into overall dependencies of key parameters and as such provide useful guidelines for subsequent investigation. In the future, this initial study phase will be expanded and other candidate power supplies similarly examined in order to select the method most compatible with design requirements.

V. OPTIMUM ENERGY TRANSFER FROM LOW IMPEDANCE PULSE NETWORKS TO ACCELERATING PLASMAS (Wilbur)

This effort is intended to give a better understanding of the conditions under which a high energy power supply, such as a capacitor bank or transmission line, will transfer its energy to an accelerating plasma with optimum efficiency. The work consists of four related studies: (1) design and development of low impedance capacitors suitable for simple assembly into pulse line configurations; (2) experimental determination of the detailed capacitor characteristics; (3) experimental investigation of the conditions for optimum transfer of energy; and (4) development of analytical techniques to support the experimental studies.

The first phase of the capacitor design and development was completed with delivery of 12 capacitor units from the manufacturer (Corson Electric Manufacturing Corp.). In order to determine the capacitor characteristics under operational conditions, the units have been arranged in a simple ladder network configuration and discharged through a resistance equal to the characteristic impedance of the network. The signatures of voltage across, and current through, the resistance are then used to synthesize the circuit which produced them. In previous semi-annual reports [47,48] data presented were based on the assumption that the capacitor units were sections of transmission line and the equations describing a transmission line were used in the mathematical description of the circuit. Recently it was found that while this was a qualitatively instructive approach, a more accurate description of the driving network could be formulated in terms of the LC ladder network shown schematically on the following page.

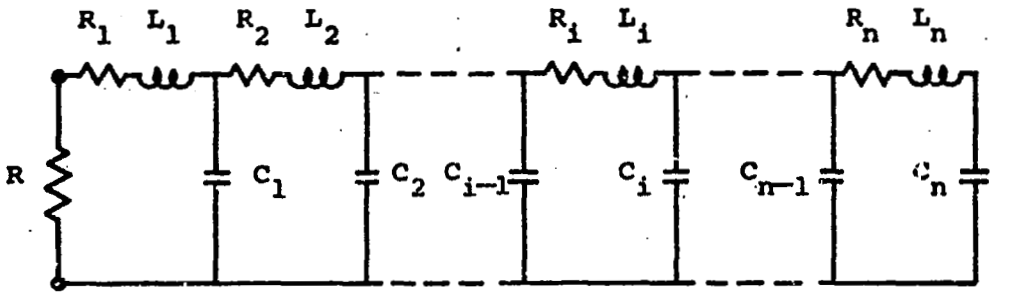

where R_i = resistance of the ith connector
L_i = inductance of the ith connector
C_i = capacitance of the ith capacitor unit
R = resistive load
R_i , L_i include the switch resistance and inductance

The 2n ordinary differential equations describing the above network can be solved simultaneously on the computer to yield the current and voltage waveforms desired for comparison with the experimental signatures. Experimental results taken with the capacitors in various arrangements agree best with the theoretical model when the average capacitor has a negligible resistance, an inductance of 7.5 nanohenries, and a capacitance of 6.35 microfarads, which are acceptably close to the separately measured values of 7.0 nanohenries and 6.5 μfd. The agreement between the theoretical model and the experimental results are illustrated for one typical case in Fig. 22. The pulse length (τ) produced by the configuration employed (one line of five units) is also defined in this figure.

The LC ladder network model of the capacitor units, which was found to give the best correlation with experi-

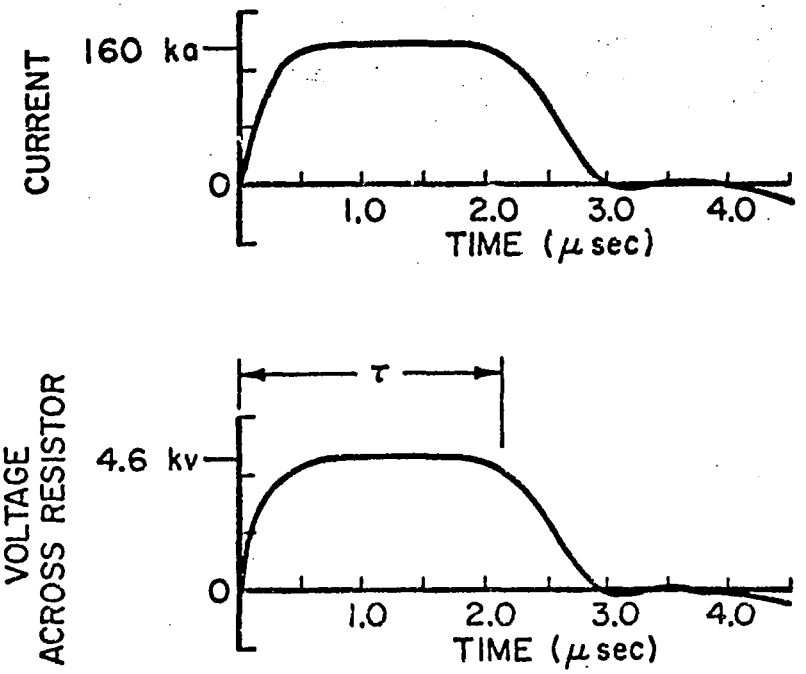

THEORETICAL RESULTS

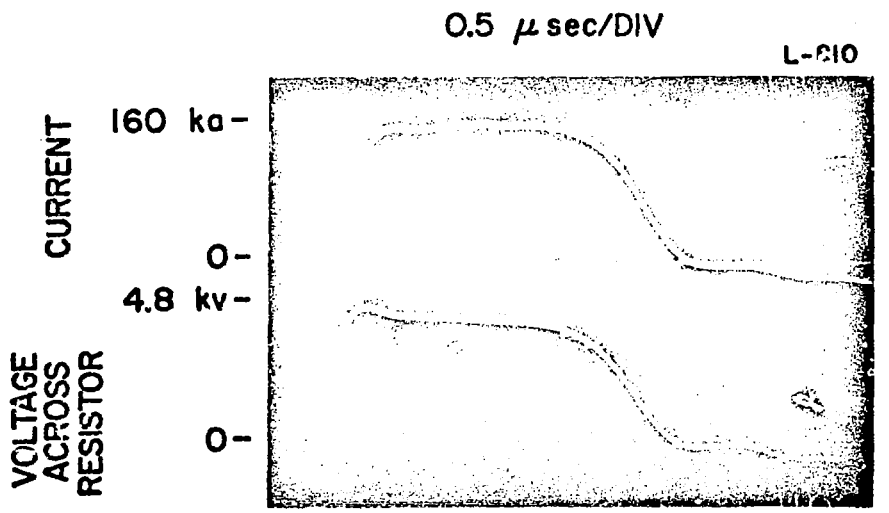

EXPERIMENTAL RESULTS

AP 25 P-213 68

THEORETICAL AND EXPERIMENTAL WAVEFORMS FROM MATCHED CAPACITOR LINE DISCHARGING THROUGH 29 m Ω RESISTOR AND 3.5 m Ω SWITCH

FIGURE 22

mental results for the case of a resistive load, has also been incorporated into the computer program describing the pulse network driving the pinch discharge. This analysis also includes an energy balance. Figure 23 shows how energy transferred to the plasma from the LC ladder network varies with the length of pulse produced by the network for the case of 100 microns of argon in the 8" pinch chamber. The pulse length is proportional to the number of elements in the ladder network and Fig. 23 is based on a power supply consisting of two ladder networks composed of 6.35 μfd, 7.5 nanohenry elements connected in parallel (0.017 ohm impedance network). E_o is the initial energy stored in the capacitors as determined from the initial voltage on the units. The pulse length is normalized by a characteristic time in the plasma acceleration profile, τ_{ej}, and the kinetic energy of the plasma sheet is evaluated at this time. In an actual thruster the appropriate τ_{ej} would be the time of ejection of the plasma, determined by the length of the thruster, but for the case of the closed chamber pinch geometry considered here, the plasma is considered "ejected" when the sheet reaches a 1" radius. One inch was selected because accurate experimental investigation is difficult at lesser radii and yet the acceleration process should be allowed to develop over as large a distance as possible in order to prevent the initiation effects from dominating the behavior of the system.

Figure 23 shows that for a current pulse longer than the "ejection" time, the efficiency of energy transfer is less than optimal. This is because there is energy left in the pulse network and in the magnetic fields associated with the discharge when "ejection" occurs. As the pulse length is decreased, less energy is left in the network and the magnetic fields at τ_{ej} and the efficiency $(KE/E_o)_{ej}$ begins to increase. As the pulse length is decreased further, the sheet accelerates less vigorously at the end of the pulse when the current is decaying. This causes the average impedance of the discharge to be less than in the case of the

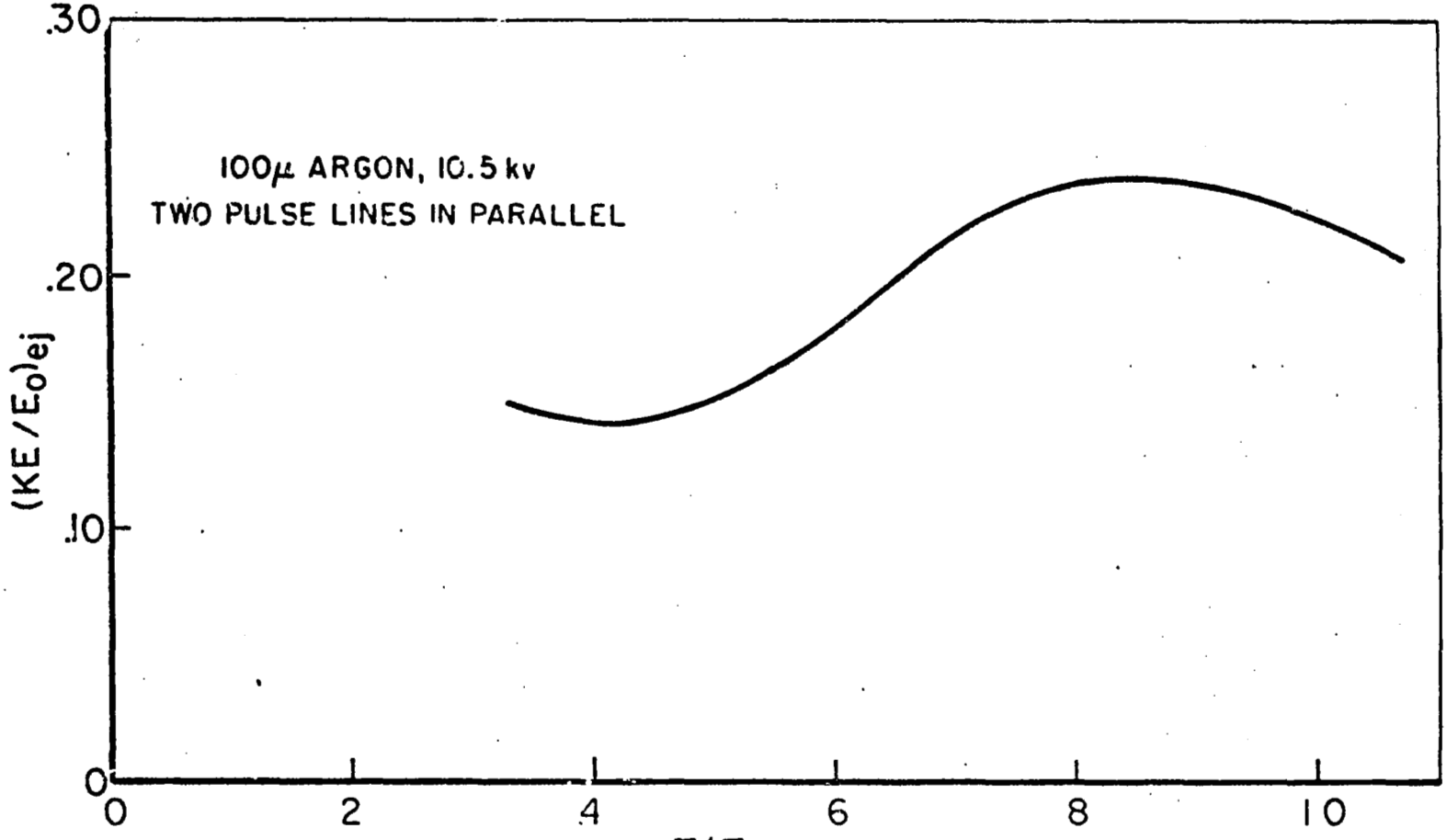

FIGURE 23

EFFICIENCY
vs
CURRENT PULSE LENGTH

longer pulses and the impedance mismatch between the line and the discharge becomes sufficiently great to cause a large fraction of the initial energy in the pulse network to be retained as reverse voltage on the capacitors. As this effect becomes more dominant, the efficiency decays. For very short pulses a secondary peak in efficiency is observed because of additional energy removal from the line during the second half cycle of the current pulse. The secondary peak is not as high as the primary one because short pulses imply a decelerating current sheet over most of the discharge and such sheets sustain greater energy losses to the thermal modes of the plasma as pointed out in Ref. [22].

Figure 24a shows theoretical curves similar to the one shown in Fig. 23 for the cases of 2, 3, 4, and 8 networks paralleled (17, 11, 8.5, and 4.25 milliohm lines). From this figure one can see the effect of the characteristic impedance of the LC ladder networks on the efficiency of energy transfer. As the pulse network impedance is decreased, the peak efficiency realized increases until the impedance of the network (Z_L) is about half of the average discharge impedance (Z_D). Further decreases in the line impedance tend to produce negligible changes in the peak efficiency.

Figure 24b contains the experimentally observed results for the case of 100 microns of argon which corresponds to the theoretical results of Fig. 24a. The kinetic energy data used is obtained in the following manner: (1) Current sheet trajectories are determined from magnetic field probe records at 2.5", 1.5", and 0.5" radii. (2) From these data, sheet velocities and ejection times are determined. (3) Kinetic energies are calculated from these velocities assuming that the sheet collects all of the mass it encounters in the discharge chamber.

The qualitative agreement between the experimental and theoretical results is reasonably good. Notice, however,

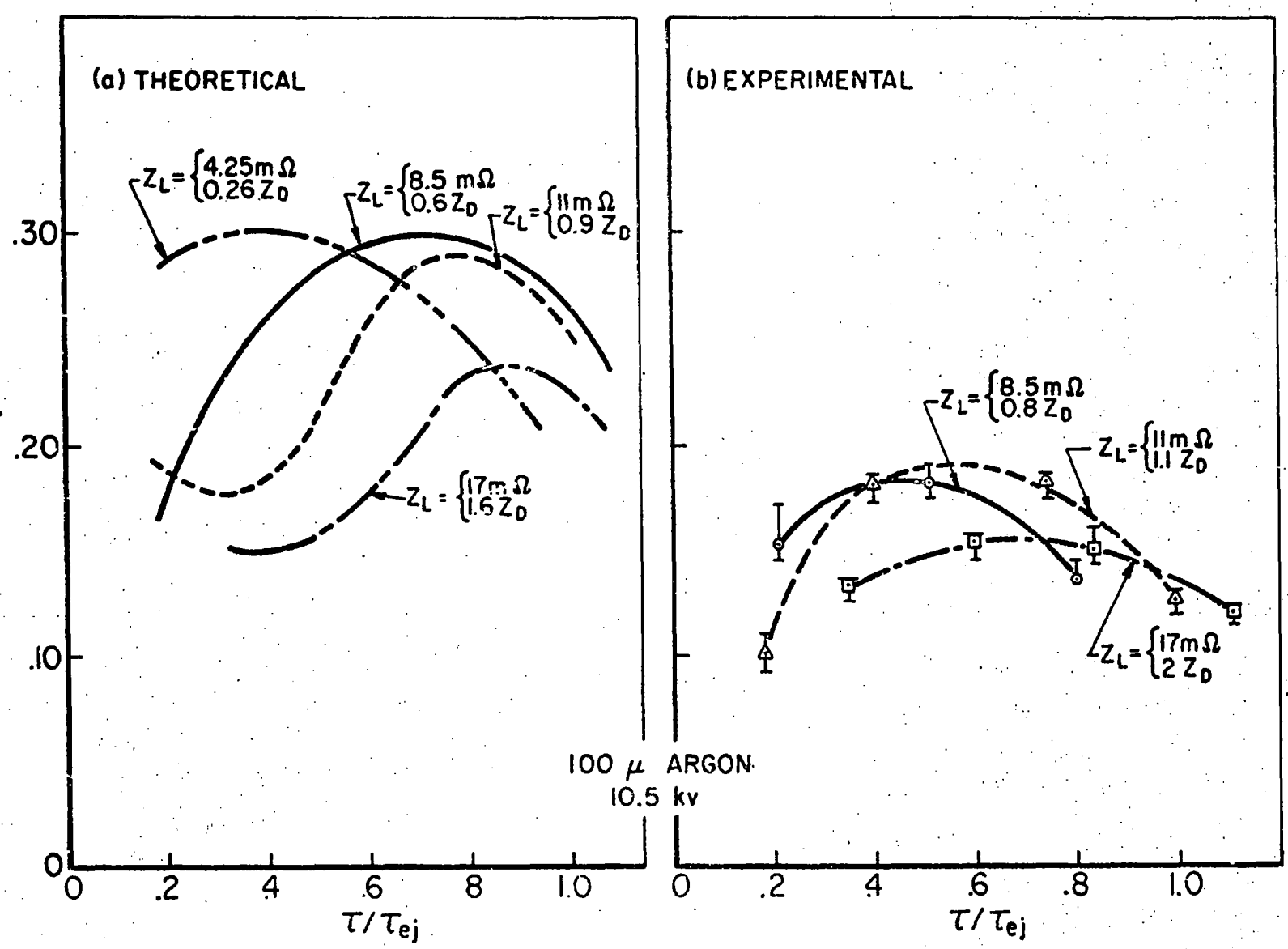

FIGURE 24

EFFICIENCY vs CURRENT PULSE LENGTH

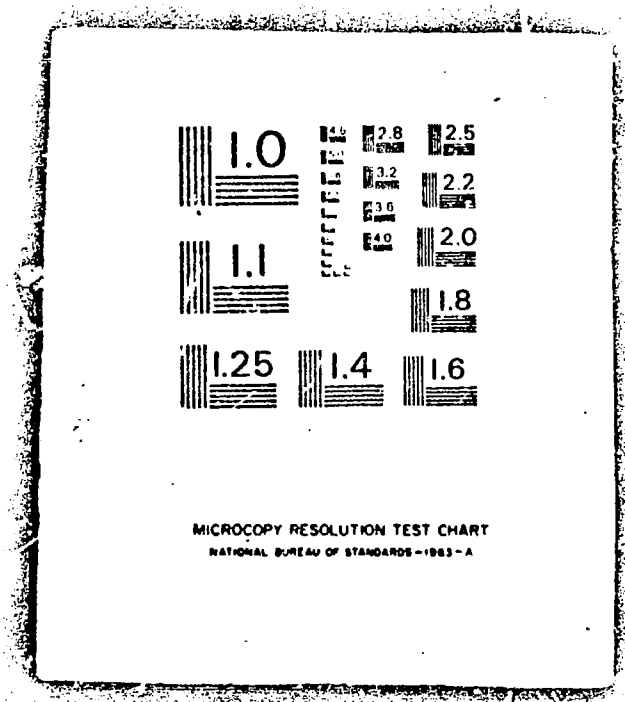

that the experimental results show a peaking of efficiency as a function of network impedance that is not observed in the theoretical results. Also, the measured efficiencies are roughly half of those predicted theoretically. These lower experimental kinetic energies are a result of lower current sheet velocities and detailed analysis of the magnetic probe records indicates that lower velocity occurs because all of the discharge current is not flowing in the thin current sheet assumed in the model. Although all of the current initially flows in a thin region when it is at the outside wall, there is a diffuse current pattern released behind the sheet as it drives inward toward the pinch configuration. This diffuse "trailing" current seems to remain stationary, and theoretically it should continue to add energy to the plasma through a $\vec{j} \times \vec{B}$ "blowing" action. In fact, it may be that a large fraction of the gas acceleration is accomplished in the region behind the current sheet in a more efficient manner than the snowplow model would predict.

The fact that all of the current is not flowing through a well-defined current sheet is manifested in several other ways experimentally. For example, Fig. 25a is an oscillogram showing the current waveform for four networks of three capacitors driving a discharge in 100 microns of argon. After the initial current rise, one sees a tendency of the current to continue to rise at a lesser slope, whereas the theoretical analysis predicts that the current decay after the initial rise time because of the increasing impedance associated with the accelerating current sheet. The fact that the total current continued to rise indicates that current paths are being established at locations other than through the main current sheet, thereby reducing the net impedance and the coupling between the external circuit and the current sheet. Figure 25b is an oscillogram of the current waveform for the same four networks of three capacitors driving a discharge in 2 mm of hydrogen (2 mm of hydrogen produces the same mass density as 100 μ argon). Here the current waveform does behave as

0.5 μsec/DIV

L-611

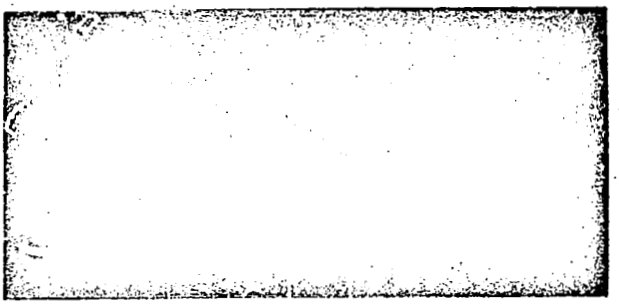

(a) 100 μ ARGON - 10.5 kv

L-736

(b) 2mm HYDROGEN - 10.5 kv

EXPERIMENTAL CURRENT WAVEFORMS

FIGURE 25

the theoretical model predicts it should, thus indicating a much closer coupling between the current sheet and external circuit. Indeed, the efficiencies observed in hydrogen are in rather good agreement with those predicted theoretically for the resistance and inductance existing in the laboratory situation, but the experimental errors involved in measuring the velocities in hydrogen are significantly larger than those in argon.

In closing, it should be pointed out that no attempt has been made to achieve ultimate efficiencies in this work. Rather, the objective has been to gain a better understanding of the mechanisms involved by devising a model that will provide insight into the experimental observations. There are large losses associated with the switch used in these experiments which could possibly be reduced. If the switch losses could be eliminated with no corresponding deterioration in the performance of the accelerator, efficiencies in excess of 50 percent are predicted by the theoretical model.

Additional studies on this problem of efficient energy transfer using different gases, gas pressures, and initial line voltages have also been conducted during this period. A more complete presentation of this work will be given in a forthcoming Ph.D. thesis.

VI. PRESSURE MEASUREMENTS IN CLOSED CHAMBER DISCHARGES (York)

Several aspects of the continuing program to map accurately the gas pressure profile through a propagating current sheet have been pursued during the present reporting period, specifically: the probe-discharge interaction has been studied in detail; precise pressure, magnetic field, and electric field data has been compiled for the specific experimental conditions of interest; and these data have been analyzed from a combined electrodynamic and gasdynamic point of view.

A previous report [51] mentioned the profiles of luminosity which appear about a probe immersed in a current sheet. In an attempt to distinguish more carefully the sources of such luminosity, simultaneous data of luminosity and $\dot{B}_\theta$ were taken at 100 μ argon in the 8" pinch chamber driven by the pulse-forming network. Kerr-cell photographs were taken with both radial and axial perspective of the probe in the chamber (Fig. 26) and compared with magnetic probe responses at the same instant of exposure. From such data it can be concluded that the discharge luminosity occurs in regions of high-current density. Reference to the catalogue of pressure probe responses then indicates that the position of the pressure discontinuity associated with a current sheet is close to the trailing edge of the luminosity profile. This result seems to be consistent with certain calculations now in progress based on a gasdynamic flow field induced by a somewhat leaky piston that exceeds the estimated escape speed of the ambient gas.

The detailed probing of the current sheet has been carried out using magnetic, electric, and pressure probes with care being taken to insure compatibility of the probing techniques. For example, in order to evaluate and eliminate all extraneous signals from the pressure probes, a null circuit has been devised by inserting a layer of insulating tape

100 μ ARGON

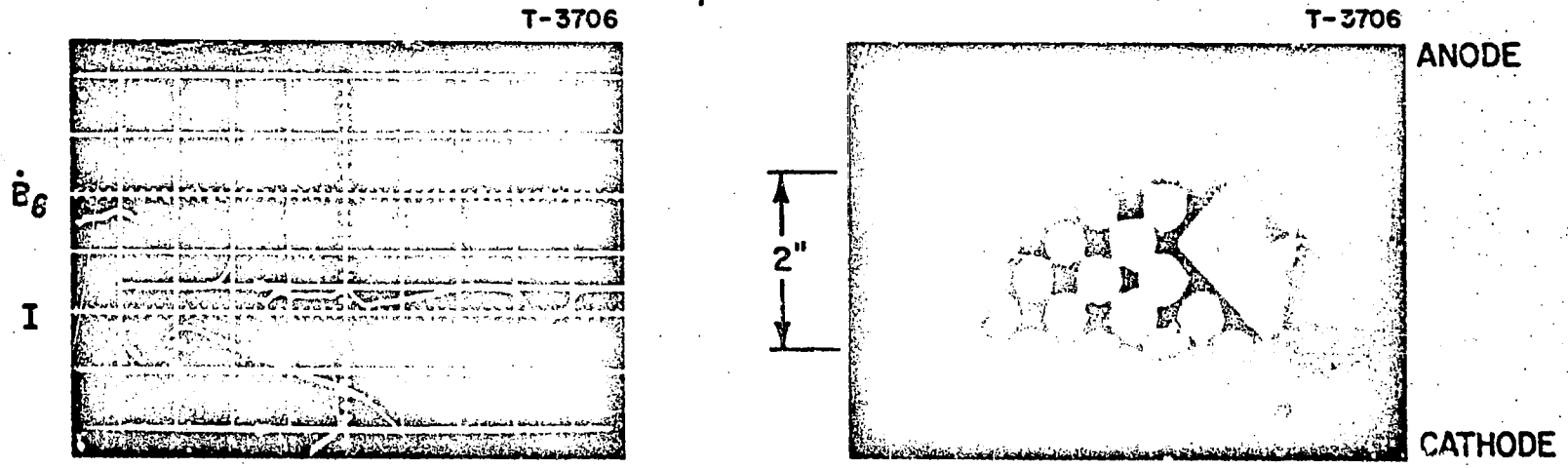

(a) RADIAL VIEW, t=1.3 μsec

1 μ sec/DIV

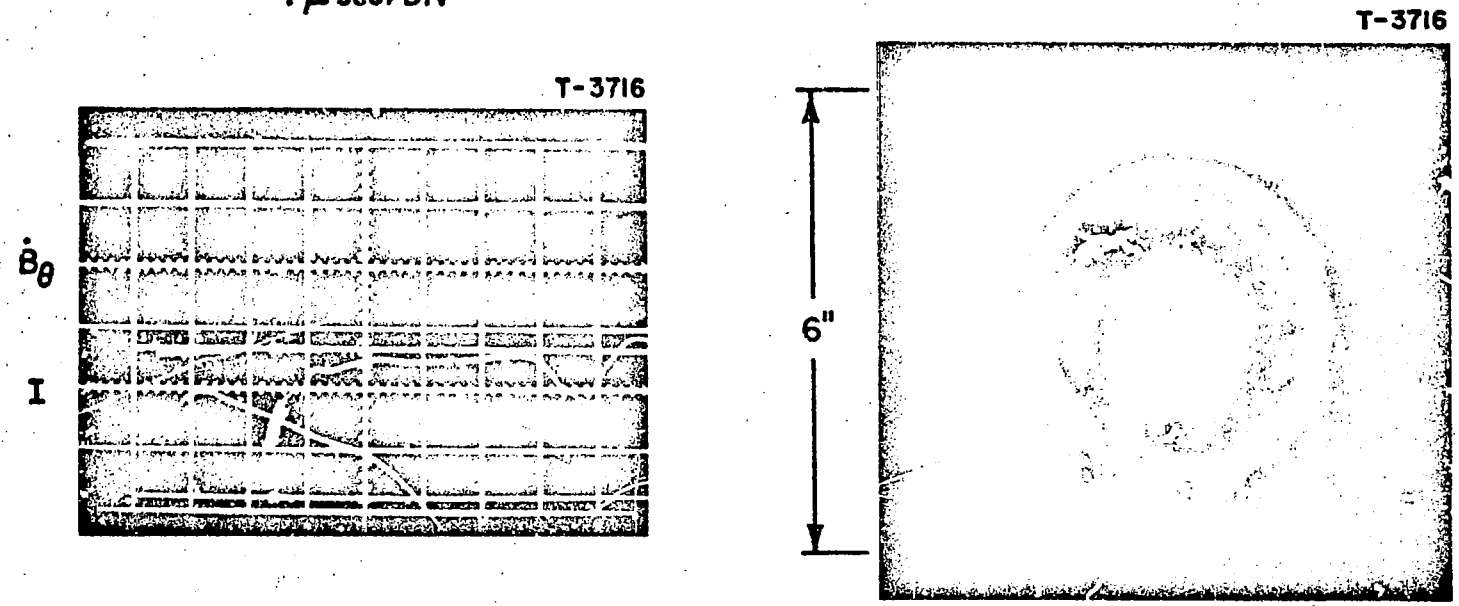

(b) AXIAL VIEW, t = 1.4 μsec

FIGURE 26

SIMULTANEOUS LIGHT AND MAGNETIC PROBE DATA

(mylar, 1 mil) between the silver paint and the crystal. In order to achieve the observed null response, it is found that the thickness of silver paint is critical.

To determine the most satisfactory gasdynamic configuration for the pressure probe, simultaneous data of pressure and $\dot{B}_\theta$ has been taken while varying the geometry of a "flow isolator" which shrouds the probe barrel. Typical results of these changes can be seen in Fig. 27, where it is evident that the presence of such an isolator distorts the current sheet profile much more than it improves the pressure response. Hence, it has been concluded that probes without isolators yield the minimum distortion of the propagating current sheet characteristics they are to determine.

A double electric probe of the ball and ring type with the electrodes embedded in a conical shape has been added as an additional diagnostic of the current sheet interior. Both the E and B probe circuits are designed to have satisfactory frequency response for this application and are calibrated using standard techniques. Also, it is found useful to record voltage signatures across the electrodes and across the current sheet by standard inner and outer dividers [43].

In the detailed surveys, current sheet data are recorded primarily on the interelectrode midplane at several radii; at a given point of interest, data are collected during three different discharges, with the common $\dot{B}_\theta$ signal used for time reference and comparison. Two internal probes (one axial, one radial) separated by a 30° cylindrical angle are used during any given experiment. The discharge is examined for symmetry and the probe positions then reversed to guarantee the time correlation of the data. Typical results, including magnetic and electric probe responses, and the responses of the pressure sensor when facing radially outward, axially toward the anode, and axially toward the cathode, respectively, all suitably adjusted to compensate for current

T-3576

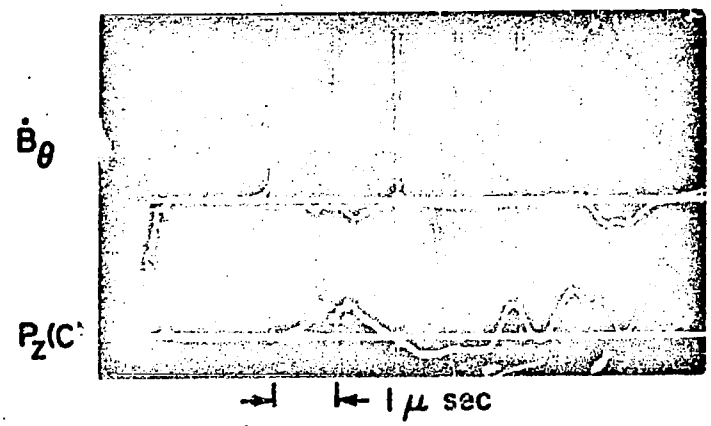

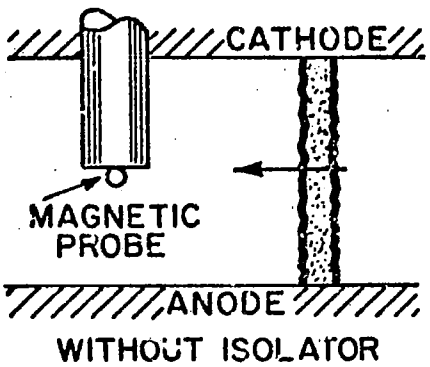

WITHOUT ISOLATOR

T-3577

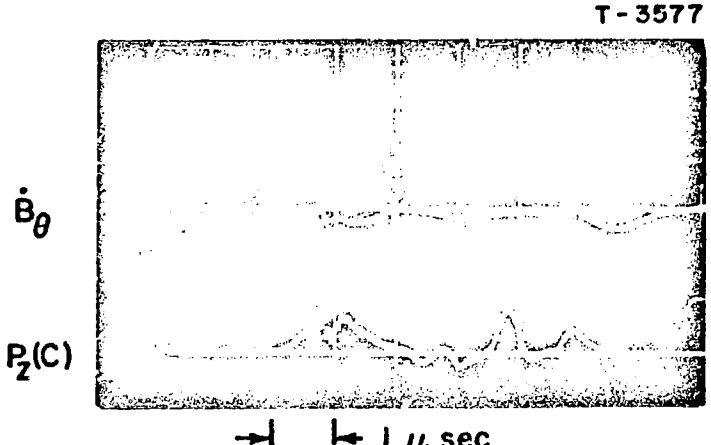

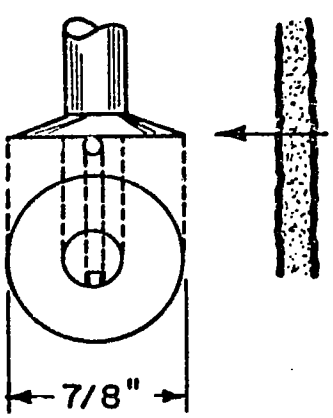

ISOLATOR

T-3578

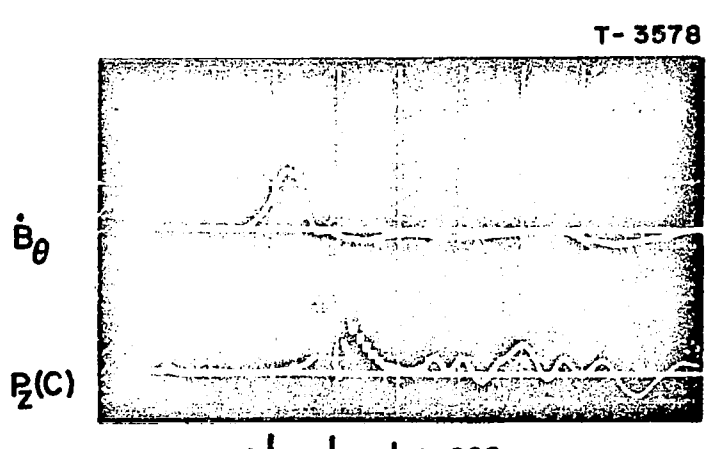

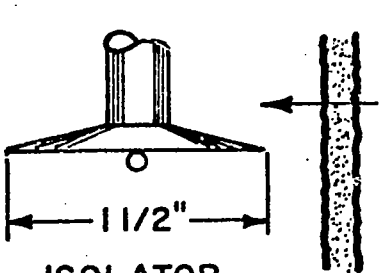

ISOLATOR

EFFECT OF FLOW ISOLATOR ON PROBE RESPONSES
(R = 2" : h = 1")

sheet arrival differences, are presented in Fig. 28. It is evident from the data generally, but perhaps most clearly on the pressure data, that there appear to be three different zones of current sheet structure. Zone I is notable as a region of current concentration with only weak but symmetric pressure response; Zone II is typified by strong but asymmetric pressure response; Zone III is evidently a region of small current density but finite pressure and field values.

Analysis of the pressure probe response presented above and its relationship to the other properties within the sheet is currently in progress. Briefly, the most important effects under consideration are those of shock wave, boundary layer, and electrostatic sheath interactions with the probe surface. This analytical formulation will be presented in entirety in a forthcoming Ph.D. thesis.

ERRATA:

Replace Fig. 28, p. 60 of text with corrected figure.

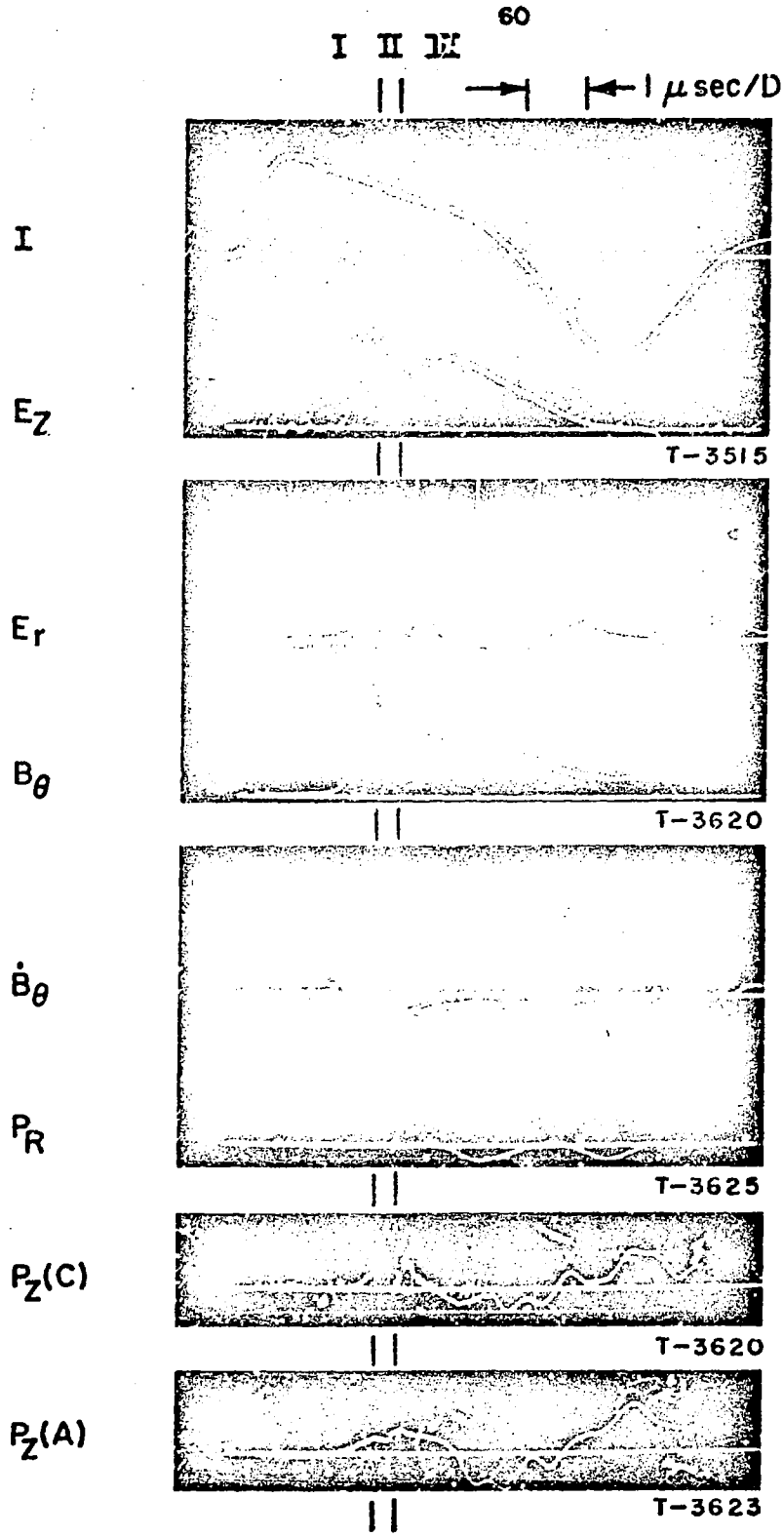

TYPICAL PROBE RESPONSES

FIGURE 28

AP 25 P-197 A 68

VII. ELECTRODE-SIZE EFFECTS ON DISCHARGE VOLTAGE (Oberth)

In the past several reports we have presented evidence of certain peculiarities in the discharge structure near the anode surface. In brief, it has been found that the current sheet attaches to the anode in the form of a broad, diffuse foot. Under certain circumstances this anode foot may divide into two, or more, regions of high-current density which then follow each other in the direction of the main sheet propagation. The extent of the anode disturbance from the surface depends primarily on the driving current waveform and may, in fact, reach as far as the chamber midplane.

The most recent experimental work has attempted to study the relationship between this anode foot and the resistive voltage drop along the current sheet. It is reasonable to expect that the anode foot involves certain dissipative processes, and since the resistive voltage drop along the sheet is an obvious index of energy loss, we may seek some correlation between the anode foot size and this resistive voltage drop.

For this purpose, closed chamber pinch discharges were monitored with an inner voltage divider constructed of an insulated metal rod inserted across the chamber electrodes to complete a circuit of which the current sheet is part. The relevance of the current sheet anode attachment in determining the resistive voltage drop was assessed by a technique of selective electrode insulation. Namely, the 8" diameter pinch electrodes were insulated by attaching to them two circular layers of 0.005" mylar, of diameter 4", 6", and 7", respectively (Fig. 29). The inner divider circuit was completed by driving the insulated rod through the insulation and into the metal electrode. In one sequence of measurements

AP 25 12 4376 68

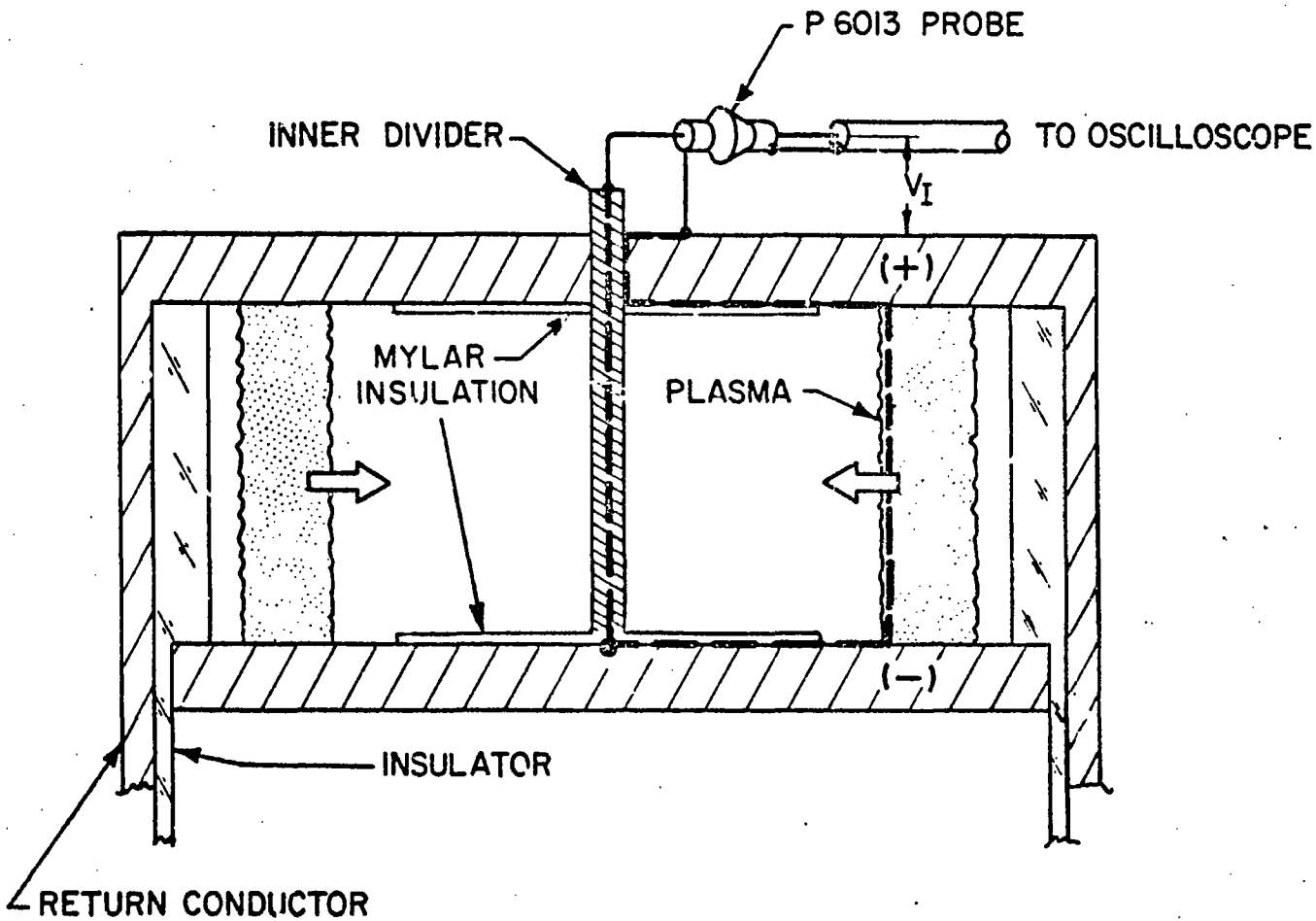

FIGURE 29

SELECTIVE ELECTRODE INSULATION EXPERIMENT

an electrode with a 6" diameter glass center section was used to provide the desired insulation.

Voltage signatures obtained from discharges in these modified chambers were found to be extremely sensitive to the surface condition of the exposed electrode area, and it was found necessary to clean the electrodes very frequently, and to compare data only from a series of consecutive discharges, to minimize the influence of this factor.

Figure 30 shows a series of oscillograms of driving current waveforms and inner divider voltage signatures for the cases where 7" diameter mylar covered, alternatively, major portions of the anode, the cathode, and both electrodes. The quoted voltage readings were taken at the time of maximum driving current, 310,000 amperes. The voltages are seen to increase in the order: both electrodes uninsulated; cathode only insulated; anode only insulated; both insulated, where it is the anode insulation which causes the most significant change.

A more complete collection of data is displayed in Fig. 31 which shows how the relative area of electrode insulation affects the current sheet resistive voltage drop. The voltage drops are found to increase with larger fractions of electrode insulation, and anode insulation is found to cause considerably higher voltage readings than cathode insulation. All of the data points were taken for current sheets propagating in 100 μ argon, driven by a 3.8 μsec current pulse of 310,000 amp maximum; two of the data points refer to the case where glass insulation is used in place of mylar, but these points agree well with the rest of the data.

Figure 32 displays how the resistive voltage drops depend upon the initial chamber pressure. This dependence although measurable, is not severe enough to obscure the electrode area effect of major interest here, and once again anode insulation is seen to cause consistently and markedly higher voltage readings than does similar cathode insulation.

AP 25 D-184 ACB

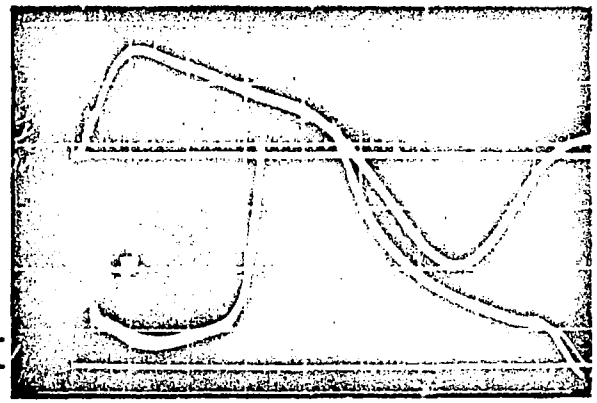

a) BOTH ELECTRODES METAL

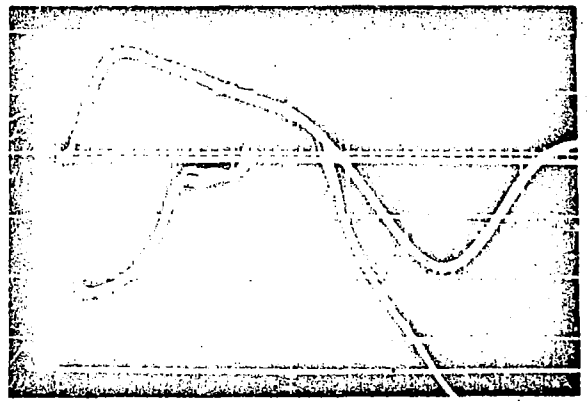

c) ANODE COVERED, r=3.5" MYLAR

1 μ sec/DIV

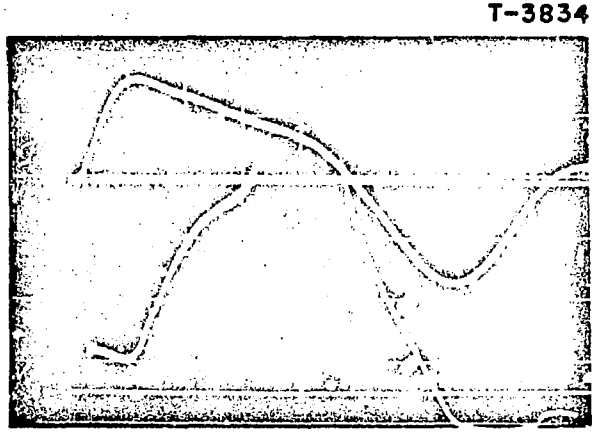

b) CATHODE COVERED, r=3.5" MYLAR

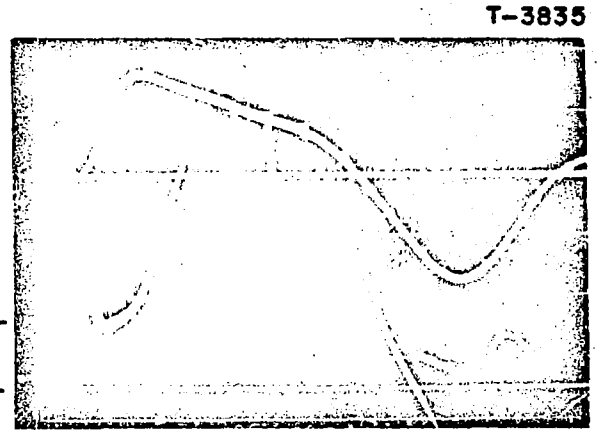

d) BOTH COVERED, r=3.5" MYLAR

INNER DIVIDER VOLTAGE SIGNATURES

FIGURE 30

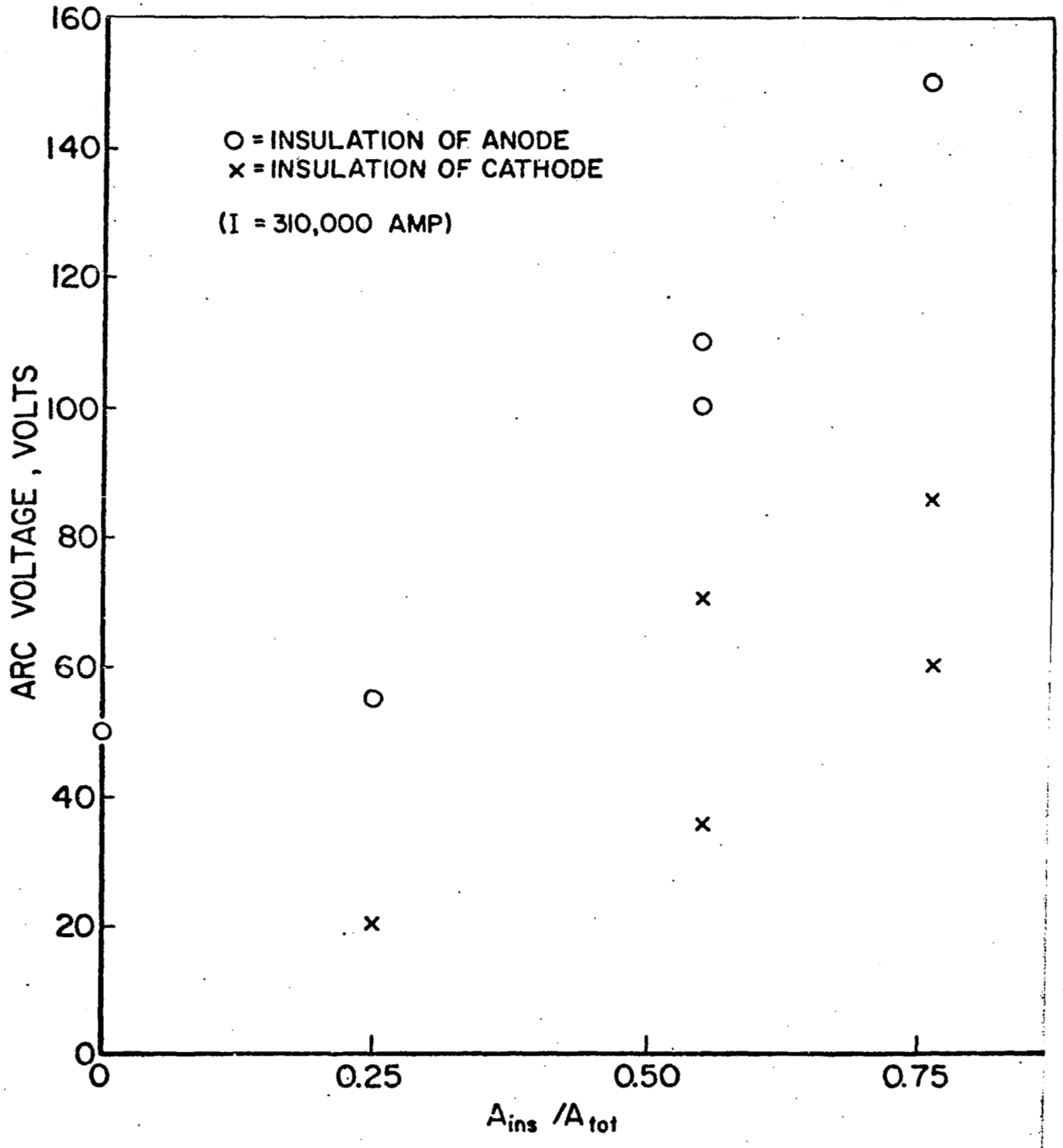

VOLTAGE ACROSS CURRENT SHEET vs FRACTION OF ELECTRODE AREA INSULATED

FIGURE 31

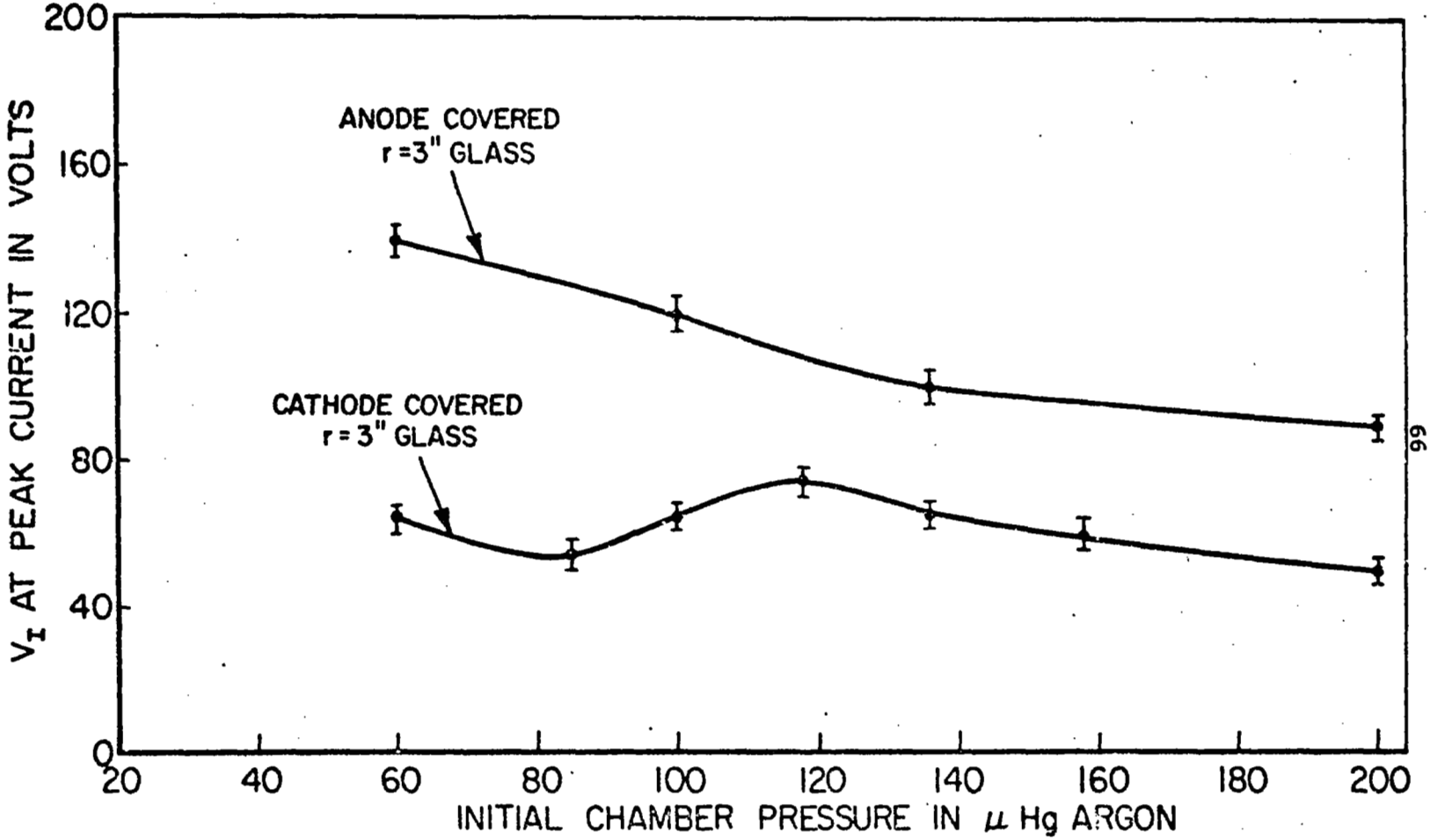

FIGURE 32

VOLTAGE vs CHAMBER PRESSURE AT PEAK CURRENT

As a tentative interpretation of these observations, we suggest the following hypothesis: The broad and diffuse anode foot structure is a manifestation of some fundamental change in the current conduction process from that prevailing in the narrow, intense current sheet which exists further from the electrode surface. Whatever this anode foot conduction mechanism may be, it requires a much larger discharge cross section to maintain comparable conductance to that of the main portion of the sheet. Partial insulation of the anode surface interferes with this broad attachment, and since the discharge current is essentially fixed by the external circuit, precipitates an increased voltage drop across the anode foot, and hence across the entire discharge path.

Anode phenomena such as these can have relevance to the observed large thermal losses associated with needless heating of the anode in MPD and other steady plasma thrusters. Better understanding of anode mechanisms may permit some reduction in these large thermal losses. For example, the above preliminary results suggest that anode losses might be reduced simply by using larger anode surface areas, thereby decreasing the resistive voltage drop associated with the diffuse anode attachment portion of the discharge. This possibility will be studied in future work.

VIII. GAS LASER INTERFEROMETRY OF CLOSED CHAMBER DISCHARGES (Bruckner)

The previous report [51] presented some preliminary interferometric measurements of time dependent electron concentrations in a 150 μ argon pinch discharge. At that time two major areas of difficulty were pointed out: (1) the lack of good reproducibility in the interferometric fringe sequences, and (2) the problem of determining unambiguously the sign of the temporal gradients in electron density.

The search for initial chamber conditions leading to reasonable reproducibility has been continued. Some interesting data were obtained at 100 μ initial argon pressure and $R/R_o = 0.55$. Two representative interferograms are shown in Fig. 33a,b. In each case the top trace represents the total current through the discharge and the bottom trace is the fringe sequence. Figure 33c shows the time history of the discharge luminosity which must, of course, be kept much smaller than the laser intensity. The corresponding time resolved electron density profiles are shown in Fig. 34. For comparison, Fig. 35 presents the 150 μ results previously reported [51].

Note that the profiles for the 100 μ case begin earlier and show a sharper rise to about the same maximum value as for the 150 μ initial pressure. The better quality of the fringes in the 100 μ case permit resolution of the inception of a "tail" in the density distribution. This supports previous indications that the current sheet does not sweep up all the mass it overtakes. At the initial pressures of 100 μ and 150 μ the ambient particle densities are respectively about 3×10^{15} and $4.5 \times 10^{15} cm^{-3}$ at room temperature. Assuming complete single ionization, it appears that the current sheet has compressed the overrun gas by factors of about 25 and 17, respectively.

p=100μ ARGON, R / Ro = 0.55

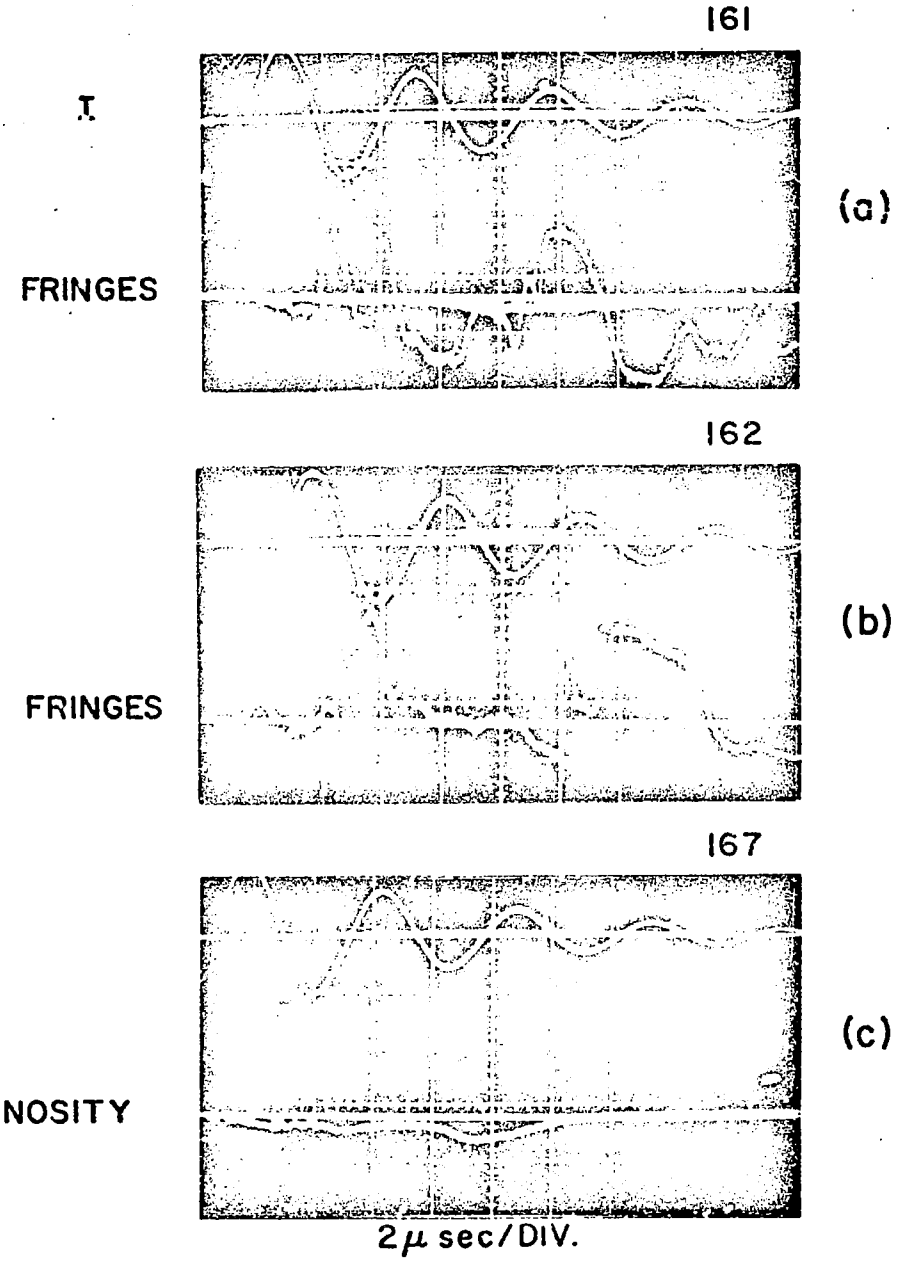

INTERFEROMETER RESPONSE
TO PINCH DISCHARGE

FIGURE 33

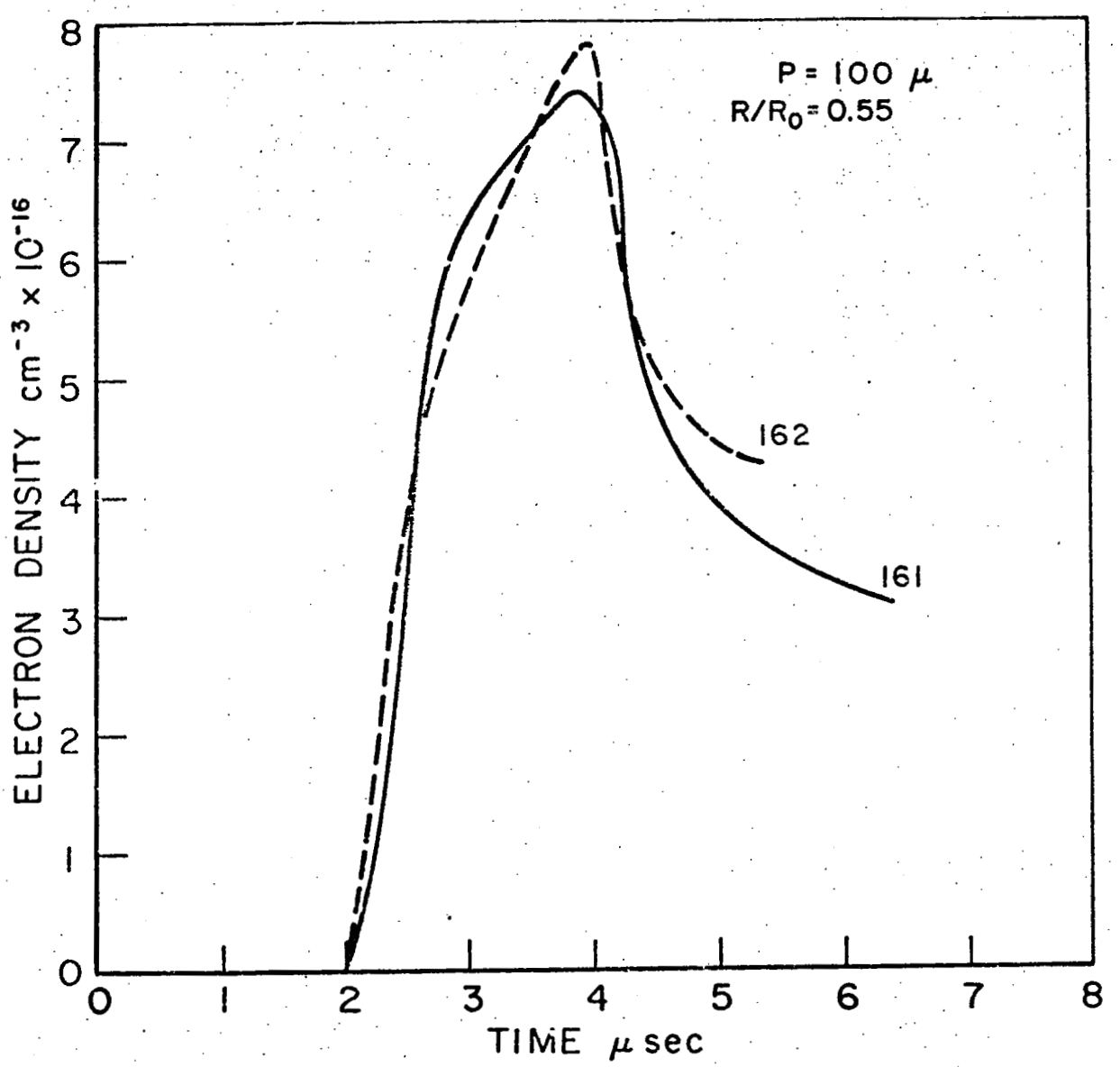

ELECTRON DENSITY PROFILE
THROUGH CURRENT SHEET

FIGURE 34

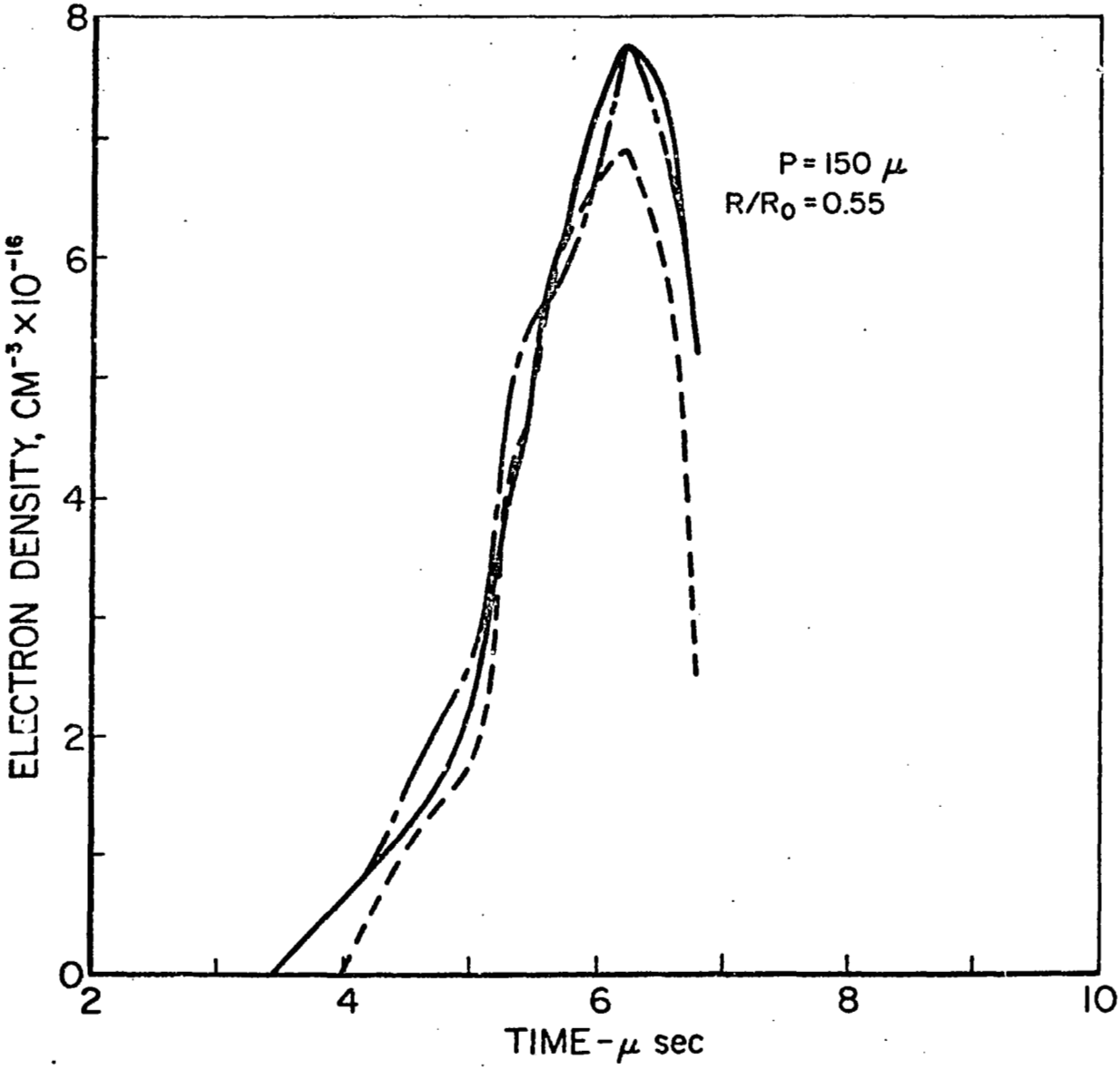

ELECTRON DENSITY PROFILE
THROUGH CURRENT SHEET

FIGURE 35

Good fringe reproducibility remained a problem, however. An examination of axial Kerr-cell photographs of discharges in the 8" device under study revealed what may well be the source of this difficulty. Figure 36 shows three such photographs, all taken at approximately the same time after discharge initiation. Note the existence of a large azimuthal disturbance in the current sheet. In each case it occurs at different angular positions. Clearly, the electron concentration through this region, or its neighborhood, could exhibit characteristics different from that through the "nominal" regions of the sheet.

In the hope of relieving this problem, the 8" device was reduced in size by the insertion of a 4" diameter cylindrical Pyrex insulator. This technique has been described in detail in one of our earlier reports [12]. The essence of the modification is that the discharge is greatly intensified, with the current sheet traversing the radius of the chamber before the external driving current has had a chance to reverse and cause secondary breakdowns. It was hoped that the increased rapidity of the process would preclude the development of the asymmetric disturbance in the current sheet. However, the intense luminosity of these sheets was greater than the maximum laser intensity, at the photomultiplier. As a result, the fringes in the laser beam were swamped by the discharge radiation, making electron density measurements impossible. A simple solution to this problem would be the use of a more powerful laser, one with an output at least an order of magnitude above the 0.3 mw available from the present instrument.

Another problem arising in our studies is that the number of fringes produced in the interferometer as the current sheet sweeps by is low (of the order of four or five). In other words, the optical length of the plasma changes little through the current sheet. This is partially due to the fact that the physical length of the plasma under obser-

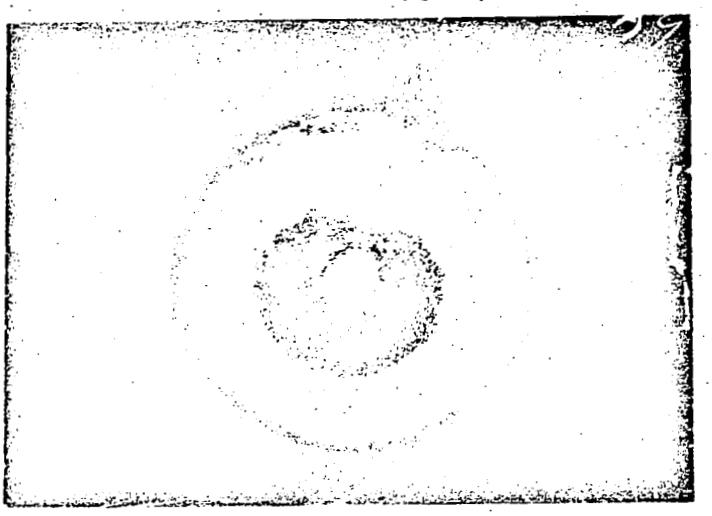

5.2 μ sec

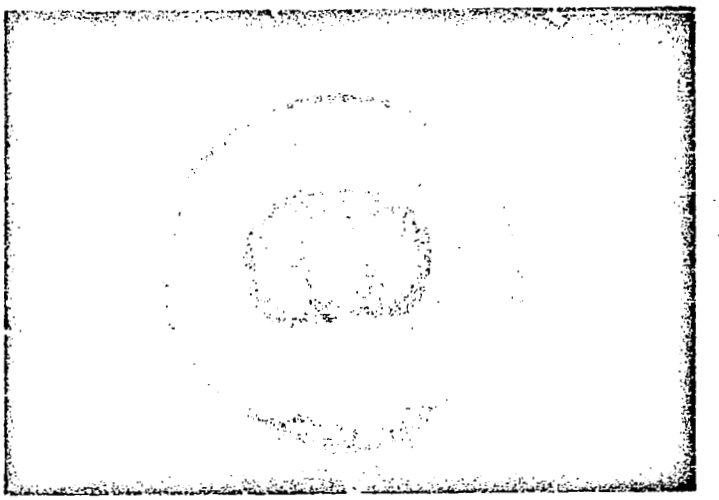

5.3 μ sec

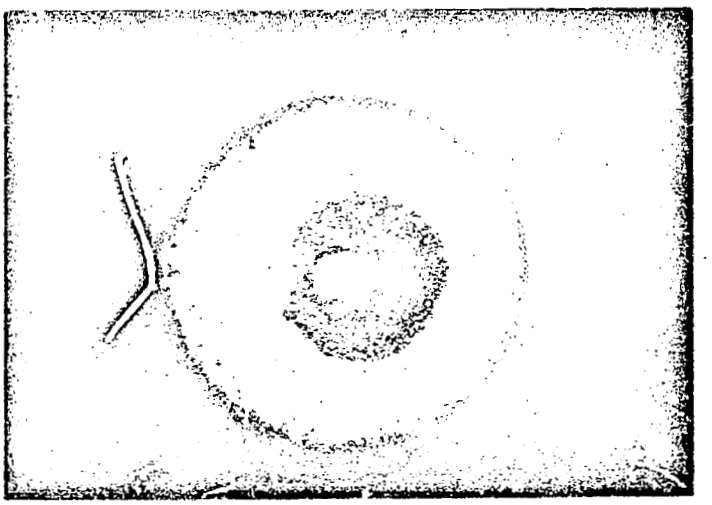

5.3 μ sec

AP 25 P-191 A 68

AXIAL KERR CELL PHOTOS OF PINCH DISCHARGE IN 170 μ ARGON (8" CHAMBER)

FIGURE 36

vation is only about 5 cm to begin with. This makes translation of the fringes to density profiles subject to large possible errors. One solution is to increase the probing wavelength. Since the present diagnostics have been carried out at a wavelength of 6328Å, (He — Ne laser) in order to increase significantly the number of observed fringes, we would have to operate in the infrared region of the spectrum. This would, of course, present the usual problems of infrared optics and detection.

Operations in the infrared may not be required, however. The original application of the laser interferometer to the pinch discharge was intended as a test of feasibility. The ultimate aim of the program is to provide diagnostic service for the more propulsion-oriented devices in our laboratory, such as the parallel-plate accelerator or the MPD arc simulator in the large vacuum facility. In these devices the optical length of the plasma under observation is significantly greater than in the pinch devices, and operations in the visible part of the spectrum should be adequate.

IX. EXPERIMENTAL STUDIES OF THE DOUBLE-FLOATING TIP ELECTRIC PROBES (Turchi)

Double-floating tip electric probes have been used in the study of pulsed plasma discharges to provide information on the distribution of electrostatic fields within the plasma and on the corresponding electric field energies present in such discharges, particularly in the current sheets [42,51]. Inherent in the use of such double probes for electric field diagnostics are assumptions on the constancy of the field over the probe tip separation, and on the nature of the interaction between the probe and the plasma flow, i.e., on the disturbance the probe introduces into its measurable.

For discharges of propulsion interest, the probe-plasma interaction is simplified in one sense, in that the electron energies are typically much less than the electromagnetic field energies characterizing the plasma acceleration process. Thus, for the floating probe case, we may neglect to first order differences in probe sheath voltages compared with the differences in plasma potential within the discharge. On the other hand, the plasmadynamic interaction of a high velocity, unsteady discharge with two probe tips and their support structure introduces major complications on the interpretation of the probe responses in such environments.

The purpose of this program is to examine systematically the validity of some of the common assumptions on field constancy and plasmadynamic interactions normally imposed on electric probe diagnostics of this type. To facilitate these studies, a variable gap probe was designed in a configuration to minimize signal distortions from plasmadynamic and electromagnetic interactions with the probe tips and their support structure. This probe employs two quasi-spherical electrode tips of equal size, maintained well away from the probe support by wires insulated with a thin coating of epoxy (Fig. 37).

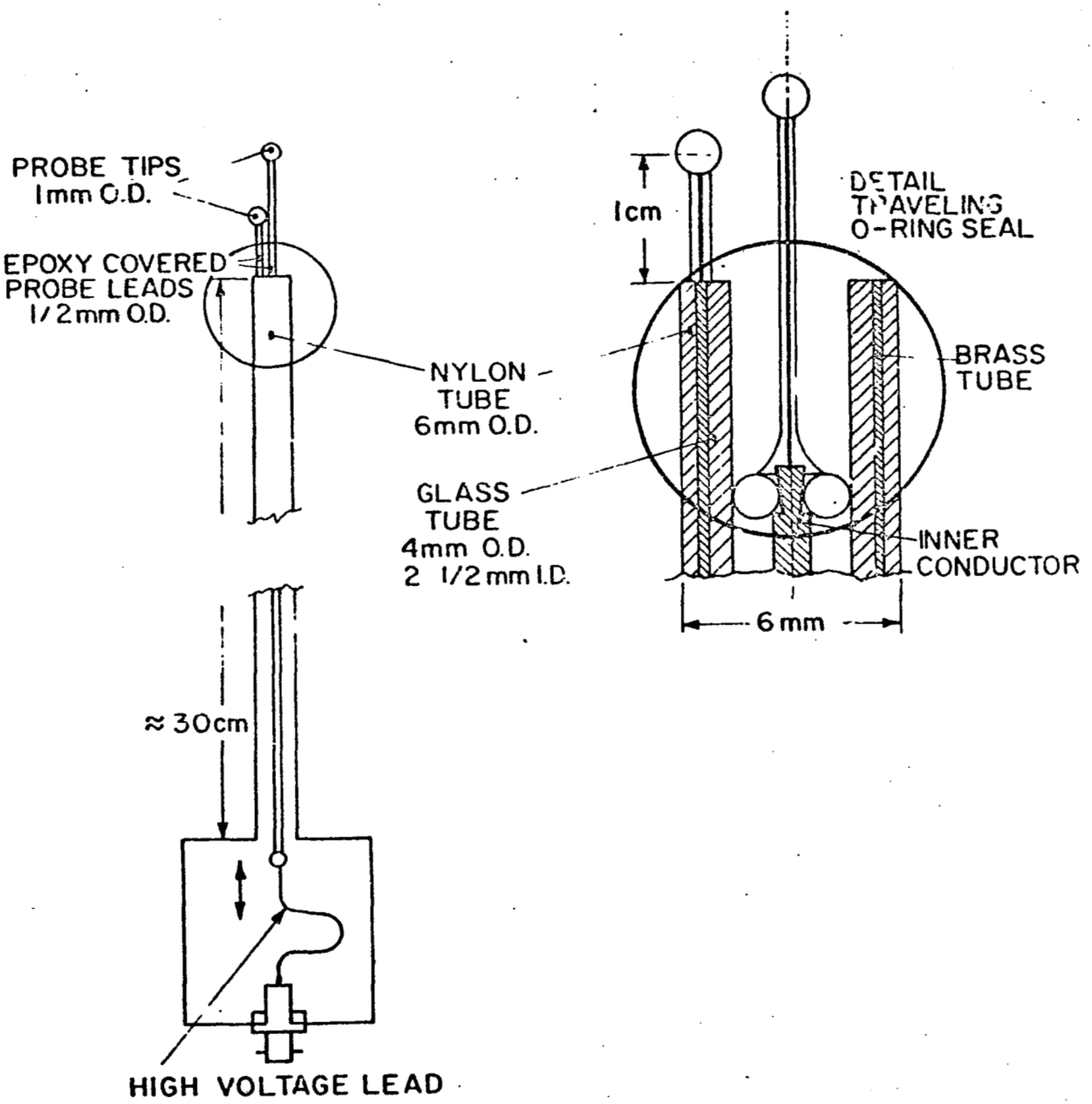

DOUBLE ELECTRIC PROBE

FIGURE 37

A traveling vacuum seal allows continuous variation of the probe tip separation over several centimeters. Initial tests with this probe displayed adequate null signals for zero tip separation and symmetric signal reversal with tip reversal. Magnetic flux pickup was eliminated by maintaining the probe tips in the plane of the magnetic field lines.

The first series of experiments with this probe investigated the variation of apparent electric field in a pinch discharge current sheet with probe tip separation. For a sequence of probe tip separations, the response was first observed with the probe tips in the plane of the magnetic field lines to prevent $\dot{B}$ pickup, and then repeated with the probe rotated 180° as a check. Each experiment was also repeated with the position of the tips reversed. The results are shown in Fig. 38. We see that the radial electric field computed on the basis of voltage difference divided by probe tip separation decreases as the tip separation is increased, indicating that the plasma potential experiences its major change over distances at least as small as 1 mm. Thus any electric probe studies on such a current sheet should use a probe of very small gap indeed, or a more tedious procedure must be employed of mapping the plasma potential vs. local radial position around the point considered with one probe tip, while the other tip is at a fixed position nearby. Then, the resulting plot may be graphically differentiated to obtain the local electric field.

In a second series of experiments designed to illuminate some aspects of the flow disturbance problem, various obstacles were placed at the probe tip to impede the flow of plasma and its electric currents. The first set of experiments used a tubular sleeve of mylar tape which extended ahead of the probe support (Fig. 39a). Tests were made for various lengths of the sleeve and the results are shown in Fig. 40 as a function of the length of the obstacle beyond the probe support. One might question whether this effect

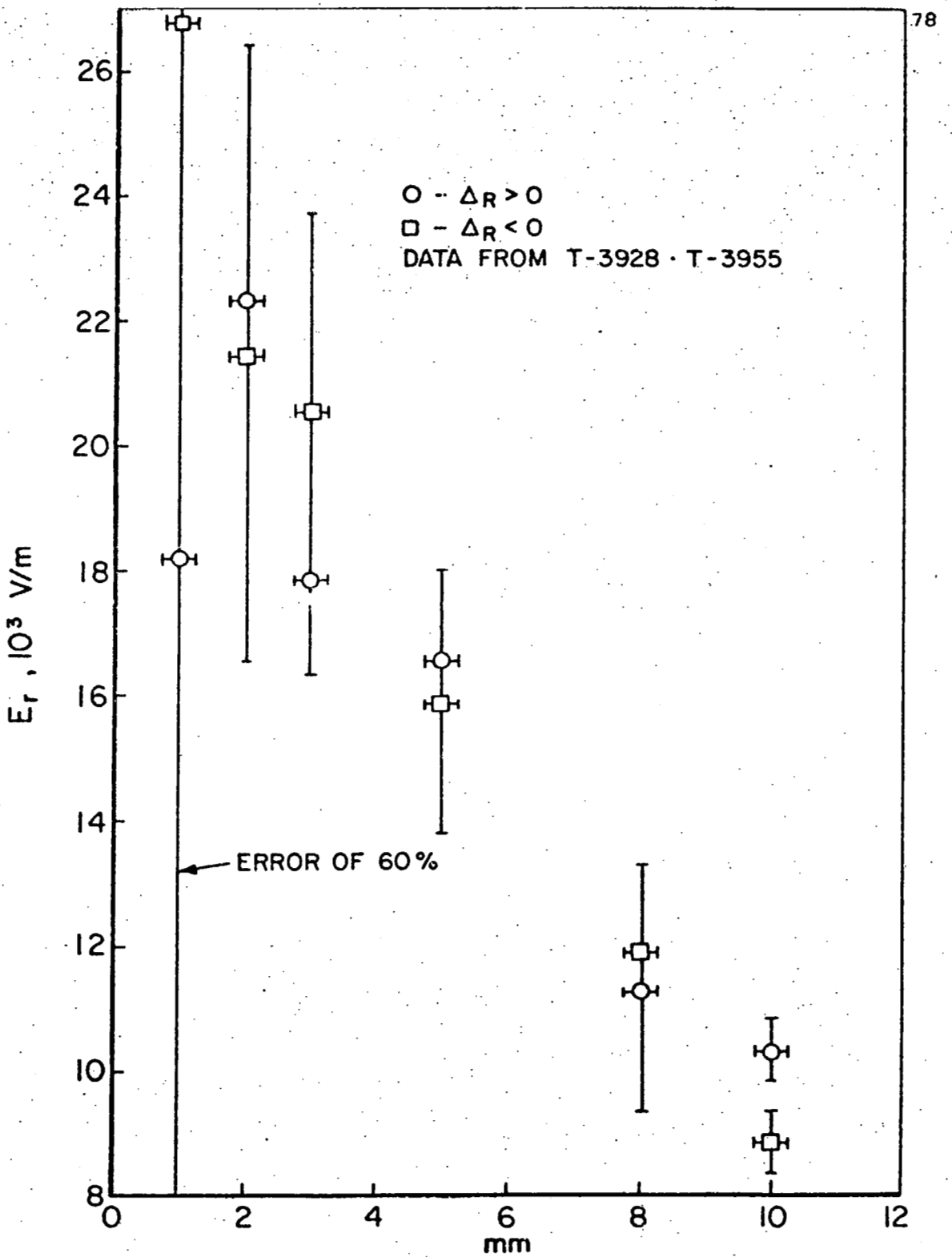

APPARENT ELECTRIC FIELD vs PROBE TIP SEPARATION

FIGURE 38

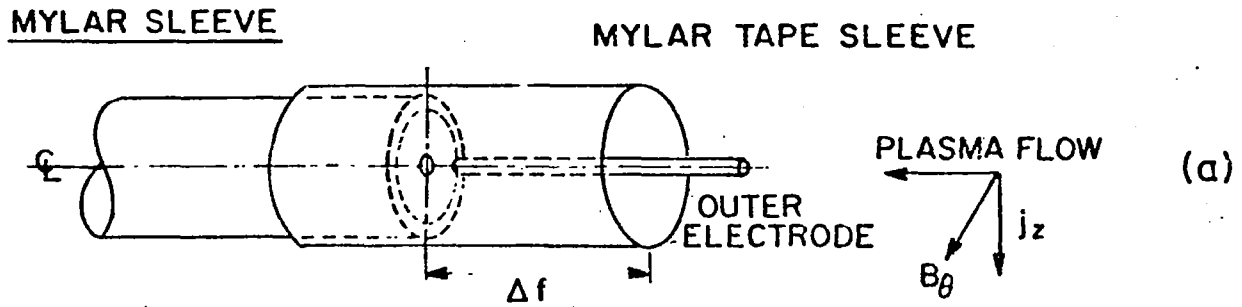

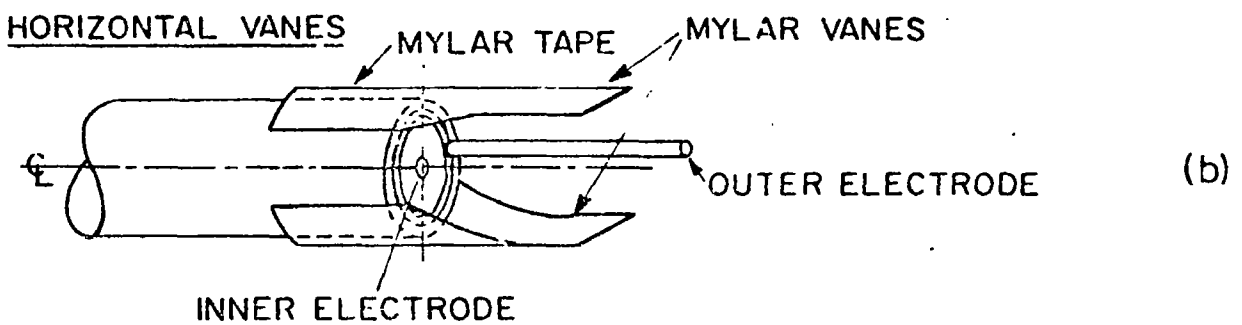

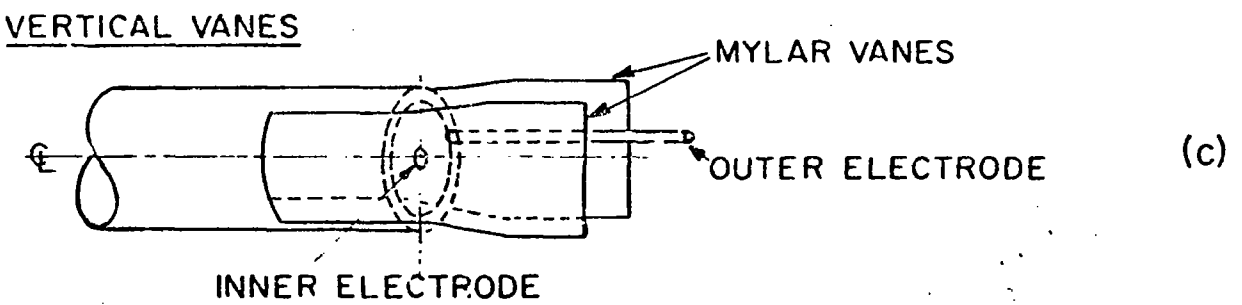

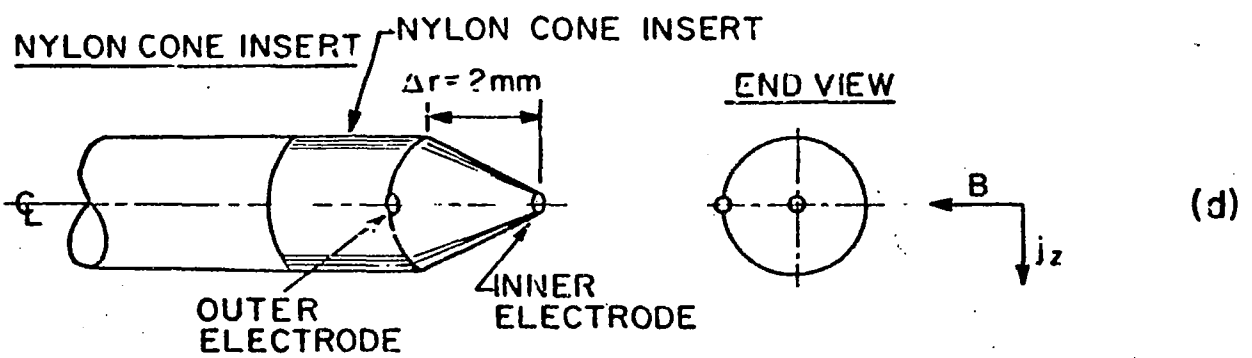

OBSTACLE EXPERIMENTS

FIGURE 39

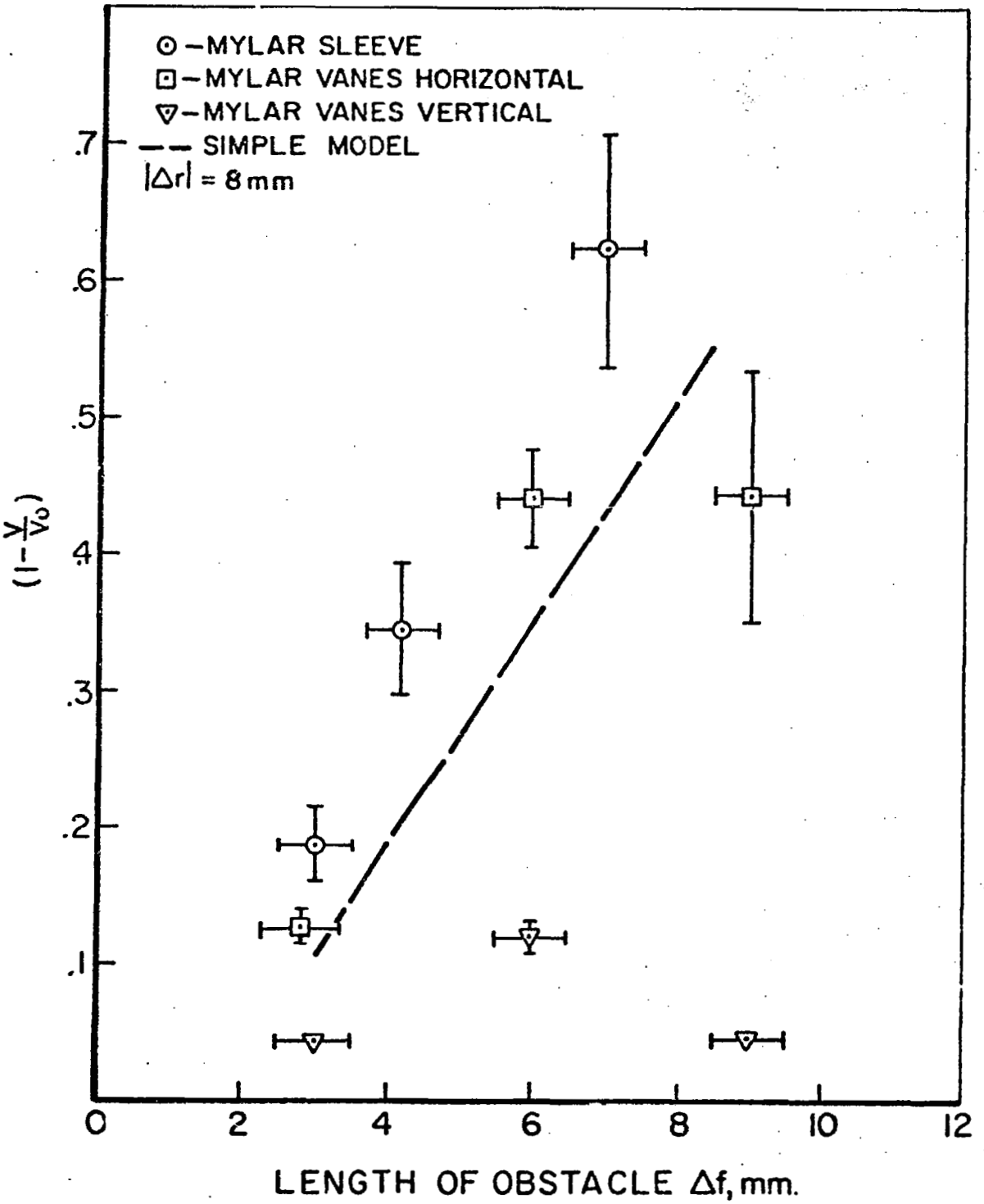

DECREASE IN PROBE VOLTAGE
vs OBSTACLE SIZE

FIGURE 40

is due to plasma cooling by the obstacle, to some mechanical interaction between the stagnating flow and the electromagnetic field, or to the interruption of the current density near the probe tips.

To pursue this point, we sought to separate the electromagnetic and gasdynamic interactions by use of sets of mylar vanes protruding beyond the probe (Figs. 39b,c). One set of vanes was aligned normal to the (axial) current vector so as to have maximum effect in cutting off the flow of axial current density near the probe tips, while still allowing the plasma to flow past the probe in nearly the usual manner. The results of such experiments with various length vanes are shown in Fig. 40. Note that the effects are comparable to those of the sleeve experiments.

To check on the effects of the vanes on the probe response when the current density is not greatly altered, the vanes were aligned parallel to the axial current. The results are also shown in Fig. 40. The disturbance is seen to be much smaller. It appears, then, that obstacles near the probe tips can have substantial effects on the probe response by disturbing the local current density patterns. The nature of this disturbance may be explored in the following simple model.

From a previous magnetogasdynamic analysis [51], we have that the radial electric field is essentially related to the axial current density via:

$$E_r = \frac{j_z B}{N_e e} \qquad (9\text{-}1)$$

that is, the radial electric field is proportional to the Lorentz force density acting in the discharge. Thus, if the local axial current density is diminished, the local radial electric field also decrease. The approach of our model is to explain such a decrease in terms of the increased length of the current conduction paths near the probe tips, forced by the obstacles. In Fig. 41 we show simplified current paths

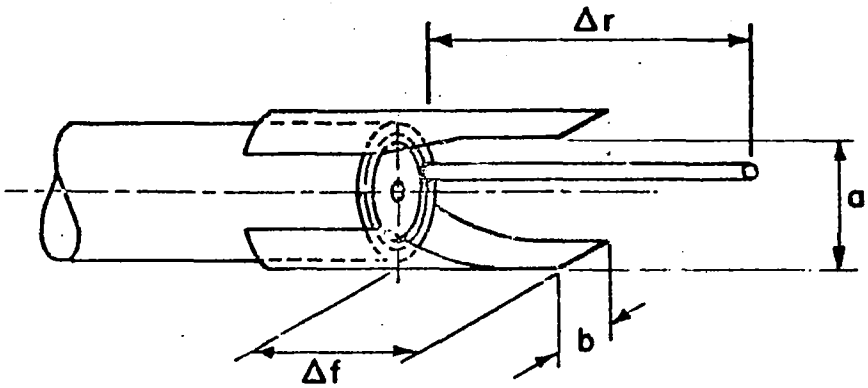

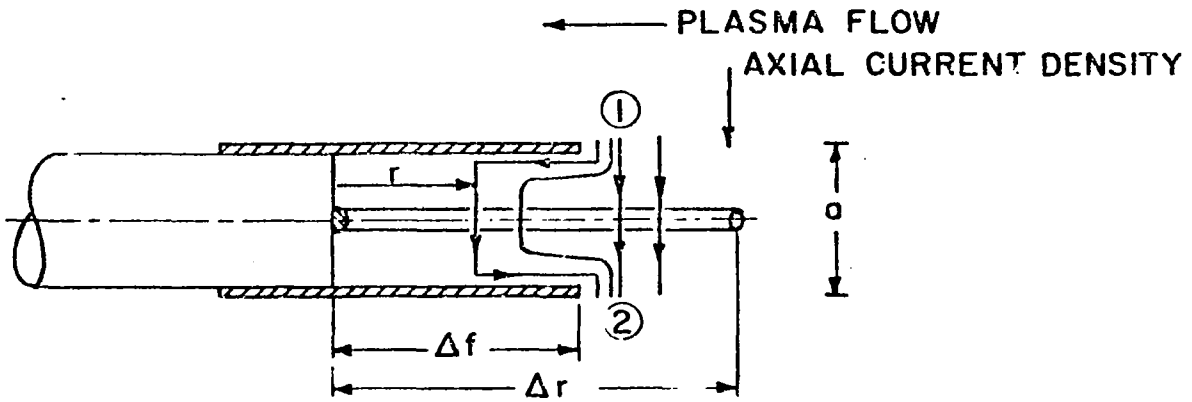

CURRENT PATH FROM ① TO ② BY WAY OF r HAS LENGTH: $l(r) = a + 2(\Delta f - r)$ IF $r \leq \Delta f$

$l(r) = a$ IF $r \geq \Delta f$

GEOMETRIC MODEL FOR OBSTACLE EXPERIMENT

FIGURE 41

near the probe tips. We assume that the plasma properties do not change greatly because of cooling or recombination effects, etc., near the insulator vanes and that the magnetic field, which is generated by the entire discharge current pattern, is not seriously affected and is approximately constant. Since the potential difference across any path between the vane edges is the same for all paths, the current carried by each path is inversely proportional to its length, $\ell(r)$. Thus, the current density at any position between the probe tips is inversely proportional to the length of the paths through that position. In other words, the voltage difference between the probe tips may be expressed:

$$V = \int_0^{\Delta r} \frac{jB}{N_e e}\, dr \propto \int_0^{\Delta r} \frac{dr}{\ell(r)} \qquad (9\text{-}2)$$

Equation (9-2) may be integrated to a detailed expression for the fractional decrease in measured voltage, which to a first approximation in the range $\Delta f \leq \Delta r$ becomes simply:

$$1 - V/V_o \approx \frac{\Delta f}{\Delta r} \qquad (9\text{-}3)$$

where V_o would be the measured value in the absence of any vanes.

This relation is also plotted in Fig. 40. Its qualitative agreement with the experimental results for the horizontal vanes suggests some validity for the concept of diffused current density as the cause of electric field weakening. The additional observed decrement of the voltage may be indicative of increased resistivity due to plasma cooling, an effect which would also explain the effect obtained with the vertical vanes.

A different sort of obstacle experiment was used to compare the results obtained by our present probe with those from conventional coaxial probes consisting of a hemispherical

center electrode and a ring outer electrode separated by an insulating cone. In our experiments, a nylon cone insert was placed over the inner probe tip, with the outer tip resting in a groove and exposed at the base of cone (Fig. 39d). With the probe tips again aligned in the plane of the magnetic field lines, several experiments were made with this arrangement, some results of which are shown in Fig. 42, along with the results of previous work with a coaxial probe. Also shown for comparison is the result of our present probe at the same tip separation, but without the nylon cone insert. Note that, while the results with the insulation cones agree rather well, they both disagree with the new probe result by about a factor of two. In light of our previous obstacle experiments, this calls into question electric probe measurements performed with insulator cone tips. In fact, we may apply our geometric model to the conical obstacle effect and obtain that the ratio of signals with and without the cone should be $2/\pi \approx 0.63$, in fairly good agreement with the experiment.

This line of research will be continued in the near future to explore the effects of probe tip area, relative flow direction, and external circuitry on the response of double-floating tip electric probes. It is hoped that these studies will provide us with the means of developing more reliable diagnostic tools for the measurement of internal electric fields. The microstructure of the plasma discharge and the physical processes by which it accelerates ionized gas are directly connected with the electric field distribution in the plasma. Thus, accurate electric field measurements are critically important to our understanding of the propulsion capabilities of pulsed plasma discharges.

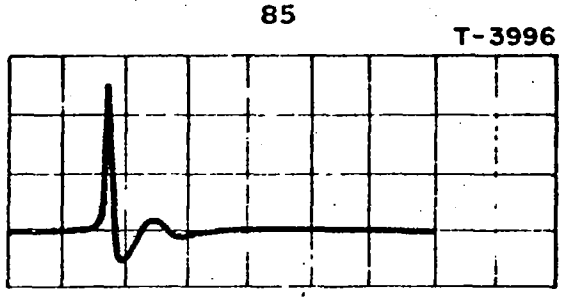

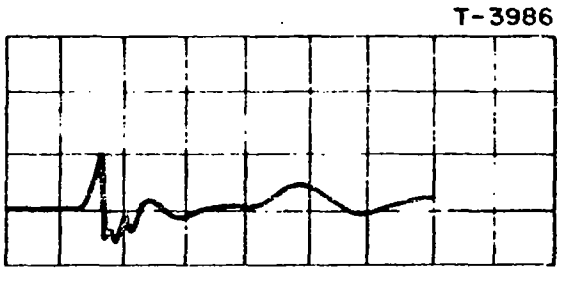

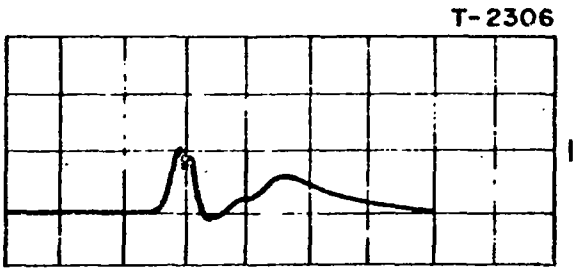

ELECTRIC PROBE RESPONSES

FIGURE 42

PROJECT REFERENCES

1. Proposed Studies of the Formation and Stability of an Electromagnetic Boundary in a Pinch, proposal for NASA Research Grant NsG-306-63, Princeton University, 5 March 1962.
2. Pulsed Electromagnetic Gas Acceleration, 1st Semi-Annual Progress Report for the period 1 July 1962 to 31 December 1962, Princeton University Aeronautical Engineering Report No. 634, January 1963.
3. "The Plasma Pinch as a Gas Accelerator," AIAA Electric Propulsion Conference, 11-13 March 1963, AIAA Preprint 63013.
4. Pulsed Electromagnetic Gas Acceleration, 2nd Semi-Annual Progress Report for the period 1 January 1963 to 30 June 1963, Princeton University Aeronautical Engineering Report No. 634a, June 1963.
5. Structure of a Large-Radius Pinch Discharge, AIAA Journal 1, 8, 1809-1814 (1963).
6. Gas-Triggered Inverse Pinch Switch, Review of Scientific Instruments 34, 12, 1439-1440 (1963).
7. A Gas-Triggered Inverse Pinch Switch, technical note, Princeton University Aeronautical Engineering Report No. 660, August, 1963.
8. "Pulsed Electromagnetic Gas Acceleration," 4th NASA Intercenter Conference on Plasma Physics, Washington, D. C., Paper No. II, 8, 2-4 December, 1963.
9. "Current Distributions in Large-Radius Pinch Discharges," AIAA Aerospace Sciences Meeting, 20-22 January 1964, AIAA Preprint No. 64-25.
10. Current Distributions in Large-Radius Pinch Discharges, AIAA Bulletin 1, 1, 12 (1964).
11. Current Distributions in Large-Radius Pinch Discharges, AIAA Journal 2, 10, 1749-1753 (1964).
12. Pulsed Electromagnetic Gas Acceleration, 3rd Semi-Annual Progress Report for the period 1 July 1963 to 31 December 1963, Princeton University Aeronautical Engineering Report No. 634b, December, 1963.
13. Pulsed Electromagnetic Gas Acceleration, renewal proposal for 15-months extension of NASA Research Grant NsG-306-63, Princeton University, 15 January 1964.
14. Pulsed Electromagnetic Gas Acceleration, 4th Semi-Annual Progress Report for the period 1 January 1964 to 30 June 1964, Princeton University Aerospace and Mechanical Sciences Report No. 634c, July, 1964.

PROJECT REFERENCES-contd

15. Gas-Triggered Pinch Discharge Switch, Princeton University Aerospace and Mechanical Sciences Technical Note No. 101, July, 1964.

16. Gas-Triggered Pinch Discharge Switch, Review of Scientific Instruments 36, 1, 101-102 (1965).

17. J. M. Corr, "Double Probe Studies in an 8" Pinch Discharge," M.S.E. thesis, Department of Aerospace and Mechanical Sciences, Princeton University, Princeton, New Jersey, 1964.

18. Exhaust of a Pinched Plasma From an Axial Orifice, AIAA Bulletin 1, 10, 570 (1964).

19. "Exhaust of a Pinched Plasma From an Axial Orifice," AIAA 2nd Aerospace Sciences Meeting, New York, New York, 25-27 January 1965, AIAA Paper No. 65-92.

20. Ejection of a Pinched Plasma From an Axial Orifice, AIAA Journal 3, 10, 1862-1866 (1965).

21. Pulsed Electromagnetic Gas Acceleration, 5th Semi-Annual Progress Report for the period 1 July 1964 to 31 December 1964, Princeton University Aerospace and Mechanical Sciences Report No. 634d, July, 1964.

22. On the Dynamic Efficiency of Pulsed Plasma Accelerators, AIAA Journal 3, 6, 1209-1210 (1965).

23. Linear Pinch Driven by a High-Current Pulse-Forming Network, AIAA Bulletin 2, 6, 309 (1965).

24. "Linear Pinch Driven by a High-Current Pulse-Forming Network," 2nd AIAA Annual Meeting, San Francisco, California, 26-29 July 1965, AIAA Paper No. 65-336.

25. E. S. Wright, "The Design and Development of Rogowski Coil Probes for Measurement of Current Density Distribution in a Plasma Pinch," M.S.E. thesis, Department of Aerospace and Mechanical Sciences, Princeton University, Princeton, New Jersey, 1965.

26. The Design and Development of Rogowski Coil Probes for Measurement of Current Density Distribution in a Plasma Pinch, Princeton University Aerospace and Mechanical Sciences Report No. 740, June, 1965.

27. Pulsed Electromagnetic Gas Acceleration, renewal proposal for 12-months extension of NASA Research Grant NsG-306-63, Princeton University, 7 June 1965.

28. Miniature Rogowski Coil Probes for Direct Measurement of Current Density Distribution in Transient Plasmas, Review of Scientific Instruments 36, 12, 1891-1892 (1965).

PROJECT REFERENCES-contd

29. Pulsed Electromagnetic Gas Acceleration, 6th Semi-Annual Progress Report for the period 1 January 1965 to 30 June 1965, Princeton University Aerospace and Mechanical Sciences Report No. 634e, July, 1965.

30. G. A. Rowell, "Cylindrical Shock Model of the Plasma Pinch," M.S.E. thesis, Department of Aerospace and Mechanical Sciences, Princeton University, Princeton, New Jersey, 1966.

31. Cylindrical Shock Model of the Plasma Pinch, Princeton University Aerospace and Mechanical Sciences Report No. 742, February, 1966.

32. Pulsed Electromagnetic Gas Acceleration, 7th Semi-Annual Progress Report for the period 1 July 1965 to 31 December 1965, Princeton University Aerospace and Mechanical Sciences Report No. 634f, January, 1966.

33. Electric and Magnetic Field Distributions in a Propagating Current Sheet, AIAA Bulletin 3, 1, 35 (1966).

34. "Electric and Magnetic Field Distributions in a Propagating Current Sheet," AIAA 5th Electric Propulsion Conference, San Diego, California, 7-9 March 1966, AIAA Paper No. 66-200.

35. "Pulse-Forming Networks for Propulsion Research," paper presented at the 7th Symposium on Engineering Aspects of Magnetohydrodynamics, Princeton University, Princeton, New Jersey, March 30-April 1, 1966 (p. 10-11 of proceedings).

36. N. A. Black, "Dynamics of a Pinch Discharge Driven by a High Current Pulse-Forming Network," Ph.D. thesis, Department of Aerospace and Mechanical Sciences, Princeton University, Princeton, New Jersey, 1966.

37. Dynamics of a Pinch Discharge Driven by a High Current Pulse-Forming Network, Princeton University Aerospace and Mechanical Sciences Report No. 778, May, 1966.

38. "Pulsed Plasma Propulsion," paper presented at the 5th NASA Intercenter and Contractors Conference on Plasma Physics, Washington, D. C., 24-26 May 1966, p. 75-81, part V of proceedings.

39. Pulsed Electromagnetic Gas Acceleration, renewal proposal for 24-months extension of NASA Research Grant NsG-306-63, Princeton University, 25 May 1966.

40. A Large Dielectric Vacuum Facility, AIAA Journal 4, 6, 1135 (1966).

41. R. L. Burton, "Structure of the Current Sheet in a Pinch Discharge," Ph.D. thesis, Department of Aerospace and Mechanical Sciences, Princeton University, Princeton, New Jersey, 1966.

PROJECT REFERENCES-contd

42. Structure of the Current Sheet in a Pinch Discharge, Princeton University Aerospace and Mechanical Sciences Report No. 783, September, 1966.

43. Pulsed Electromagnetic Gas Acceleration, 8th Semi-Annual Progress Report for the period 1 January 1966 to 30 June 1966, Princeton University Aerospace and Mechanical Sciences Report No. 634g, July, 1966.

44. Electromagnetic Propulsion, Astronautics and Aeronautics 4, 69 (1966).

45. W. R. Ellis, Jr., "An Investigation of Current Sheet Structure in a Cylindrical Z-Pinch," Ph.D. thesis, Department of Aerospace and Mechanical Sciences, Princeton University, Princeton, New Jersey, 1967.

46. "Current Status of Plasma Propulsion," AIAA 2nd Propulsion Joint Specialist Conference, Colorado Springs, Colorado, 13-17 June 1966, AIAA Paper No. 66-565.

47. Pulsed Electromagnetic Gas Acceleration, 9th Semi-Annual Progress Report for the period 1 July 1966 to 31 December 1966, Princeton University Aerospace and Mechanical Sciences Report No. 634h, January, 1967.

48. Pulsed Electromagnetic Gas Acceleration, 10th Semi-Annual Progress Report for the period 1 January 1967 to 30 June 1967, Princeton University Aerospace and Mechanical Sciences Report No. 634i, July, 1967.

49. "Current Pattern Stabilization in Pulsed Plasma Accelerators," AIAA Electric Propulsion and Plasmadynamics Conference, Colorado Springs, Colorado, 11-13 September 1967, AIAA Paper No. 67-656.

50. An Investigation of Current Sheet Structure in a Cylindrical Z-Pinch, Princeton University Aerospace and Mechanical Sciences Report No. 805, July, 1967.

51. Pulsed Electromagnetic Gas Acceleration, 11th Semi-Annual Progress Report for the period 1 July 1967 to 31 December 1967, Princeton University Aerospace and Mechanical Sciences Report No. 634j, January, 1968.

52. Current Pattern Stabilization in Pulsed Plasma Accelerators, AIAA Bulletin 4, 9, 433 (1967).

53. Jahn, R. G.: "Physics of Electric Propulsion," McGraw-Hill Book Company, New York, 1968.

END

DATE

FILMED

OCT 7 1968